The Thesis Committee for Karla Anne Kruse
Certifies that this is the approved version of the following thesis:

Characterization of High-Calcium Fly Ash for Evaluating the Sulfate Resistance of Concrete

APPROVED BY
SUPERVISING COMMITTEE:

Supervisor:

Kevin J. Folliard

Raissa Ferron

Characterization of High-Calcium Fly Ash for Evaluating the Sulfate Resistance of Concrete

by

Karla Anne Kruse, B.S.Ar.E.

Thesis

Presented to the Faculty of the Graduate School of

The University of Texas at Austin

in Partial Fulfillment

of the Requirements

for the Degree of

Master of Science in Engineering

The University of Texas at Austin

May 2012

Acknowledgements

Many individuals contributed to the success of this project. Without these individuals, my work would have led to many more dead ends and to a lot more stress.

To my family, I know you had no idea what I was researching for these two years, but I appreciate the support anyway. Always remember that "previous" concrete is not old concrete!

To my boyfriend, Anthony, I think I read more of your dissertation than my thesis, but I appreciate the open forum to bounce ideas around. It wasn't always easy, but it will be worth it. Get ready for the cold year we have ahead of us!

To my project advisor, Dr. Folliard, I appreciate the opportunity to work on my first fly ash project to realize I wanted to pursue a materials background. Thank you for your breadth of knowledge and your willingness to share it with me. Your playful mindset for the little things in life will resonate with me for a long time.

To my co-advisor, Dr. Ferron, thank you for your technical assistance and for reviewing this thesis.

To my colleague on this project, Andy, we grew a lot over these few years. I wish you the absolute best.

I appreciate all of the assistance from other members at the University of Texas at Austin. Thano, thank you for always hearing my footsteps walking down the hallway to ask you yet another question and answering me. Thank you for sitting with me in front of the Rietveld computer getting just as frustrated as I was. Dr. Juenger, thank you for your guidance in project meetings over these past two years. To Sherian and Mike, thank you for all of your support and guidance. I will miss the great times I have had at the lab over the past four years.

And finally, I want to thank TxDOT for the financial support through this project and the resources over these two years.

Abstract

Characterization of High-Calcium Fly Ash for Evaluating the Sulfate Resistance of Concrete

Karla Anne Kruse, M.S.E.

The University of Texas at Austin, 2012

Supervisor: Kevin J. Folliard

Concrete structures are often exposed to sulfates, which are typically found in groundwater and soils, in agricultural run-off, in industrial facilities, and in other source points. These sulfates may attack concrete and significantly shorten the service life of concrete due to reactions between sulfate ions and concrete constituents. These reactions form expansive and deleterious compounds that lead to cracking and spalling of the concrete. This reaction is a function of the sulfate solution but also the physical, chemical, and mineralogical properties of the cement and supplemental cementitious materials (SCMs). It is widely understood that the addition of some fly ashes, by-products of coal combustion power plants, improve the sulfate resistance of the concrete but some fly ash additions actually reduce the sulfate resistance. This project aims to understand this relationship between fly ash and sulfate resistance. Using sulfate testing results on mortar previously obtained at The University of Texas at Austin, this research evaluated the mineralogical, chemical, and physical characteristics of fly ash and

attempted to link these measured characteristics (or combinations thereof) to sulfate resistance of concrete.

Table of Contents

List of Tables

List of Figures

Chapter 1: Introduction

1.1 Introduction

Concrete has been a major construction material for hundreds of years and is the most widely used construction material today. With the ability to alter mix designs, use recycled components, and create a cost-effective product, concrete appears to be a relatively sustainable material. However, concrete can be affected by various durability-related problems that can shorten its service life. External chemical sulfate attack is one example of a durability problem that has plagued concrete structures throughout the world. The research described in this thesis is aimed at providing insight into how to best characterize fly ash in order to gain insight into sulfate resistance of concrete containing fly ash.

1.2 Project Needs

This project was specifically aimed at improving the sulfate resistance of concrete containing fly ash. Past research has shown that using low-calcium fly ash can significantly improve sulfate resistance, whereas some high-calcium fly ashes may have little impact on sulfate resistance or may even reduce sulfate resistance (Drimalas, 2007). Although calcium content is a reasonable first-order index for predicting sulfate resistance, there are fly ashes with similar CaO contents that may show significant departures in their effects on sulfate resistance. Thus, the need exists for characterization methods that better correlate with sulfate resistance, especially given the rapidly changing situation with fly ash availability and changes in coal sources, combustion processes, and emission controls.

1.3 Statement of Objective

This thesis aims to characterize fly ash with regard to sulfate resistance. This project builds on previous work funded under TxDOT Project 4889 at the University of Texas at Austin, which tested many different fly ashes and created an extensive database of concrete and mortar durability testing results. This project has the unique advantage of this database of testing results, which allows for greater focus on testing the fly ashes to fully understand the material under investigation.

1.4 Organization of Thesis

This thesis is divided into eight chapters, this introduction being the first. The literature review for sulfate attack and fly ash is presented in Chapter 2. Chapter 3 describes the testing methods and equipment used in this thesis. The materials used are described in Chapter 4, along with the results from sulfate expansion tests. Chapter 5 summarizes the results of various tests on fly ashes to characterize their chemical, mineralogical, and physical properties. Chapter 6 presents the results from hydration and microstructural studies on paste and mortar containing fly ash, including an in-depth study evaluating the effects of sulfate exposure on the type and amount of hydration and reaction products. Chapter 7 discusses and synthesizes the key findings from this study, and Chapter 8 presents the main conclusions from this work and identifies areas for future research.

1.5 Nomenclature

The following nomenclature will be used throughout this thesis:

Table 1: Nomenclature

Notation	Cement Chemistry Name
A	Al_2O_3
C	CaO
F	Fe_2O_3
H	H_2O
K	K_2O
N	Na_2O
S	SiO_2
$	SO_3
C_2S	Di-calcium silicate
C_3S	Tri-calcium silicate
C_3A	Tri-calcium aluminate
C_4AF	Tetra-calcium aluminoferrite
$C_3A(C\$)_3H_{32}$	Ettringite
$C_3A(C\$)H_{12}$	Monosulfate
CH	Calcium hydroxide
C-S-H	Calcium silicate hydrate
C-A-H	Calcium aluminate hydrate

Chapter 2: Literature Review

This chapter presents a brief literature review of the mechanisms of sulfate attack and mitigation techniques. The background and material properties of fly ash are then presented, including how fly ash affects the sulfate resistance of concrete.

2.1 SULFATE ATTACK

Sulfate attack is a durability concern for concrete members. It involves the reaction of sulfate ions and concrete constituents. Sulfate attack is quite complex, and there are different forms of sulfate attack that manifest themselves in concrete; the attack can be chemical and/or physical in nature and the source of sulfate can be either internal or external to the concrete. A brief summary of sulfate attack will be presented herein, but the main focus of this thesis will be on the resistance of fly ash mortar and concrete to external, chemical sulfate attack.

2.1.1 External Sulfate Attack

External sulfate attack may be either physical or chemical. Physical sulfate attack is referred to as salt crystallization or salt weathering and is caused by sulfate salts that penetrate into the concrete and cause deterioration on the concrete exterior. This physical form of attack does not alter hydration products within the concrete, but rather the damage is caused by phase changes in the sodium sulfate solution that exert expansive stresses within the concrete (Skalny, Marchand, & Odler, 2002). However, sulfates can also penetrate the concrete and react with constituents to form ettringite and gypsum, which can be detrimental to the concrete. According to ACI 201.2R-01, sodium, potassium, calcium, and magnesium sulfates are responsible for this concrete deterioration. Concrete in contact with gypsum rich sources exhibit sulfate attack in

Texas, while sodium and magnesium sulfate sources tend to show even greater durability issues elsewhere in the United States (Drimalas, 2007).

2.1.1.1 Physical Sulfate Attack

Physical sulfate attack, sometimes called salt crystallization or weathering, involves the concentration and precipitation of sulfate salts near the concrete surface that leads to surface scaling. Most commonly, concrete is in contact with sulfates in soils from groundwater, but sulfates are also introduced from industrial waste and fertilizers. These sulfates wick up the concrete by capillary action and can penetrate the concrete due to its porous nature. The resulting distress is due to a conversion from a low to a higher hydrate phase and a resulting volume increase due to crystallization pressure. Theoretically, the transition from the anhydrous thenardite to the decahydrate mirabilite results in a 314% volume increase (Haynes & Bassuoni, 2011); however, in laboratory experiments, the levels of expansion measured are much lower (Folliard & Sandberg, 1994) but certainly high enough to cause near-surface distress in concrete. These phase transitions occur due to a change in temperature and/or humidity, as shown in Figure 1.

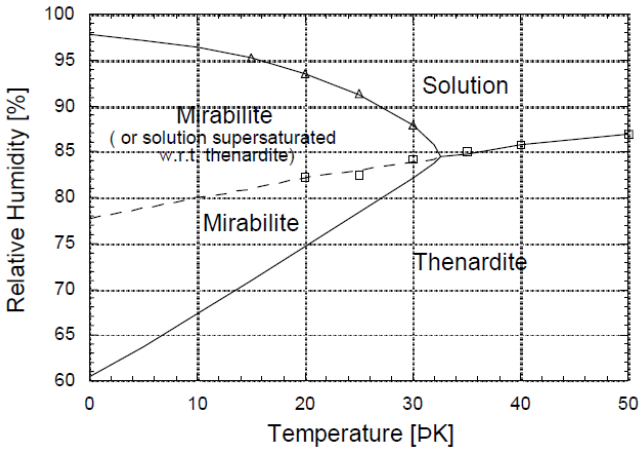

Figure 1: Mirabilite-Thenardite Transition (Flatt & Scherer, 2002)

2.1.1.2 Chemical External Sulfate Attack

The deterioration in this type of sulfate attack is due to the formation of ettringite and gypsum. This is a consequential attack due to a series of actions. Sodium sulfate solution reactions are presented below due to their frequency in nature and literature, but the attack can also be caused by magnesium sulfate and calcium sulfate, or any combination of the three aforementioned sulfate salts.

First, to set the stage for discussing sulfate attack, it is important to first consider the hydration products that form in typical portland cement concrete. Most important to strength gain, the calcium silicates, C_3S and C_2S, react with water to form calcium silicate hydrate (C-S-H) and calcium hydroxide (CH). The C-S-H is responsible for binding the concrete together for strength gain. In the presence of a pozzolan, such as fly ash, the pozzolan will react with the CH to form more beneficial C-S-H. Any leftover CH is available for reaction with sulfate ions.

Sulfate ions can penetrate the concrete due to the porosity of the mix, type of ions, and the sulfate concentration. These sulfate ions are usually found in the groundwater. These ions, sodium sulfate shown below, react with remaining CH to form gypsum, shown in Equation 1 (Folliard K. , 2010).

$$\boxed{CH + N_2\bar{S}H_{10} \rightarrow C\bar{S}H_2 + 2NH + 8H}$$

Calcium Hydroxide + Sodium Sulphate → Gypsum + Sodium Hydroxide + Water (1)

This gypsum can react with monosulfate, C_3A, and calcium aluminates to produce ettringite. See the reaction between gypsum and monosulfate in Equation 2 (Folliard K. , 2010). Monosulfate is present due to the reaction of C_3A, water, and ettringite during cement hydration. Ettringite can also be formed due to the reaction between calcium

aluminate hydrates and sodium sulfate, shown in Equation 3, and due to the reaction between calcium aluminate sulfates and gypsum.

$$C_3A(C\bar{S})H_{12} + 2C\bar{S}H_2 + 16H \rightarrow C_3A(C\bar{S})_3H_{32}$$

Calcium Monosulphoaluminate + Gypsum + Water → **Ettringite** (2)

$$2C_3AH_{12} + 3N_2\bar{S}H_{10} \rightarrow C_3A(C\bar{S})_3H_{32} + 2AH_3 + 6NH + 17H$$

Tri-Calcium Aluminate Hydrate + Sodium Sulphate → **Ettringite** + Aluminum Hydroxide + Sodium Hydroxide + Water (3)

Through the above processes, gypsum and ettringite are formed. The formation of gypsum leads to a loss of mass and paste cohesion because gypsum is water soluble. The formation of ettringite from monosulfate leads to expansion and cracking as ettringite occupies about twice as much volume as monosulfate (Neville, 1996).

2.1.1.3 Thaumasite

Thaumasite is a naturally occurring mineral similar in appearance to ettringite. The destruction of concrete is due to the transition from C-S-H into thaumasite, and as a result, the paste essentially loses its entire binding capacity. Thaumasite forms at low temperatures, especially 0-5 °C, in the presence of calcium, carbonate, silica, sulfate, and water. Thaumasite is generally more of an issue when limestone fillers are used in the concrete mix design due to the introduction of calcium carbonate. This is a slow reaction that takes 6 months to 1 year, but it can be even slower at slightly higher temperatures up to 15 °C (Bensted, 1999).

2.1.2 Internal Sulfate Attack

To better understand internal sulfate attack, some key aspects of typical portland cement hydration are worth noting. Calcium sulfates are added to the clinker in the cement production process. Gypsum is often the form of this added sulfate, but alkali sulfates are present in the clinker due to the cement manufacturing process. The addition of gypsum controls setting time and increases strength. The gypsum reacts with water and C_3A from the cement to form ettringite, shown in Equation 4.

$$C_3A + 3C\overline{S}H_2 + 26H \rightarrow C_3A(C\overline{S})_3H_{32}$$

Tri-Calcium Aluminate + Gypsum + Water → **Ettringite** (4)

This ettringite is referred to as blocking ettringite because it coats the C_3A grains to slow down the hydration reaction. This reaction will continue until all of the C_3A or gypsum reacts. If there is an excess of C_3A, it becomes available for reaction with ettringite and water to form monosulfate. If there is even more C_3A present, it hydrates and forms calcium aluminate hydrate (C-A-H). Sulfate attack and expansion occur as the monosulfate reacts with gypsum and water and converts back to ettringite. See Equation 5 for the chemical equation for this reaction (Skalny, Marchand, & Odler, 2002).

$$C_4A\overline{S}H_{12} + 2C\overline{S}H_2 + 16H \rightarrow C_6A\overline{S}_3H_{32}$$

Monosulfate + Gypsum + Water → Ettringite (5)

When ettringite is accompanied by the absorption of water, expansion occurs. It is important to note that if ettringite forms early during hydration, the concrete can

accommodate the expansion. However, if ettringite continues to form after hardening, expansion and cracking will result (Tishmack, Olek, & Diamond, 1999).

2.1.2.1 Delayed Ettringite Formation

Delayed ettringite formation (DEF) is a type of concrete distress due to the formation of ettringite in hardened concrete. This is known to be a result of high curing temperatures because ettringite dissolves at these higher temperatures. Sulfate and alumina get trapped in the inner C-S-H layer. The sulfate and alumina are slowly released, leading to the formation of ettringite at later ages (Folliard K. , 2010). When this ettringite is accompanied by water absorption, it leads to detrimental expansion.

2.2 SULFATE ATTACK MITIGATION

ACI recommends using low permeability concrete and concrete components appropriate for mitigating sulfate resistance as the best defense to sulfate attack (ACI201.2R-01, 2001). For both types of sulfate attack, the permeability of the concrete is a very important factor to limit the ingress of sulfate ions. This is achieved by lowering the water to cementitious ratio (w/cm), as shown in Table 2 (ACI201.2R-01, 2001). Proper curing of the concrete is also essential to the permeability of the concrete. Vapor barriers and other membranes can be utilized to prevent the ingress of sulfates as well.

Table 2: Sulfate Attack Mitigation Requirements (ACI201.2R-01, 2001)

Severity of potential exposure	Water-soluble soluble sulfate (SO_4)*	Sulfate (SO_4)* in water, ppm	*w/cm* by mass, max.†‡	Cementitious material requirements
Class 0 exposure	0.00 to 0.10	0 to 150	No special requirements for sulfate resistance	No special requirements for sulfate resistance
Class 1 exposure	> 0.10 and < 0.20	> 150 and < 1500	0.50‡	C 150 Type II or equivalent§
Class 2 exposure	0.20 to < 2.0	1500 to < 10,000	0.45‡	C 150 Type V or equivalent§
Class 3 exposure	2.0 or greater	10,000 or greater	0.40‡	C 150 Type V plus pozzolan or slag§
Seawater exposure	—	—	See Section 2.4	See Section 2.4

Using sulfate resistant cements is also featured in ACI guidelines, as shown in Table 2. Decreasing the C_3A content of the cement will decrease the amount of ettringite formed. Type II and V cements are permitted for this use per ASTM C 150 due to their low C_3A content, 5% and 8%, respectively. Type V cements should not be used in excess of 25% due to the involvement of the alumina in aluminoferrite phase of C_4AF with sulfate attack (Bhatty & Taylor, 2006). The correlation between C_3A content and sulfate attack can be seen in Figure 2 – the higher the C_3A content of the cement, the higher the level of deterioration that was visually observed.

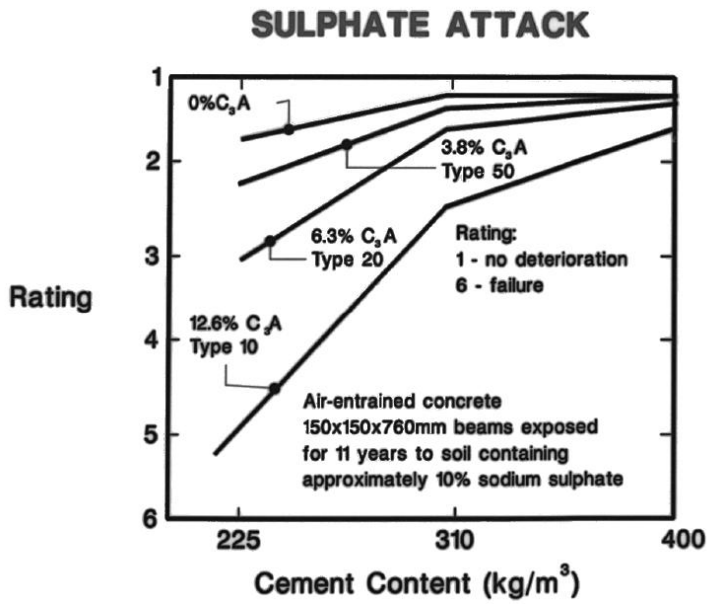

Figure 2: Sulfate Attack and Cement Content (Kosmatka & Panarese, 1994)

Using supplementary cementitious materials (SCMs) is another way to increase sulfate resistance. The use of pozzolanic SCMs converts CH into C-S-H, thereby reducing the amount of CH that can be readily attacked by sulfate salts. In addition, using SCMs as a replacement for portland cement reduces the C_3A content of the binder system, reducing the potential for ettringite formation and subsequent expansion and cracking. It should be noted, however, that certain high-calcium fly ashes may actually contain C_3A, and this may have a significant impact on sulfate resistance. Performance testing, typically using ASTM C 1012, is allowed by ACI 201 (and ACI 318) to allow one to test a specific SCM (or SCMs), provided that the mortar mixture meets the expansion limits (see Table 3).

Table 3: Exposure Classification Expansion Limits (ACI201.2R-01, 2001)

Severity of Potential Exposure	Cementitious Material Requirements	Expansion Limits
Class I	C150 Type II	≤ 0.10% at 6 months
Class II	C150 Type V	≤ 0.10% at 1 year
Class III	C150 Type V plus pozzolan or slag	≤ 0.10% at 18 months

Overall, sulfate attack depends on where the sulfates originate, the concentration of the sulfates, and the types of sulfates. The temperature and relative humidity can play an important role as well especially for DEF and thaumasite formation. The constituents in the concrete, such as the type of cement, SCMs, and w/cm ratio, are the most important factors that can impact sulfate resistance. This thesis will only focus on the effects of fly ash type and dosage on the resistance of mortar and concrete to external, chemical sulfate attack.

2.3 FLY ASH

2.3.1 Fly Ash Background

Fly ash is a by-product of coal combustion power plants which is often used in concrete. Fifty million tons of fly ash is produced annually in the United States with 10-12% being used in concrete (ACI 232.R-96, 1996). Fly ash enhances the properties of concrete when used effectively. With typical replacement percentages of 15-25%, less cement is used resulting in fewer CO_2 emissions from cement manufacturing plants and a lower overall cost of concrete. Fly ash reduces the heat of hydration, reduces permeability and improves concrete resistance to durability issues such as alkali silica reaction (ASR), sulfate attack, and DEF.

Fly ash particles are heterogeneous, fine particles carried away by flue gas and caught by mechanical or electrostatic precipitators in coal combustion power plants. With temperatures in excess of 2700 °F, non-organic matter in the coal forms molten droplets which are quenched. This process forms glassy spheres, mostly solid but some hollow, with a smooth surface. These particles range in size from 0.5-200 μm with a range of densities from 123 lb/ft^3 to 187 lb/ft^3 (ACI 232.R-96, 1996).

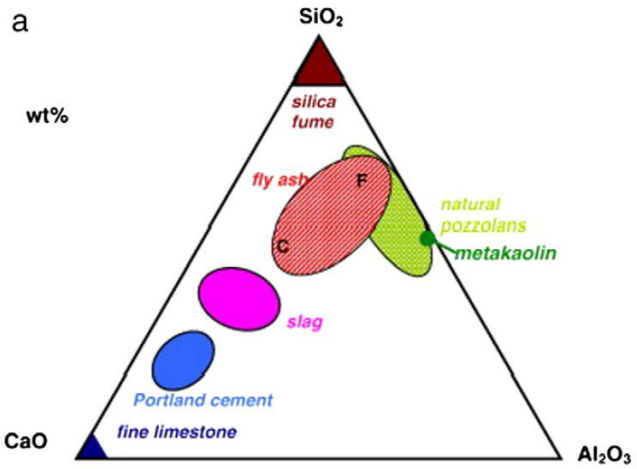

Figure 3: Cementitious Materials Ternary Diagram (Scrivener & Nonat, 2011)

The composition of the fly ash changes drastically with the parent coal burned in the power plant, the combustion conditions, and cooling regimes. Due to the wide variety of fly ash compositions, it is difficult to characterize this material. In the United States, there are two main classification groups for fly ash, shown in Table 4. ASTM identifies these groups as Class F and Class C ashes. Class F ashes are produced from the burning of anthracite or bituminous coal. The total silica, alumina, and iron oxide content must be greater than 70%. This classification usually refers to the lower calcium ashes. Class C ashes are produced from the burning of lignite or sub-bituminous coal.

The total silica, alumina, and iron oxide content must be greater than 50% for this classification (ASTM C 618, 2008). Class C ashes are the higher calcium ashes, refer to Figure 3. Although not recognized as an identifier by ASTM, ashes greater than 20% calcium oxide content are referred to as Class C ashes in the United States. However, in Canada, a mid-level of fly ash is referred to as Class CH. Based on past research, Canada may begin classifying fly ash in terms of calcium oxide content. The United States, Canada, and the United Kingdom all have different criteria for the classification of fly ash even though bulk oxide content is the basis for most characterizations.

Table 4: ASTM C 618 Fly Ash Classification (ASTM C 618, 2008)

Class	Description	Requirements
F	-Anthracite or bituminous coals -Pozzolanic	$SiO_2 + Al_2O_3 + Fe_2O_3 \geq 70\%$
C	-Lignite or sub-bituminous coals -Pozzolanic and cementitious	$SiO_2 + Al_2O_3 + Fe_2O_3 \geq 50\%$

Fly ash is a pozzolanic material. ASTM defines a pozzolan as "a siliceous or siliceous and aluminous material that in itself possesses little or no cementitious value but will, in finely divided form and in the presence of moisture, chemically react with calcium hydroxide at ordinary temperatures to form compounds possessing cementitious properties" (ASTM International, 2011). This pozzolanic reaction results in greater strength gain and reduced permeability attributed to SiO_2 and Al_2O_3 components. Class F and C ashes are pozzolanic; however, Class C ashes also exhibit cementitious properties, meaning they can harden and gain strength when mixed only with water and not cement. This reaction is due to the reactive crystalline phases found in higher-calcium ashes reacting with water.

2.3.2 Fly Ash Changes

The United States Congress passed the Clean Air Act in 1990 in an attempt to reduce the harmful emissions of the coal-burning power plants by controlling the SO_2 and NO_x emissions. This Act required the power plants to use low-NO_x burners. This increases the percentage of unburned carbon in the fly ash, which can significantly impact water demand and workability in a concrete mix. To control SO_x emissions, scrubbers, such as SO_3, were added due to the presence of pyrite and gypsum in the parent coals. A reaction with lime and alkalis resulted in sulfur scrubbing the fly ash particles (ACI 232.R-96, 1996). The main effect of this Act was the switch from using any locally available parent coal to coals from the Powder River Basin, an area in the western region of the United States. This region is now the largest coal producing region in the United States. The coal from this region is lignite or sub-bituminous coal, which creates a higher calcium oxide content of the output fly ash. These coals have lower amounts of SO_2 to help control the emissions due to the high cost of adding scrubbers. This coal is also close to the surface requiring fewer resources to mine the Powder River Basin. This increase in calcium in the output fly ash can lead to problems including increased heat of hydration, increase in set time, and decreased resistance to sulfate attack.

2.3.3 Fly Ash Mineralogy

Fly ash composition has three components: inorganic material comprised of crystalline and amorphous phases, organic material, and fluid material found in the organic and inorganic material. Each part of the fly ash can be classified according to time of formation. Primary phases undergo no phase transformations. Secondary phases are formed during coal combustion and include the silicates and oxides. The tertiary phases were formed during fly ash transport and include portlandite and gypsum. The

main elements of the fly ash are: O, Si, Al, Ca, Fe, C, K, Mg, H, Na, Ti, N, P, Ba, and other trace elements (Vassilev & Vassileva, 2007).

When the fly ash particles are cooling, the rate of cooling affects the formation of the inorganic matter. A slow cooling results in larger, crystalline particles whereas a fast cooling results in smaller, 1-5 μm glassy particles (Hemmings & Berry, 1988). The crystalline and amorphous phases make up the fly ash.

Fly ash currently is classified by its bulk oxide content. Refer to Table 5 for typical bulk fly ash compositions. The CaO, SiO_2, Al_2O_3, and Fe_2O_3 make up the majority of the fly ash. As the CaO increases, the other three oxides listed above decrease. As CaO increases, the SO_3 and alkalis (Na_2O and K_2O) increase as well. The more iron in the fly ash, the greater the density; the greater the carbon in the fly ash, the lower the density (ACI 232.R-96, 1996). The loss on ignition (LOI) is related to the carbon content in the fly ash, which effects water demand and workability. LOI is higher for Class F ashes than Class C because of the presence of more unburnt carbon.

Table 5: Typical Fly Ash Bulk Composition (ACI 232.R-96, 1996)

Table 2.1—Example bulk composition of fly ash with coal sources

	Bituminous	Subbituminous	Northern Lignite	Southern Lignite
SiO_2, percent	45.9	31.3	44.6	52.9
Al_2O_3, percent	24.2	22.5	15.5	17.9
Fe_2O_3, percent	4.7	5.0	7.7	9.0
CaO, percent	3.7	28.0	20.9	9.6
SO_3, percent	0.4	2.3	1.5	0.9
MgO, percent	0.0	4.3	6.1	1.7
Alkalies,* percent	0.2	1.6	0.9	0.6
LOI, percent	3	0.3	0.4	0.4
Air permeability fineness, m^2/kg	403	393	329	256
45 µm sieve retention, percent	18.2	17.0	21.6	23.8
Density, Mg/m^3	2.28	2.70	2.54	2.43

* Available alkalies expressed as Na_2O equivalent.

2.3.3.1 Crystalline Phases

Crystalline phases account for 5-50% by mass of the fly ash (Hemmings & Berry, 1988). The ten main crystalline phases are (McCarthy, Solem, Manz, & Hassett, 1190):

1. Anhydrite ($CaSO_4$) –found in most Class C ashes and is a result of the Cao, SO_2 and O_2 in the furnace, it increases with an increase in SO_3 and is involved with ettringite formation
2. Mullite (A_3S_2) –found more in Class F ashes, not reactive
3. Quartz –in all fly ash
4. Melite –a solid solution of akermanite and gehlenite found in Class C ashes and related to MgO content
5. Merwinite –found in Class C ashes and related to MgO content
6. Periclase (crystalline MgO) –ASTM C 618 limits MgO to ≤ 5% due to soundness issues, found in Class C ash
7. C_3A – in all Class C ashes, forms ettringite responsible for sulfate expansions
8. Magnetite (Fe_3O_4) – known as spinel

9. Hematite (Fe_2O_3) - common in F ash
10. Lime (crystalline CaO) –found in all Class C ashes and some Class F ashes, free lime participates in hydration reactions and dissolves to increase the pH greater than 12, usually at 2-5% because if all of the free lime doesn't react initially then it'll react with portlandite and result in soundness issues (Roy, Luke, & Diamond, 1985)

The crystalline phases are identified through x-ray diffraction (XRD), specifically identifying which phases are reactive and those that are stable. The reactive phases most vulnerable to sulfate attack are C_3A, gehlenite, periclase, and anhydrite (Carrasquillo & Tikalsky, 1993). The reactive C_3A component is responsible for ettringite formation and associated expansion, but it is not in large enough quantities to solely cause full deterioration (Carrasquillo & Tikalsky, 1992). The stable phases do not participate in hydration reactions or reactions with sulfates.

2.3.3.2 Amorphous Phases

Amorphous particles are the circular particles 1-5 μm in diameter. These particles are formed due to quenching of particles, resulting in disordered, lack of crystal structures, making them harder to characterize. This lack of crystal structure is due to "rapid cooling, network isomorphic substitution, and cation modification" (Hemmings & Berry, 1988). Parent coal with a low calcium results in aluminosilicate glass. Parent coal with higher levels of calcium result in calcium aluminosilicate glass, a known reactive phase in Class C ashes (ACI 232.R-96, 1996). It is the presence of the calcium aluminosilicate glass which makes Class C ashes more reactive than Class F ashes.

The amount of amorphous phases is found by subtracting the amount of crystalline phases from the total bulk mass. This is discussed in the testing methods section, Section 3.3.

2.3.4 Fly Ash and Sulfate Attack

Fly ash is used as a supplementary cementitious material in concrete to enhance strength properties, reduce permeability, and reduce heat of hydration to name a few technical benefits. Adding fly ash into a concrete mixture can also improve the resistance of sulfate attack.

It is generally understood that Class F ashes improve the sulfate resistance, but Class C ashes decrease the sulfate resistance. Class C ashes contain C_3A, which is responsible for ettringite formation and resulting expansions. See Figure 4 for the relationship of cement C_3A with expansions. As the calcium oxide content increases past 20%, the percent C_3A begins to increase rapidly (Folliard K. , 2010). Class C ashes have a reduced pozzolanic nature compared to Class F ashes as well. Therefore, Class C ashes are not as effective at consuming CH and converting it into C-S-H. Class C ashes also contain reactive glassy calcium-aluminate phases (Folliard K. , 2010).

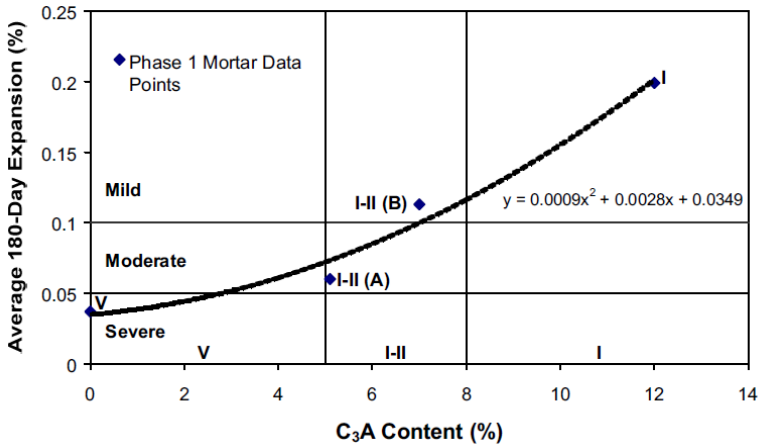

Figure 4: Average Expansions versus C_3A Content for Portland Cement Mortar (Stephens & Carrasquillo, 2000)

In addition, Class C ashes increase the amount of expansion and decrease the time to failure as the fly ash replacement levels increase (Tikalsky & Carrasquillo, 1992). Refer to Figure 5 to see this relationship. This relationship is due to more reactive crystalline phases of anhydrite, lime, periclase, sodalite, and C_3A present in high calcium fly ashes. Class F ashes do not contain these reactive phases and only the inert crystalline phases of mullite, quartz, ferrite spinel, and hematite (Carrasquillo & Tikalsky, 1992).

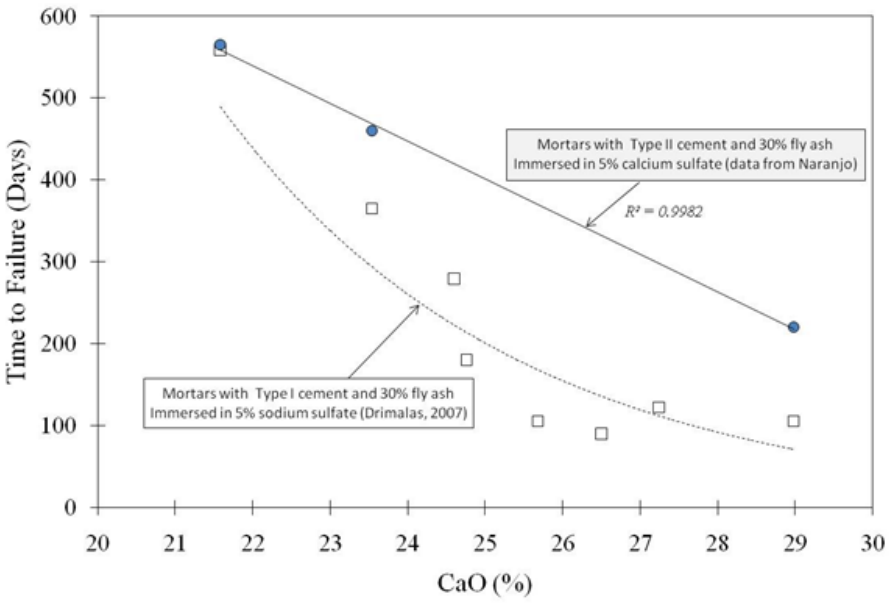

Figure 5: Relationship between CaO content and Time to Failure (Folliard K. , 2010)

Dunstan acknowledged that C_3A content was related to sulfate durability because it is the reactive aluminate compound responsible for ettringite formation. He argued that C_3A in combination with alumina and C_4AF was the contributing factor to sulfate resistance though. Alumina itself is introduced from mullite (A_3S_2) as a non-reactive crystalline phase. However, in high calcium ashes, there are other crystalline phases that do contain alumina. The glassy alumina in calcium-alumina-silicate glass is more reactive with sulfates because of the formation of monosulfate and calcium alumina hydrates (Tishmack, Olek, & Diamond, 1999) and lies in the gehlenite region (C_2AS) on the $CaO\text{-}SiO_2\text{-}Al_2O_3$ ternary diagram. As calcium content increases, the glass turns into calcium aluminosilicate glass and reactivity increases. Refer to Figure 6 to see this transition to reactive glass phase with an increase in calcium content, left to right on x-axis.

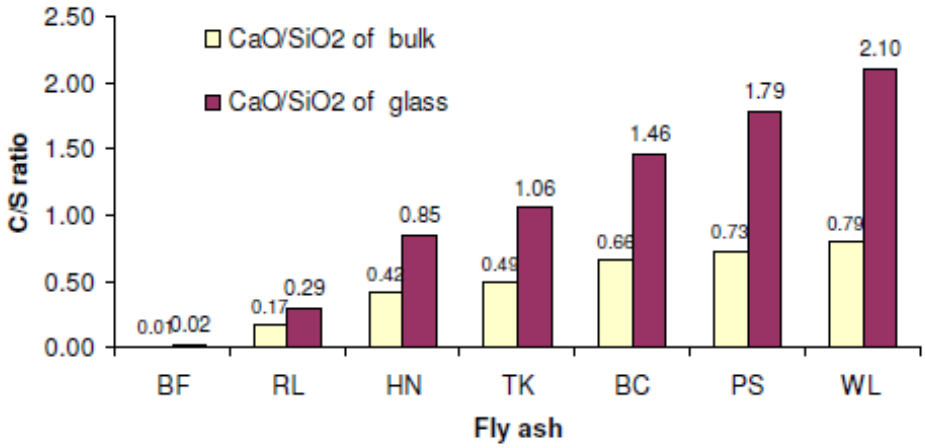

Figure 6: C/S Ratio of Fly Ash Compositions (Folliard K. , 2010)

Plotting fly ash on the ternary diagram may be useful to indicating sulfate resistance. Refer to Figure 7 for these regions on the ternary diagram. If the fly ash falls within the mullite region, it typically has good sulfate resistance. If the fly ash falls within the gehlenite region, the ash typically has reduced sulfate resistance (Dunstan, 1980). Watt and Thorne continued this theory to say that the amount of iron oxide (Fe_2O_3) could be used to determine sulfate durability for Class F ashes. It is stated that ettringite can be iron-rich or iron-poor, and the iron-rich ettringite particles will not cause expansion (Kalousek & Benton, 1970). Iron found in fly ash may be related to the type of ettringite, and the theory stated that an increase in iron oxide reduced sulfate expansion (Watt & Thorne, 1965-66). Later research conducted at The University of Texas at Austin found no linear relationship between iron oxide content and sulfate resistance as proposed (Carrasquillo & Tikalsky, 1992).

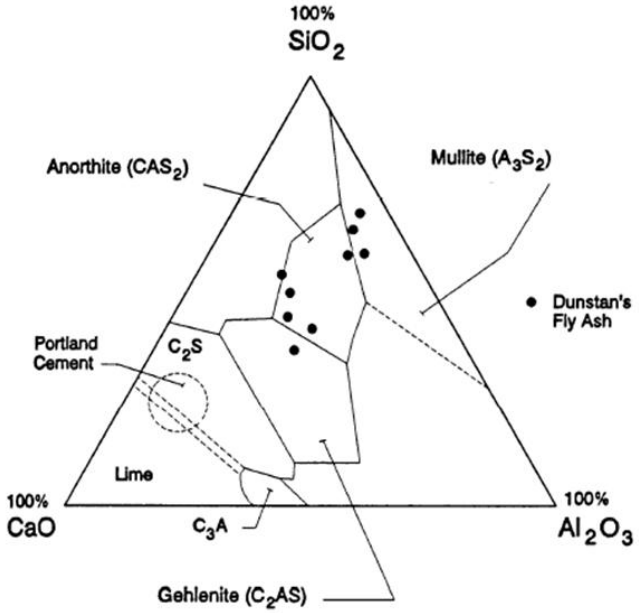

Figure 7: CaO-SiO_2-Al_2O_3 Ternary Diagram (Day, 2000)

Dunstan proposed a resistance factor that related calcium and iron content. Sulfate resistance is proportional to calcium oxide content greater than 5% and inversely related to the amount of iron oxide. This R-factor is found by the following Equation 6 where C is CaO and F is Fe_2O_3 in percentages.

$$R = (C - 5)/F \qquad (6)$$

If the R value is less than 1.5, the fly ash had good resistance to sulfate attack, but if the value exceeds 3.0, the ash has poor resistance (Dunstan, 1980).

Critics say that this R-factor does not account for the sources of ettringite formation. Manz proposed a revised model that included fly ash reactive crystalline components. This model was based on two parameters, the calcium aluminate potential (CAP) and the calculated sulfate equivalent (CSE). CAP is calculated using bulk oxide contents identified in XRF analysis and subtracting inert crystalline compounds identified

through XRD and Rietveld analysis. The CAP equation is presented below in Equation 7 and CSE formula in Equation 8 (Bhatty & Taylor, 2006).

$$CAP = (C^* + A^* + F^*) / S^* \quad (7)$$

C* = Bulk CaO – Reactive crystalline CaO (lime, anhydrite, C_2S) – inert crystalline CaO (melillite, merwinite)

A* = Bulk Al2O3 – inert Al_2O_3 (mullite)

F* = Bulk Fe2O3 – inert crystalline Fe_2O_3 (hematite, spinel)

S* = Bulk SiO2 – inert crystalline SiO_2 (quartz, mullite)

$$CSE = \text{Anhydrite} + 1.7\$ \quad (8)$$

This relationship is plotted on an x-y graph shown in Figure 8. As the CSE parameter increases, the fly ash becomes more sulfate resistant. The problem with this proposed model is that it neglects the combined role of cement and fly ash reaction products.

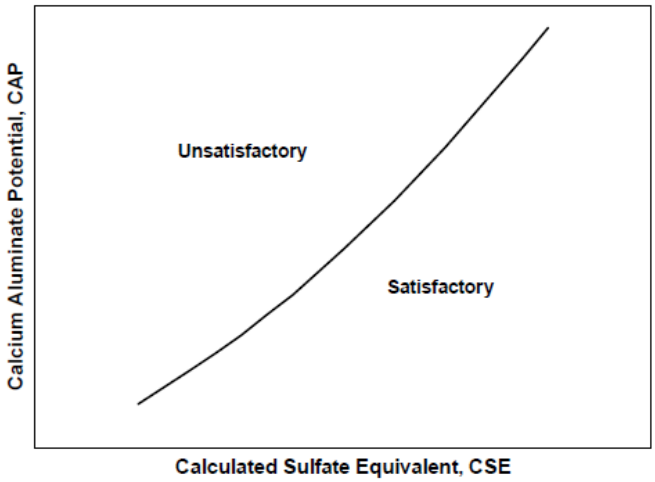

Figure 8: Relationship between CAP and CSE and Sulfate Resistance (Bhatty & Taylor, 2006)

Another proposed model based on Dunstan's original model was created by Hartmann and Mangotich. This model introduced an oxide durability factor (ODF) to predict sulfate resistance. See Equation 9 for this calculation (Bhatty & Taylor, 2006). As the ODF value decreases, the sulfate resistance of the concrete increases.

$$\text{ODF} = (\text{Bulk CaO in fly ash and cement}) * \text{Free lime} / (\text{Bulk } SiO_2 \text{ in fly ash and cement}) + (\text{Bulk } Al_2O_3 \text{ in fly ash and cement}) + (\text{Bulk } Fe_2O_3 \text{ in fly ash and cement}) \quad (9)$$

This equation was important because it took into consideration the composition of the fly ash and of the cement since both constituents add reactive components to the concrete. However, the cement and fly ash hydration products are more important than their individual contributions. This equation also emphasizes the importance of alumina in the concrete.

The three proposed models highlighted the role of crystalline phases, but later research proposed the glassy phase as a more important factor for sulfate resistance. Fly ashes that have high-calcium glass discharge calcium aluminates that when mixed with sulfates form expansive products. Through a study conducted at the University of Texas at Austin, the composition of the glassy portion was important in determining the sulfate resistance of fly ash. The type of cement used, presence of entrained air, slump and different curing length had little effects on the sulfate resistance of fly ash mixtures. It was concluded that even using sulfate-resistant cement, with little or no C_3A, did not affect sulfate resistance if a poor fly ash was used in the concrete mix. It was recommended to use fly ash in a sulfate environment if calcium oxide is less than 10% but not acceptable for use if calcium oxide is greater than 25%. For those ashes whose calcium oxide falls within this range, it is recommended to perform testing and observe

the sulfate resistance in addition to noting where the ash falls on the ternary diagram shown in Figure 7 (Tikalsky & Carrasquillo, 1993). The effects of calcium oxide and sulfate resistance were tested by Tikalsky, but he did not observe the trend of poor resistance with increasing calcium content for all ashes studied. However, he still did not advocate the use of high calcium ashes in sulfate environments due to their potential to expand (Tikalsky P. J., 1989).

As for the effect of fly ash on delayed ettringite formation, it is believed that the alumina oxide (Al_2O_3) content is the contributing factor because of its role in ettringite stability. Class F and C ashes can be used to control DEF; however, more Class C replacement is needed to control the expansion (Folliard K. J., 2006).

There is still not a full understanding of the mechanism(s) contributing to sulfate resistance. A general acceptance that Class F ashes are suitable and Class C are not suitable tends to exist today, but this is not entirely accurate, and the need to safely use Class C fly ash in a sulfate environment will become more critical as coal sources change and fly ashes tend to increase in CaO content.

Chapter 3: Testing Methods

This chapter describes the various test methods and equipment used to characterize fly ash, evaluate microstructure of paste and mortar, and evaluate other key aspects linked to fly ash and sulfate attack.

3.1 X-RAY FLUORESCENCE

All of the fly ashes were analyzed with x-ray fluorescence (XRF) to evaluate the bulk oxide contents. High energy x-rays excite the fly ash, which emit fluorescent, or secondary, x-rays. These secondary x-rays are used to qualitatively and quantitatively identify the oxides in the sample. XRF can be used to determine amorphous content by subtracting the crystalline amount by the total bulk oxide amount found with XRF.

3.2 PARTICLE SIZE

Particle size in this thesis was measured by two different methods: laser diffraction and No. 325 sieving. A laser diffraction machine uses a laser to plot the particle size distribution of a fly ash, or any material. An electron in the electron cloud removes light from the light beam due to interaction of the light beam and the material and then re-emits that light causing light scattering. This scattering is due to reflection, refraction and diffraction of the light due to this interaction (Webb, 2000). The light can also be absorbed. The machine analyzes the interaction of the material particles and the light based on the diffraction pattern and matches the analyzed pattern to a mathematically calculated model. This mathematical model is estimated using the Mie or Fraunhofer theory. The diffraction pattern is created due to the beam shot through the particles suspended in a dispersive agent and being diffracted, deviation due to a light ray traveling close to a particle. A Fourier transform lens focuses the diffracted light beam to convert incident energy into electric signals. The angle between the incident and

diffracted light is related to the particle size (Cyr & Tagnit-Hamou, 2001). The dispersive agent recommended by NIST is isopropyl alcohol due to its high viscosity and increased reproducibility (Ferraris, Bullard, & Hackley). The broader the particle size distribution, the greater the packing density of the mixture and resulting greater workability.

Particle size distribution was also performed with a No. 325 wet sieve analysis as required and outlined in ASTM C 618 and C 311/430 respectively. The code requires that no more than 34% of the material can be retained on the No. 325 sieve. Coarser materials contain more unburnt carbon, affecting LOI, and larger particles affect the material's reactivity. The coarser the fly ash, the lower the pozzolanic activity index (PAI). As particle size increases, the amount of quartz (crystalline SiO_2) increases and calcium containing products decreases. As the particle size increases, the number of spherical particles decreased. Most crystalline material was found to be larger than No. 325 sieve (Joshi, Natt, Day, & Tillerman, 1985).

3.3 X-RAY DIFFRACTION

X-ray diffraction (XRD) qualitatively identifies the crystalline phases of the fly ash sample. In this technique, electrons hit a solid sample and x-rays are emitted. When the x-rays hit a crystal structure, some x-rays diffract based on this crystal structure but other x-rays penetrate further into the sample until colliding into a crystal. The machine reads all of the angles of diffracted, scattered x-rays and their intensities to create a pattern. These patterns are plotted, creating a diffractogram as seen in Figure 9 relating diffracted intensity to diffraction angle.

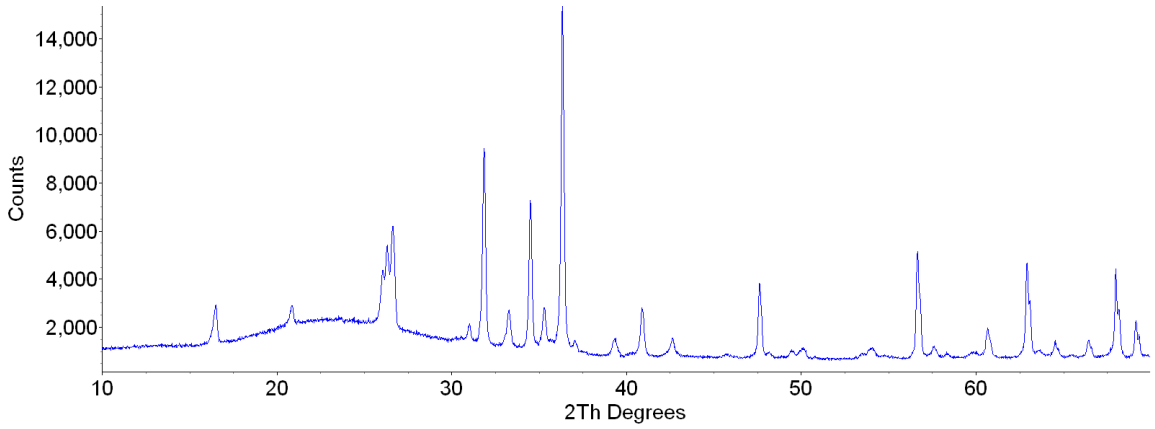

Figure 9: XRD Pattern of a Fly Ash

With a high intensity scan, major and minor crystalline phases can be identified. A major match involves the match of 3 peaks of that phase. For a very detailed analysis, a quantitative analysis called Rietveld QXRD (RQXRD) is possible. Rietveld uses an internal standard, zincite in this project, with a computer program called Topas manufactured by Bruker-AXS. This program uses a curve-fitting algorithm to match crystal structures to the peaks identified in the XRD scan. Refining each crystal structure enables the user to more accurately fit the peak and/or intensities identified. During sample preparation, the fly ash powder is packed with a flat, glass surface. This alters the orientation of the crystals but is corrected with refining the preferred orientation, the tendency for crystals to be oriented in a specific way. Refining is continued until the residual is small. R values less than 10 were deemed acceptable in this analysis. The output crystalline percentages were then adjusted to the known amount of added internal standard, 10% was used for these analyses, and values were back calculated to remove this known addition. It is these values that will be presented in the results of this thesis. The amount of amorphous phases can also be calculated by subtracting the total crystalline percentage without the internal standard from 100%.

Zincite, ZnO, was chosen as the internal standard based on previous research. One study examining different internal standards compared rutile, zincite, and alumina. Internal standard selection should be based on grain size due to smaller sizes obtaining more accurate intensities due to sufficient particle diffraction. Based on a 5-phase mixture, rutile had the lowest weighted relative error at 5.3%. Zincite and alumina had almost double the error at 10% and 11% respectively (Winburn, Lerach, Jarabek, Widsom, Grier, & McCarthy, 2000). In another test, rutile was found to have a large refined March-Dollase coefficient, which deals with preferred orientation and is a problematic issue for using Rietveld for amorphous content analysis (De La Torre, Bruque, & Arand, 2001). A third research project compared alumina and zincite and found alumina was a better choice for cement Rietveld analysis (Wei, Yao, & Wang, 2012). Rutile, zincite, and alumina are all suitable choices as an internal standard; however due to the desire to use Rietveld to identify the total amorphous content, rutile was deemed an unsuitable choice. Due to the significant cost increase of alumina over zincite, zincite was deemed the most cost-effective internal standard for this project.

3.4 SCANNING ELECTRON MICROSCOPY

To identify the composition of the amorphous phases of the fly ashes, samples were analyzed with a scanning electron microscope (SEM). This machine employs an electron beam to penetrate about 1 μm deep into a sample. This beam focuses on a point and detectors read signals and convert them into intensities on the attached computer to create an image.

One image of interest is the secondary electron signal. These signals produce information about the surface topography. These are created due to a beam hitting valence electrons, which resultantly are emitted from the atom. These valence electrons

are attracted to a detector, which produces a signal proportional to the number of electrons it has attracted (Chancey, 2008). See Figure 10 for a secondary electron image.

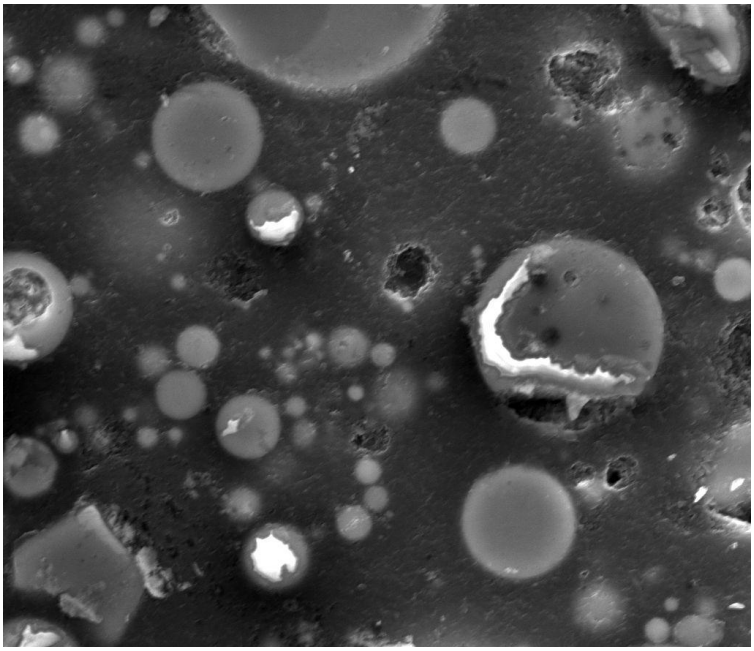

Figure 10: Secondary Electron Image of Fly Ash

Another image of interest is the backscattered electron image. This image is created due to electrons from the electron beam being reflected from the specimen. A detector identifies the amount of electrons reflected. As the atomic number increases, the more reflected electrons present. Therefore, brighter spots in an image mean a higher atomic number than the darker spots. See Figure 11 for a backscattered electron image.

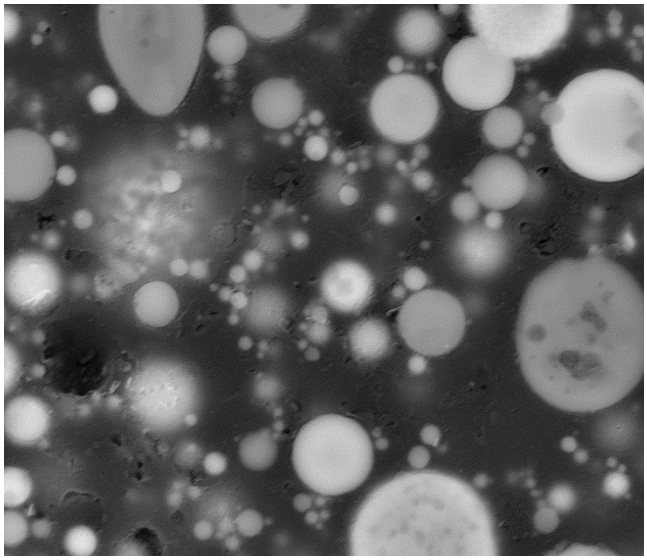

Figure 11: Backscattered Electron Image of Fly Ash

An energy-dispersive x-ray analyzer (EDXA) was used to point count amorphous particles. This was performed in the computer program Espirit. As the beam hits the specimen surface, x-rays are emitted that are characteristic of the specimen's elemental composition. Therefore, this technique is used to identify the elemental make-up of the amorphous particles. As mentioned in the literature review, the amorphous particles are the spherical particles of 1-5 μm in diameter. These amorphous particles were identified by measuring circular particles with a built-in measuring tool. Only those particles 1-5 μm in diameter were selected for the point analysis. Analysis of 150-200 amorphous particles constituted a comprehensive analysis of the fly ash specimen. These particles were quantitatively investigated for eight elements: calcium, aluminum, iron, sodium, potassium, silicon, oxygen, and carbon. These elements were converted into oxides, and each point was plotted on a ternary diagram for further analysis. For more information on ternary diagrams, refer to the literature review background and Section 5.3.2 for these results.

3.5 REACTIVITY

A patent was issued to Dodson in 1980 for a simple test to identify reactive fly ashes. This test was initially created to identify early strength characteristics of fly ashes, but there appears to be a correlation between high early strength and poor sulfate resistance found in TxDOT Project 4889. This test involves the mixing fly ash with tartaric acid solution, boiling the solution, and cooling covered for 3 hours. After this waiting period, the height of the mixture is measured. If the product exceeds 20 mm in height, the fly ash is considered reactive (Dodson & Roberts, 1980). See Figure 12 for differences in height of the gel product formed as a result of this procedure.

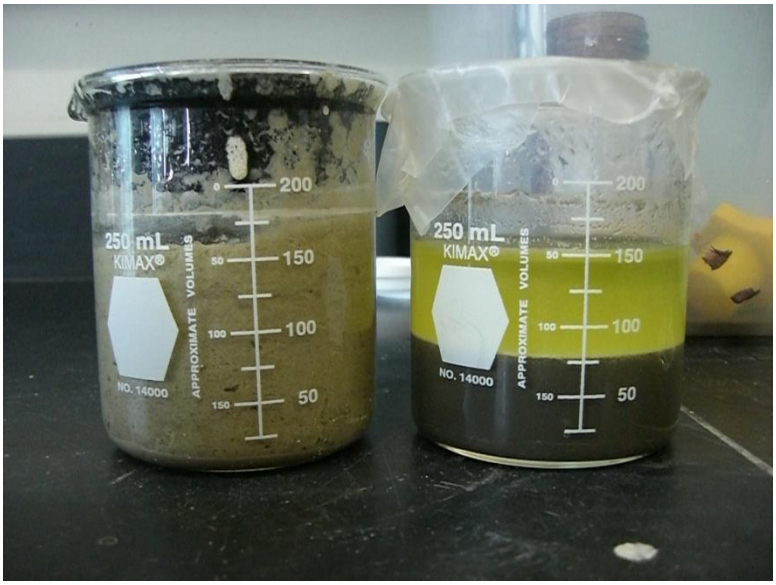

Figure 12: Reactivity Gel Product

3.6 CALORIMETRY

Heat of hydration is the heat produced from the reaction of Portland cement and water. This heat is greatly influenced by C_3A and C_3S content of the cement, but also the

w/c ratio, fineness of the particles, and the curing temperature. There are five stages of hydration, shown in Figure 13.

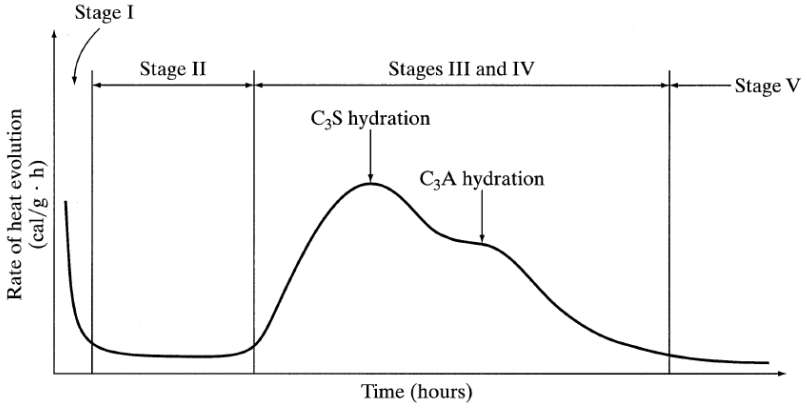

Figure 13: Portland Cement Hydration (Mindess & Young, 1981)

Stage I is the dissolution of solids phase where water is introduced into the mixture. Stage II is the induction period and involves the slow dissolution of C_3S. The acceleration period occurs in Stage III where CH crystallizes and C-S-H forms on the surface of grains. The mixture begins to harden here. This C-S-H layer thickens and controls the rate of reaction in Stage IV. Hydration here is controlled by diffusion. In Stage V, hydration products continue to fill empty space and continue until full hydration. These stages hold true with the introduction of SCMs, especially fly ash, in the mixture.

Heat of hydration curves are generated by the use of an isothermal calorimeter. This thesis aimed to plot the heat of hydration of all fly ash studied with different cement replacement percentages and at different temperatures, following protocol outlined in ASTM C1679, using an isothermal calorimeter ADIACAL TC produced by Grace. Also, by removing the mixtures at predetermined times from the calorimeter, stopping

hydration, and scanning in XRD, it is possible to observe crystalline phase formation as a product of hydration time. For those samples identifying hydration products, a scan range of 5° to 70° 2θ degrees, step 0.02, and 4 sec dwell was employed for an average scan of 3.5 hours. This timed calorimetry was performed on a select number of fly ashes to observe microstructural development.

The isothermal calorimetry curves were used to observe the heat flow during hydration, the cumulative heat release, and the activation energy. By observing the heat flow graphs, like that shown in Figure 13, one can compare the hydration differences between the fly ashes, between different replacement percentages, and between the different mixing temperatures. Identifying the length of the dormant period, the time and height of C_3A and C_3S peaks, and the slopes of the acceleration and deceleration time will allow for a quantitative comparison of all the mixtures. The cumulative heat release is another interesting plot. It is calculated by Simpson's Rule of integration of the heat flow curve. This plot shows the strength development of the mixture. The third interesting heat of hydration parameter is activation energy, the energy required to start a reaction. This calculation is based on Arrhenius equation, shown in Equation 10.

$$k = Ae^{-E_a/RT} \tag{10}$$

The variable k is the reaction rate coefficient, A the proportionality constant, Ea the activation energy, R the ideal gas constant 8.314 J/mol-K, and T the temperature in Kelvin. The constant Ea is often called the "apparent" activation energy because Ea is a representative average over a range of temperatures. Activation energy is a function of temperature and the degree of hydration. In general, Ea decreases with the increase of Class F replacement. Ea increases with increasing Class C replacement of a low C_3A,

low equivalent alkali (Na_2O_e) cement but does not change when Class C replaces a high C_3A, high N_a2O_e cement. In a study looking at the fly ash oxide values, CaO content was the only oxide found to correlate with activation energy (Riding, Poole, Folliard, Juenger, & Schindler, 2011).

Through previous research, it is known that fly ash with higher CaO and C_3A content exhibit more heat release early in the hydration process and also show poor sulfate resistance. The fly ash that forms monosulfate rather than ettringite in the early hydration stages show poor sulfate resistance as well due to the transformation of monosulfate to ettringite and associated cracking. The higher calcium ashes are more reactive. The fly ashes that delay hydration, or an elongated Stage II, show improved sulfate resistance (Dhole, 2008).

3.7 SULFATE IMMERSION

The testing to observe the sulfate exposure on hydration products was based on previous collaborative work performed at the University of New Brunswick with Rajaram Dhole and Dr. Michael Thomas (Dhole, 2008). Fly ash was mixed with calcium hydroxide and an alkaline solution to create a paste with a w/c of 0.45. These pastes were cured over water at 38 °C for 28 days. At the end of curing, samples were crushed and a small amount was run in XRD to identify hydration products and the remainder was immersed in sodium and calcium sulfate solutions for 90 days. At the end of sulfate immersion, the samples were run in XRD again to re-identify and re-quantify hydration products. An investigation in the impact of the sulfate solution on the hydration products was conducted and linked to the sulfate resistance of the fly ashes.

Mehta's research proposed that the formation of hydration products at the time of sulfate immersion is the most important factor in determining sulfate resistance. If

monosulfate and C-A-H is formed initially, then these products will convert to ettringite over time and cause detrimental expansion. If ettringite formed initially, it would remain as a stable product and the mixture would exhibit good sulfate resistance. Mehta's work directly refuted Dunstan's R factor, outlined in Section 2.3.4, finding some ashes that failed according to Dunstan's equation but performed satisfactorily (Mehta, 1986). This observation that Class C ashes initially produced monosulfate was also observed in work performed by Tishmack. This was a result of more alumina and less SO_3 in the mixture (Tishmack, Olek, & Diamond, 1999).

Other work investigated the hydration product formation of high lime fly ashes. The Class C ashes formed calcium hydroxide from free lime and formed gypsum from anhydrite; however, calcium hydroxide and gypsum were converted into ettringite. This formation was due to the reactive glassy phases in the higher calcium ashes. The Class F ashes formed no ettringite but rather only gypsum from the anhydrite (Tokyay & Hubbard, 1992).

Chapter 4: Concrete Durability Results

4.1 INTRODUCTION

This chapter presents information about the selected materials used for this thesis. This chapter also presents the sulfate attack testing results conducted in a previous testing program at the University of Texas at Austin under TxDOT Project 0-4889.

4.2 MATERIALS

4.2.1 Fly Ash

Eighteen different fly ashes were used in this research. These fly ashes were selected based on completed sulfate attack testing results at UT-Austin and to obtain a wide variety of fly ashes used. The bulk oxide contents presented in Table 6 are based on testing performed by TxDOT Materials Lab in Cedar Park, Texas. The fly ash identification numbers were generated based on increasing calcium oxide content of the fly ashes under investigation due to the established relationship between calcium content and sulfate resistance.

Table 6: Fly Ashes Tested XRF Results

Fly Ash	Chemical Composition										
ID	SiO_2	Al_2O_3	Fe_2O_3	Sum of Oxides	CaO	MgO	SO_3	Na_2O	K_20	Na_2O_e	LOI
FA-1	53.8	29.5	4.6	87.9	1.1	0.7	0.1	0.4	2.2	1.9	1.8
FA-2	51.4	20.7	7.1	79.2	10.2	3.0	0.3	0.4	1.3	1.3	
FA-3	55.3	17.8	7.6	80.7	10.6	2.3	0.4	0.3	1.1	1.0	0.2
FA-4	51.6	22.8	3.8	78.2	11.9	2.0	0.5	0.2	0.8	0.7	1.1
FA-5	42.9	21.6	4.3	68.8	13.6	2.5	0.9	8.1	0.4	8.4	0.4
FA-6	49.9	18.1	7.8	75.8	14.5	2.8	0.7	0.3	0.9	0.9	0.4
FA-7	45.7	21.0	5.1	71.9	15.3	3.6	0.5	0.8	0.8	1.3	0.5
FA-8	34.9	19.2	5.5	59.6	17.2	3.5	2.8	8.4	0.4	8.6	0.7
FA-9	37.4	18.9	6.5	62.9	21.0	4.3	1.1	1.2	0.4	1.4	0.1
FA-10	33.9	19.3	6.4	59.5	22.9	4.6	0.8	1.2	0.3	1.4	0.2
FA-11	34.4	18.4	6.6	59.4	23.1	4.6	1.3	1.2	0.4	1.4	0.3
FA-12	33.5	19.4	6.0	58.9	24.3	5.4	1.1	1.2	0.3	1.4	
FA-13	31.8	18.6	6.4	56.8	24.7	4.4	2.4	1.1	0.3	1.3	0.3
FA-14	32.5	19.3	6.0	57.7	25.4	4.4	1.2	1.1	0.2	1.2	0.5
FA-15	30.8	19.5	5.6	56.0	25.5	4.5	1.4	1.2	0.3	1.4	0.3
FA-16	32.0	17.2	5.8	55.0	25.8	6.1	1.9	1.3	0.3	1.4	
FA-17	30.9	17.3	5.8	53.9	26.6	7.8	2.3	1.4	0.2	1.5	
FA-18	27.1	17.1	5.8	50.0	29.2	6.2	3.5	1.1	0.2	1.2	0.6

The fly ash background is as follows:

- FA-1: a low CaO, fly ashes this low are not available in Texas, imported from NC
- FA-2: from Texas
- FA-3: large quantities used in central Texas, from Texas
- FA-4: large quantities used in central Texas, from Texas
- FA-5: high-alkali from Michigan, produced from Powder River Basin Coal
- FA-6: from Texas
- FA-7: produced in Texas, low CaO fly ash previous to plant changes compared to FA-10
- FA-8: high-alkali from Southern Canada, produced from Powder River Basin Coal
- FA-9: produced in Texas
- FA-10: produced in Texas, higher CaO compared to FA-7 fly ash after plant changes that is currently produced
- FA-11: produced in Texas
- FA-12: from Arkansas
- FA-13: produced in Texas, used in precast concrete applications
- FA-14: from Texas
- FA-15: produced in Texas, most commonly used in central Texas
- FA-16: from Texas
- FA-17: from Oklahoma
- FA-18: known very poor sulfate resistance, produced in Texas

According to the criteria presented in Table 6, FA-1 thru FA-7, with the exception of FA-5, are Class F fly ashes. FA-5 has low calcium content for a Class C ash. The remaining ashes are Class C ashes based on the sum of oxide content.

See Appendix A for the relationship between oxide contents from the XRF results. Because of the debate about classifying ashes based on calcium oxide content, especially in Canada, these figures plot the oxides generated by XRF testing versus calcium oxide content.

4.2.2 Cement

The cement used in testing is Type I-II cement commonly used in central Texas. The XRF data for the cement is shown in Table 7. The Bogue values were calculated using ASTM C150-07 calculations.

Table 7: Cement XRF Values

Cement ID	C-1	C-2
SiO_2	18.95	20.04
Al_2O_3	5.35	4.49
Fe_2O_3	2.57	3.63
CaO	63.87	63.8
MgO	1.14	0.72
SO_3	3.27	3.02
Na_2O	0.113	0.037
K_2O	0.9	0.62
TiO_2	0.23	0.21
Mn_2O_3	0.049	0.096
P_2O_5	0.34	0.305
Cl	0.007	0.0063
ZnO	0.0108	0.007
Cr_2O_3	0.0122	0.0149
LOI	2.99	2.75
CO_2	1.806	1.759
C_3S	58	54
C_2S	11	16
C_3A	10	6
C_4AF	8	11

C-1 is high alkali cement whereas C-2 is lower alkali cement. C-1 was used in ASTM C1012 testing due to the requirement that cement C_3A content must be greater than 8%. C-2 was used in calorimetry and sulfate reactivity testing.

4.3 ASTM C1012

ASTM C1012 is a widely used test method to evaluate the external sulfate attack resistance of blended cements with SCMs. The test involves casting mortar bars, curing until they reach a specified strength, and placing the bars in a 5% sodium sulfate solution. Other sulfate solutions may be used; however, only the effect of sodium sulfate was studied in this research. Measurements are taken over a period of 18 months with a change of solution at each measurement. The expansion limits are listed in Table 8.

Table 8: Fly Ash Expansion Limits for ASTM C1012 (ASTM C 618, 2008)

Sulfate resistance of blended cement	Expansion (maximum) at 6 months, %	Expansion (maximum) at 12 months, %
Moderate	0.10	—
High*	0.05	0.10
Very high	—	0.05

*If expansion at 6 months is >0.05% but expansion at 12 months is <0.10%, blended cement is considered to have high sulfate resistance.

This project utilized past data from previous University of Texas projects to minimize the number of ASTM C1012 samples cast. See Table 9 for the summary showing which ashes were tested as part of this thesis. The previous work was conducted by Dr. Thano Drimalas and John Christopher Clement at the University of Texas at Austin.

Table 9: ASTM C1012 Testing Summary

	Previous Results	Needed
FA-1	x	
FA-2		x
FA-3		x
FA-4	x	
FA-5		x
FA-6	x	
FA-7		x
FA-8		x
FA-9	x	
FA-10		x
FA-11	x	
FA-12		
FA-13	x	
FA-14	x	
FA-15	x	
FA-16	x	
FA-17		
FA-18	x	

FA-12 and FA-17 were not analyzed by the ASTM C1012 testing due to delays in acquiring these samples.

4.4 RESULTS

In general, high calcium ash offered poor resistance to sulfate attack as compared to low calcium ashes. Compared to the control of 100% cement, most of the Class C ashes failed at comparable measurements. See Figure 14 for a representative Class F ash performance and Figure 15 for a representative Class C ash performance compared to the control mixture. The red x represents bar failure. Graphs presenting ASTM C1012 expansions for each fly ash are presented in Appendix B.

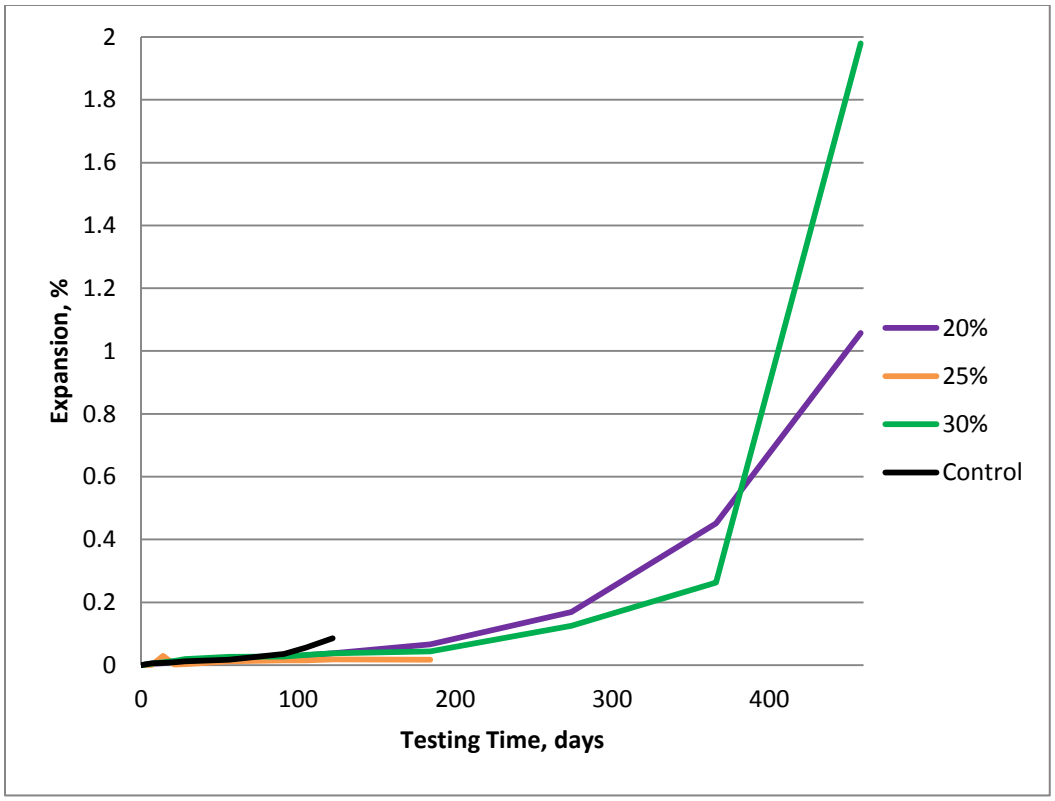

Figure 14: Typical Class F Fly Ash ASTM C1012 Data

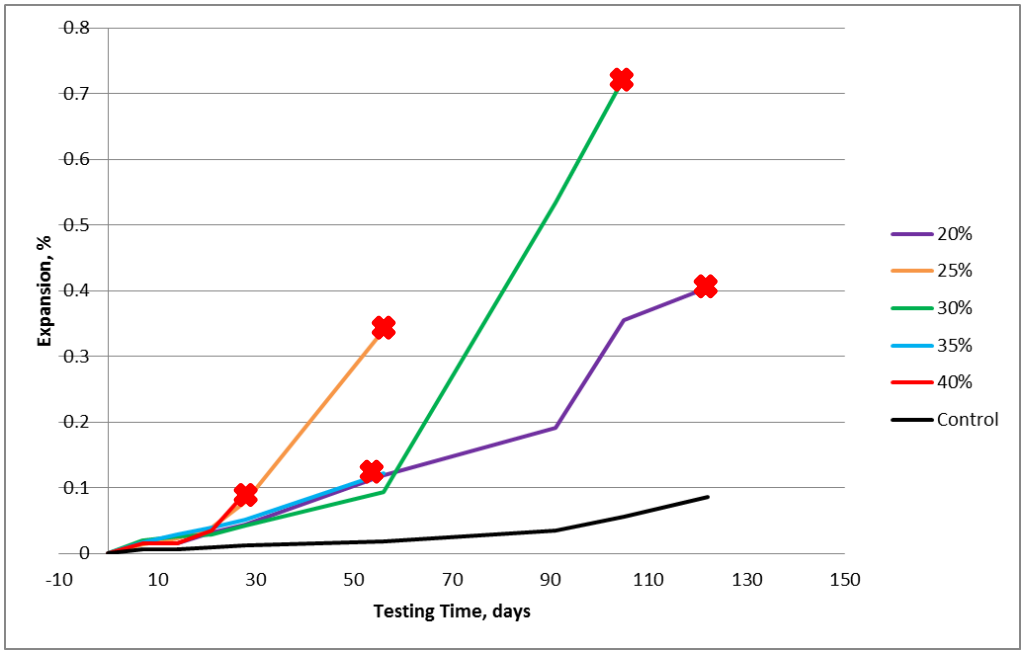

Figure 15: Typical Class C Fly Ash ASTM C1012 Data

Another way to observe this data was the time to failure. Failure occurs when the bars exceed 0.1% expansion at one year or when all of the bars became unreadable. See Figure 16 for the time to failure plot of all the fly ashes. Notice that for all replacement levels, the highest calcium Class C ashes failed much faster than the other ashes studied. High calcium fly ashes at 40% replacement had the highest linear correlation, meaning that as the calcium content increased, the expansion increased.

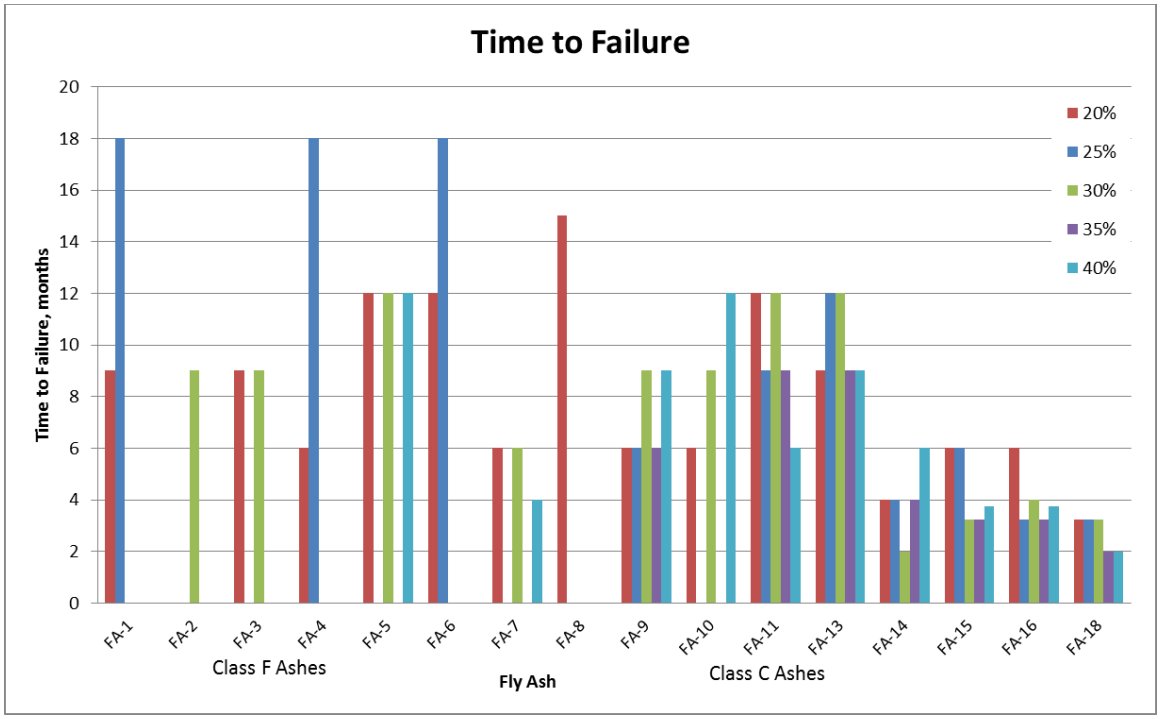

Figure 16: Time to Failure Data

The average time to failure values are plotted in Figure 17. It can be seen that the average time to failure for Class F ashes was much higher than that of the Class C ashes for the same replacement percentages. As the replacement percentage increased for a Class F ash, the sulfate resistance improved or the time to failure increased. There was a slight inverse relationship for time to failure and increasing Class C replacement percentage, meaning as replacement percentage increased, expansion increased. However, these correlations were very weak ones.

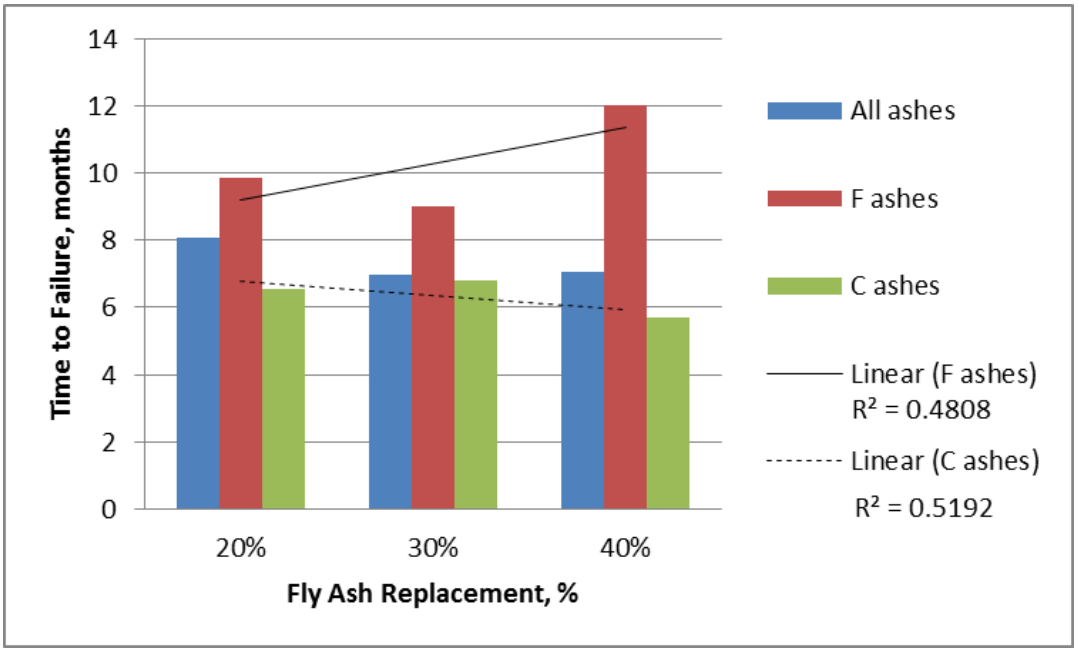

Figure 17: Average Time to Failure

4.5 Discussion

Previous work has showed that Class F ash improves the sulfate resistance of the mixture. In general, Class C ash had an increase in expansions compared to a control and had a decreased resistance to sulfate exposure, often resulting in complete sample degradation. The results shown in Figure 17 confirm this finding. The effect of the replacement percentage of Class F ashes on expansion varied with the type of cement used. As replacement with Class C ashes increased, there was also an increase in expansions (Stephens & Carrasquillo, 2000). In this work, as the replacement percentage of Class F ashes increased, the expansion decreased. The testing results from this thesis and previous testing displayed in Figure 17 agreed with the findings on replacement percentages.

Comparing the time to failure results with the XRF data for the ashes seen in Table 6, there were a few interesting items to note. When the calcium oxide content is

greater than 25%, the sulfate resistance was quite poor. FA-14 through FA-18 have calcium oxide content in excess of 25%, and as seen in Figure 16 these ashes had a significant decrease in time to failure compared to the other ashes.

In literature, if the alumina, iron, and silica oxide sum, which will be referred to as sum of oxides, is greater than 70% and the silicon dioxide value is greater than 40%, the fly ash will improve the sulfate resistance. The ashes with silicon dioxide values greater than 40%, which was all of the Class F ashes, had improved sulfate resistance. FA-6 had the longest average time to failure out of the ashes that have failed and interestingly the highest iron oxide content.

It is interesting to look at the performance of the two high alkali fly ashes, FA-5 and FA-8. These two ashes have the highest alkali content by a factor of around 6 compared to the other ashes. They are both classified as Class C ashes; however, FA-8 has greater calcium content. Refer to the XRF data presented in Table 10. As shown in Figure 18, all samples containing FA-5 failed at 12 months whereas most FA-8 specimens have not yet failed to date. FA-5 had significantly higher expansions at the 18 month reading for all replacement percentages. These two ashes have differing silica and sulfur oxide contents. This relationship will be analyzed more in depth in the later sections of this thesis.

Table 10: XRF Values for High Alkali Fly Ashes

Chemical Composition	Fly Ash	
	FA-5	FA-8
SiO_2	42.9	34.9
Al_2O_3	21.6	19.2
Fe_2O_3	4.3	5.5
Sum of Oxides	68.8	59.6
CaO	13.6	17.2
MgO	2.5	3.5
SO_3	0.9	2.8
Na_2O	8.1	8.4
K_20	0.4	0.4
Na_2O_e	8.4	8.6
LOI	0.4	0.7

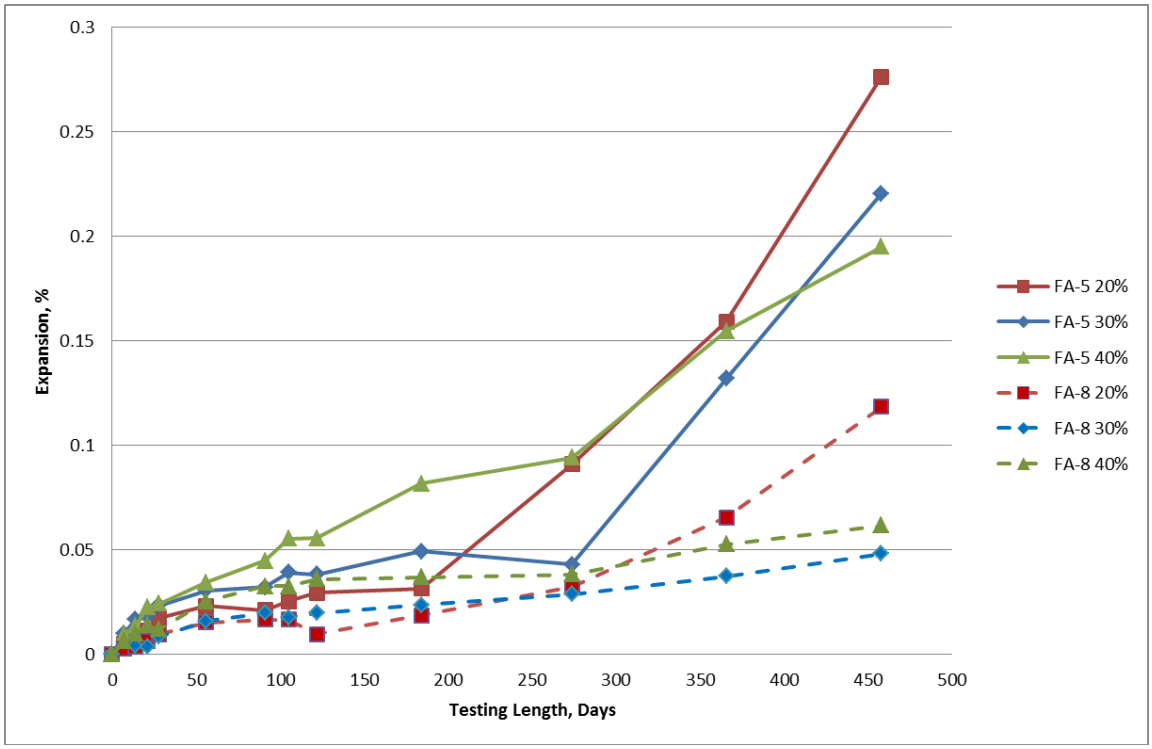

Figure 18: ASTM C1012 Results for the Two High-Alkali Fly Ashes

The following were trends found when analyzing the XRF data in Table 6 with expansion data at 15 weeks and 9 months plotted in Figure 19. The fly ashes are listed in

order of increasing CaO content. The 15 week data was used for comparison purposes due to most every specimen under investigation having a valid reading at this length of time. The 15 week expansion data may not be indicative of true sulfate expansion performance due to the possibility of large expansions later in the testing regime. Therefore, trends looking at expansions at 9 months were observed in the same manner as the 15 week expansion data. On this plot, the bars for each fly ash are 20%, 25%, 30%, 35%, and 40% fly ash replacement. Not all replacement percentages were tested for every fly ash. Also, if there is a 15 week but no 9 month reading, the bars failed before this reading.

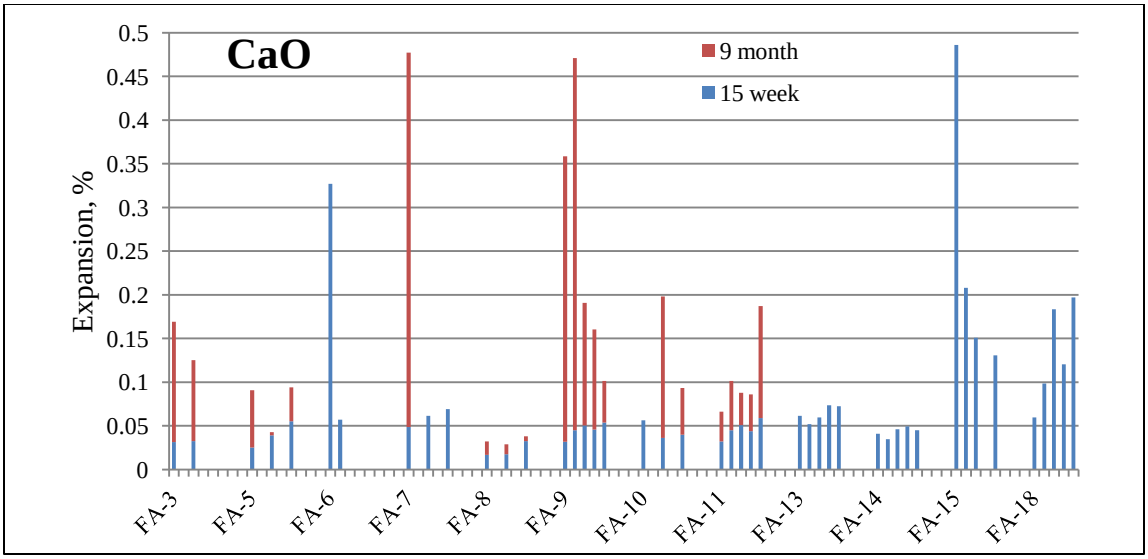

Figure 19: Comparison of XRF Calcium Oxide Contents with ASTM C1012 Expansions at 15 weeks and 9 months

FA-6, FA-15, and FA-18 had the largest 15 week expansions. The XRF data for these ashes is presented in Table 11. There seemed to be no similarities between all three ashes for any oxide value.

Table 11: XRF Data for FA-6, FA-15, and FA-18

Chemical Composition	Fly Ash		
	FA-6	FA-15	FA-18
SiO_2	49.9	30.8	27.1
Al_2O_3	18.1	19.5	17.1
Fe_2O_3	7.8	5.6	5.8
Sum of Oxides	75.8	56.0	50.0
CaO	14.5	25.5	29.2
MgO	2.8	4.5	6.2
SO_3	0.7	1.4	3.5
Na_2O	0.3	1.2	1.1
K_20	0.9	0.3	0.2
Na_2O_e	0.9	1.4	1.2
LOI	0.4	0.3	0.6

Plots comparing the expansions at 15 weeks and 9 months and XRF oxides were generated to see if any trends existed between oxides other than calcium, shown in Figure 19, and expansions. These plots are presented below in Figure 20 where the x-axis ashes have increasing oxide contents.

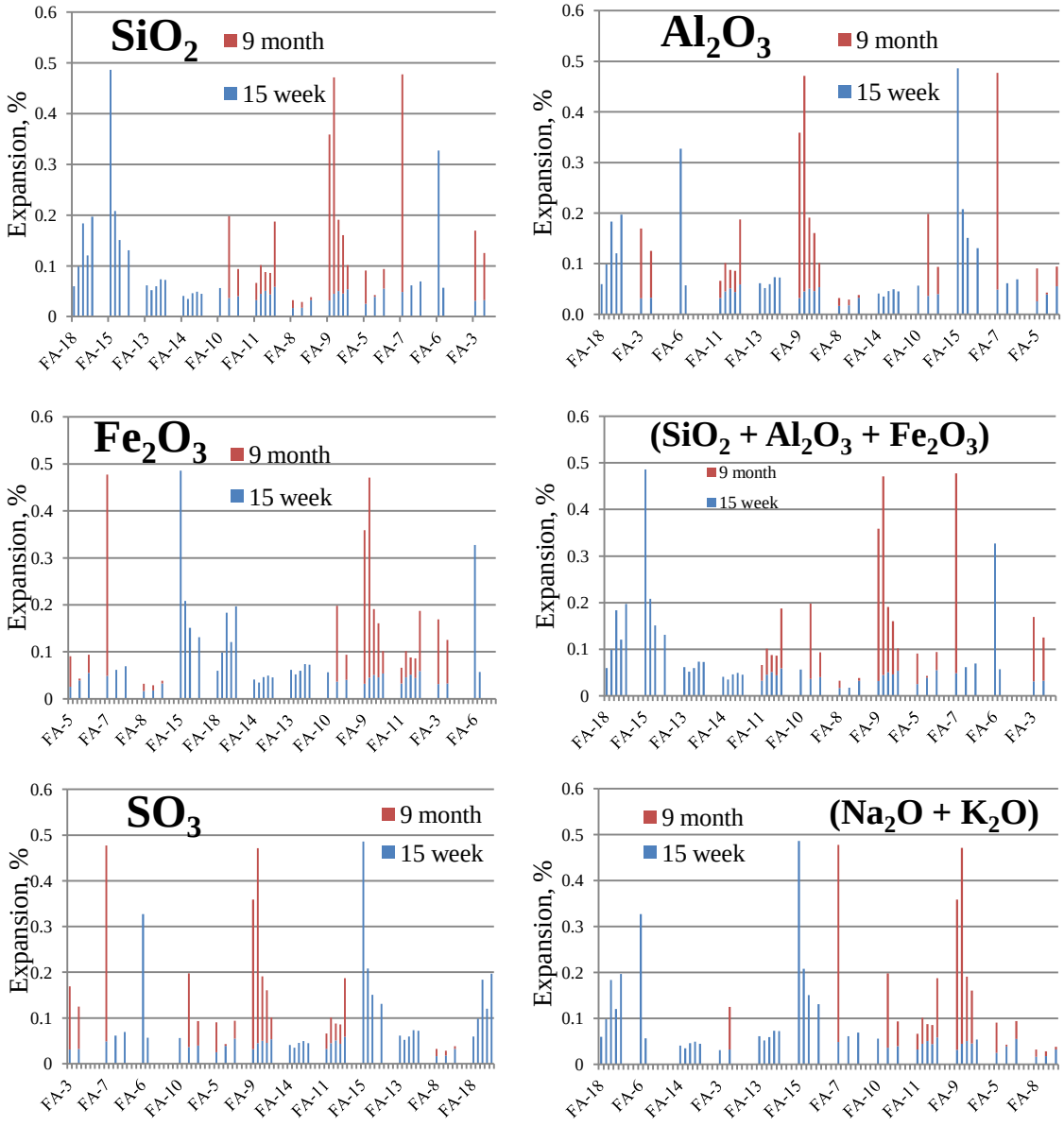

Figure 20: Comparisons between XRF Oxides and ASTM C1012 Expansion Data

When considering the general trends between 15 week and 9 month expansion and XRF data, the following relationships were observed:

- SiO_2: At 15 weeks, the lower the SiO_2 content, the greater the expansion. At longer testing periods, the lower SiO_2 contents had expansions large

enough to break all specimens and render a 6 month reading unattainable. The higher the SiO_2 content, the lower the expansions.

- Al_2O_3: There does not appear to be a trend with Al_2O_3 at any testing age.
- Fe_2O_3: The highest expansions had Fe_2O_3 content around 6.0%, the mean of the XRF values. These specimens had the largest 15 week expansions and unreadable bars at 9 months. The fly ashes with the lowest and highest Fe_2O_3 values had less expansion.
- Sum of oxides: The lower the sum of the oxides, the greater the expansion at 15 weeks. This correlated to the greatest expansions breaking all specimens at 9 months as well. For the ashes with largest sum of oxide values, the expansions were less. FA-6 is the only outlier to this conclusion.
- CaO: At 15 weeks, the fly ashes with the largest expansions had the highest CaO contents. This held true for the later testing ages. FA-6 is the only outlier again for this conclusion.
- SO_3: The higher the SO_3 content, the larger the expansions at 9 months. FA-6 is an outlier to this argument as well.
- $Na_2O + K_2O$: Note this is the sum of the alkalis, not Na_2O_e. The larger the sum of the alkalis, the less the expansions. FA-3 was an outlier to this finding.

4.6 SUMMARY

In general, the ASTM C1012 results presented correlate with findings from other research studies. The lower calcium ashes had improved sulfate resistance while the greater the calcium, the lower the sulfate resistance. Also, as Class C ash replacement

percentage increased, the expansion increased. No strong relationship was observed between Class F ash replacement and expansion.

Chapter 5: Fly Ash Characteristics

This chapter contains the testing results that describe the nature of the fly ash, including its composition, and fly ash testing independent of its reaction with cement during hydration studies.

5.1 Composition and Particle Size Distribution

5.1.1 Testing

5.1.1.1 XRF

The XRF data was performed at TxDOT's Materials Department in Cedar Park, Texas. Testing was performed on a 1 kW Wavelength Dispersive S4 Explorer manufactured by Bruker-AXS. TxDOT utilized fusion pellets as the preferred XRF method over pressed pellets to obtain a truly homogeneous sample removing the particle size effect and to obtain a higher accuracy output.

5.1.1.2 Particle Size Distribution

Particle size distribution was evaluated using laser diffraction and wet sieving through No. 325 sieve. For laser diffraction, the instrument used was a Spraytec by Malvern Instruments, Inc. with Spraytec software. The material refractive index was 1.5 with an imaginary index of 0.1. This machine uses degassed isopropyl alcohol as the dispersive agent. The fly ash is added to the dispersant, and a stirrer suspends the particles and shoots them through a small separation between 2 glass plates. A laser shoots through the glass plates and measures the diameters of the particles traveling through the plates. The diameter of 10%, 50%, and 90% are numerically reported in addition to a particle size distribution plot.

The wet sieving procedure was followed as outline in ASTM C430.

5.1.2 Results

5.1.2.1 XRF Results

The XRF results were presented in Section 4.2 in Table 6 and Table 7. The XRF values will continuously be used throughout the following results in an attempt to understand the presented results pertaining to sulfate attack.

5.1.2.2 Particle Size Distribution Results

Research conducted on fly ash particle size and sulfate resistance states that the coarser fly ash particles have increased expansion. In fine fly ash particles, the glass content increased over that of coarser particles so reactivity was enhanced. The finer particles also lead to a more dense cement matrix though due to the fine particles decreasing the pore volume. Due to the enhanced reactivity and reduced permeability, the finer fly ash particles had good sulfate resistance (Chindaprasirt, Homwuttiwong, & Sirivivatnanon, 2004). This research was conducted creating mortar containing only the fine fly ash particles, mortar containing only the medium particles, and mortar containing only the coarse particles. This work failed to characterize the effect of a wide particle size distribution range of fly ash particles in a mortar matrix on sulfate resistance. Another research project aimed to characterize different fly ash sizes by their mineralogy from XRD. As the size of the fly ash increased, the amount of calcium-bearing compounds decreased and the amount of quartz increased. McCarthy conducted a test that found the opposite results from fly ash size and mineralogy though. It was found that quartz did take part in the pozzolanic reaction and the amount of glass in all of the sizes was the same. Any material greater than 75 μm was found to be nonreactive (Joshi, Natt, Day, & Tillerman, 1985).

The particle size distributions for the fly ashes in this study are displayed in Figure 21. The S-shape curve shown for each fly ash shows a relatively even distribution of all sizes with no missing sizes present for all fly ashes. This range of sizes ensures good packing density to create less permeable concrete.

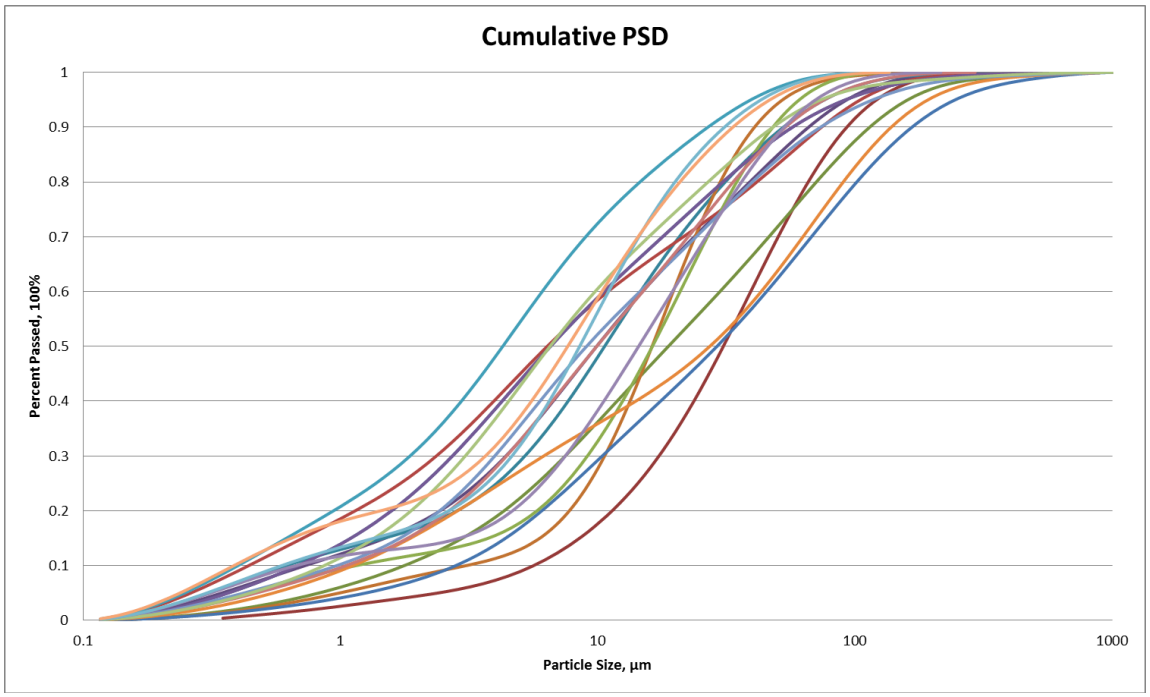

Figure 21: Fly Ash Particle Size Distribution

The particle size results are shown in Figure 22. In general, as the CaO content of the ashes increased, the particle size decreased. From the argument posed above that finer particles have better sulfate resistance due to their better packing density, the Class C ashes should have larger particle diameters. However, this result was not observed, suggesting that it is the mineralogy and reactivity of the fly ash that most affect sulfate resistance. It is proposed that these higher calcium ashes have poor sulfate resistance due to a finer, more reactive fly ash due to greater surface area of the particles. The research

performed by Joshi stating larger particles contain more quartz used in pozzolanic reactions was confirmed by the testing results (Joshi, Natt, Day, & Tillerman, 1985). The Class F ashes were comprised of larger particles and were more pozzolanic than the Class C ashes. Joshi also stated that particles greater than 75 µm were nonreactive. The lower calcium ashes had the greatest content of 75 µm and greater particles. If more of the ash is nonreactive, it will have better sulfate resistance due to sulfate ions attacking fewer reactive components. LOI is related to particle size. LOI is increased with increasing unburnt carbon content and is usually higher for Class F ashes. The greater the carbon content of the ash, the lower the density (ACI 232.R-96, 1996). This relationship was confirmed here, and there was a correlation between LOI and D(50).

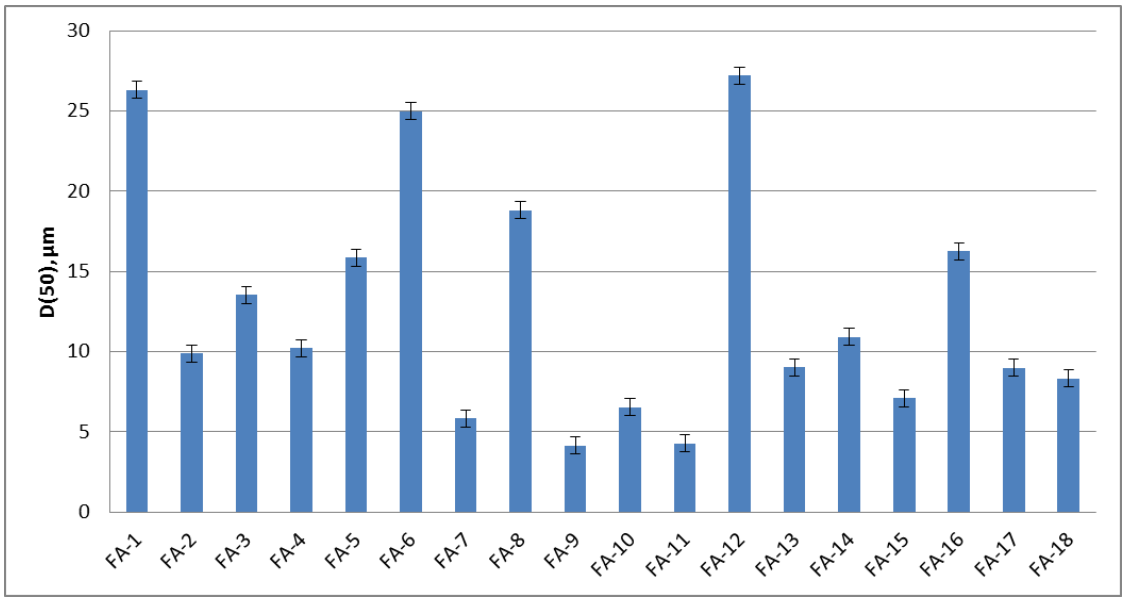

Figure 22: Average Particle Diameter by Mass

Out of the lower calcium ashes that performed well in sulfate environments, only FA-7 had a very short time to failure. This ash had the smallest particle size diameter compared to the other Class F ashes. FA-5 and FA-11 had similar time to failure data but

drastically different particle diameters. FA-2, FA-4, and FA-14 had similar particle diameters but very different sulfate expansions. FA-9 and FA-11 had the smallest average particle diameter; however, these ashes did not have the worst sulfate performance. The worse sulfate resistant ashes, FA-14 thru FA-18, had moderate average particle diameters.

The results from the No. 325 wet sieve standard are presented in Figure 23. All of the ashes passed the requirement that no more than 34% of the material can be retained on the No. 325 sieve.

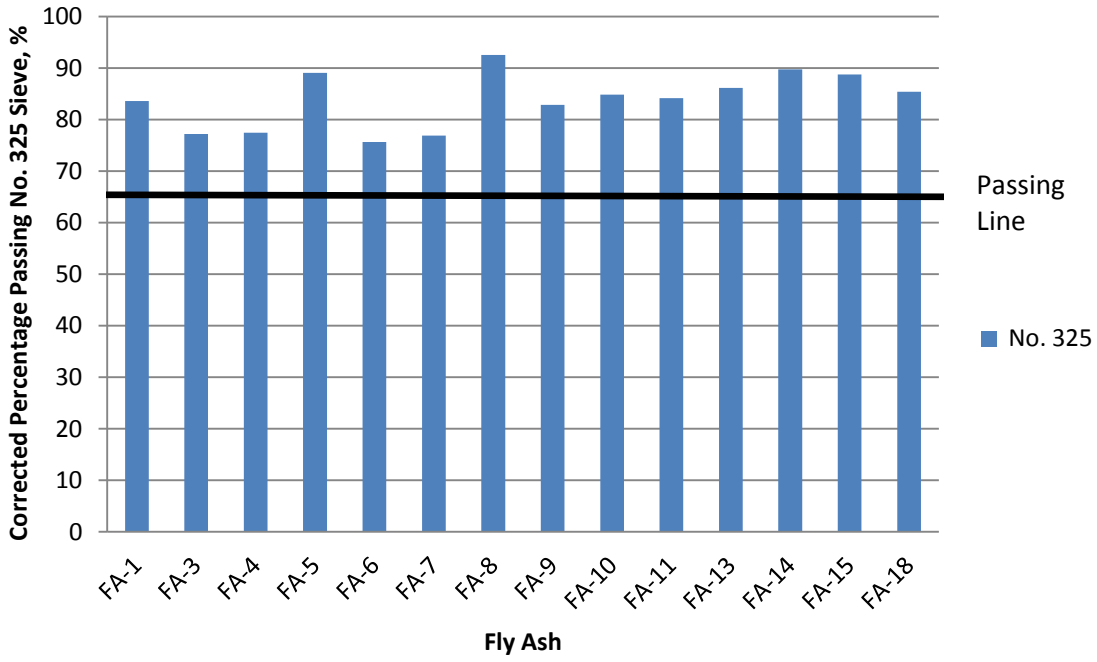

Figure 23: Fly Ash Fineness by the 45-µm (No. 325) Sieve

In general, there does not appear to be a definite correlation between particle size diameter and sulfate resistance. There was a general trend of increasing calcium content with decreasing average particle diameter and increasing expansion. No other oxide

values correlated to particle size diameter. As average particle size decreased, sulfate resistance decreased in this study.

5.2 Crystalline Phase Composition

5.2.1 Testing

The pure powder fly ash samples were examined through XRD analysis. Tests were run on Siemens D500 diffractometer with scan parameters of 10° to 70° 2θ degrees, step 0.02, and 8 sec dwell. The average scan time was 6.75 hours per fly ash powder sample for a high intensity scan. Rietveld was performed on all scans to identify the major crystalline phases. The Rietveld analysis was adjusted until the best fit regression analysis had a correlation coefficient value under 10.

5.2.2 Results

5.2.2.1 Reactive vs. Non-Reactive

Based on previous research stating which crystalline phases are reactive and those that are not, the phases identified through Rietveld analysis were categorized based on their reactivity. The following were considered reactive phases: anhydrite, merwinite, periclase, sodalite, lime, C_3A, C_4AF, C_2AS, C_2S, and arcanite. These results are presented in Figure 24. The lower calcium ashes had a greater percentage of non-reactive crystalline phases whereas the higher calcium ashes had a greater percentage of reactive crystalline phases. This correlates with the poor sulfate resistance of higher calcium ashes. Note the large percentage of reactive phases in FA-17 and FA-18.

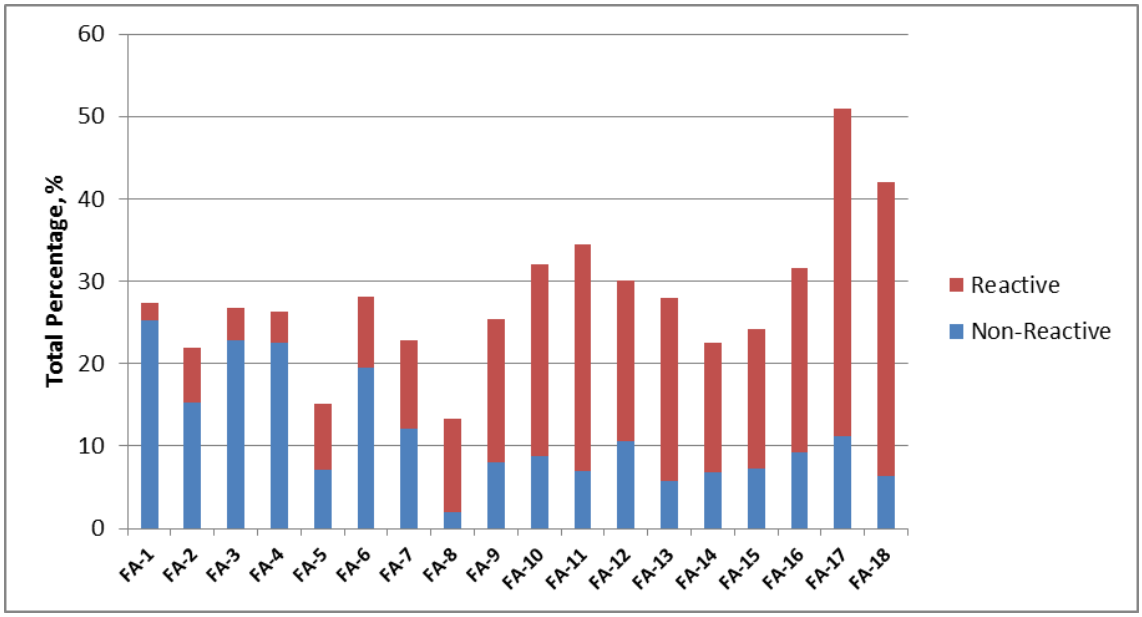

Figure 24: Breakup of Crystalline Phases of Power Fly Ash XRD

There were trends observed between XRF oxides and amount of reactive phases.

- SiO_2: The lower the SiO_2 content, the more reactive phases present. The observation also exists for the sum of the oxides. These two oxides are the opposite of the CaO results shown in Figure 24.
- Al_2O_3: The lower the Al_2O_3 content, the more reactive phases present. The exceptions are FA-3, FA-6, and FA-8.
- Fe_2O_3: The moderate Fe_2O_3 contents contain the most reactive phases.
- SO_3: The lower the SO_3 amounts, the more content of reactive phases. The exception is FA-8.
- Na_2O_e: The middle Na_2O_e values contain the most reactive phases. FA-17 and FA-18 are the exceptions.

5.2.2.2 Crystalline Phases

As for the main crystalline phases outlined in Section 2.3.3.1, a more in depth look follows. Anhydrite, a reactive phase involved in ettringite formation, was somewhat increased for the higher calcium ashes, but there was a large amount for FA-18. FA-18 had one of the shortest time to failures or the poorest sulfate resistance. In previous research, anhydrite was thought to be released at later stages of hydration to form ettringite. This phase is linked to DEF and resulting durability issues (Dhole, 2008). More mullite, a non-reactive phase, was found in Class F ashes. More merwinite was found in Class C ashes. This result matches what was expected and was related to MgO content. More quartz was observed in Class F ashes, supporting the PSD results that quartz was involved in the pozzolanic reaction and found in lower calcium ashes. See these relationships in Figure 25.

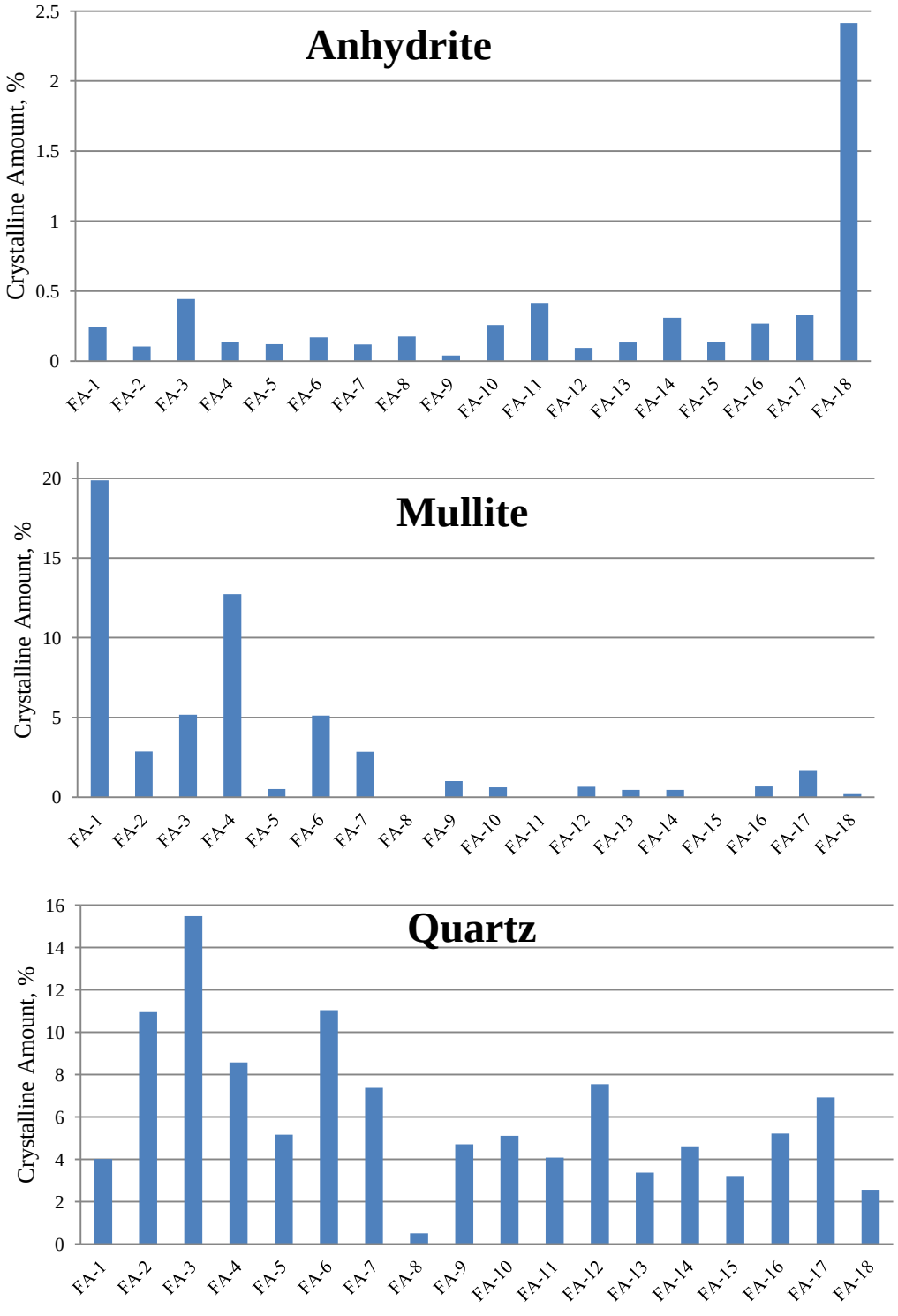

Figure 25: Select Crystalline Phase Amounts in Powder Fly Ash XRD

The C_3A content is a very reactive crystalline phase known to be related to sulfate performance. See the relationship with C_3A in Figure 26. The C_3A content increased with increasing calcium content which also correlated to poor sulfate performance. FA-16 had a very low percentage of C_3A but a very short time to failure. FA-16 had a very high percentage of periclase though, which is another reactive crystalline phase. FA-6 had a large amount of C_3A, which could explain the large expansion at 15 weeks noted previously.

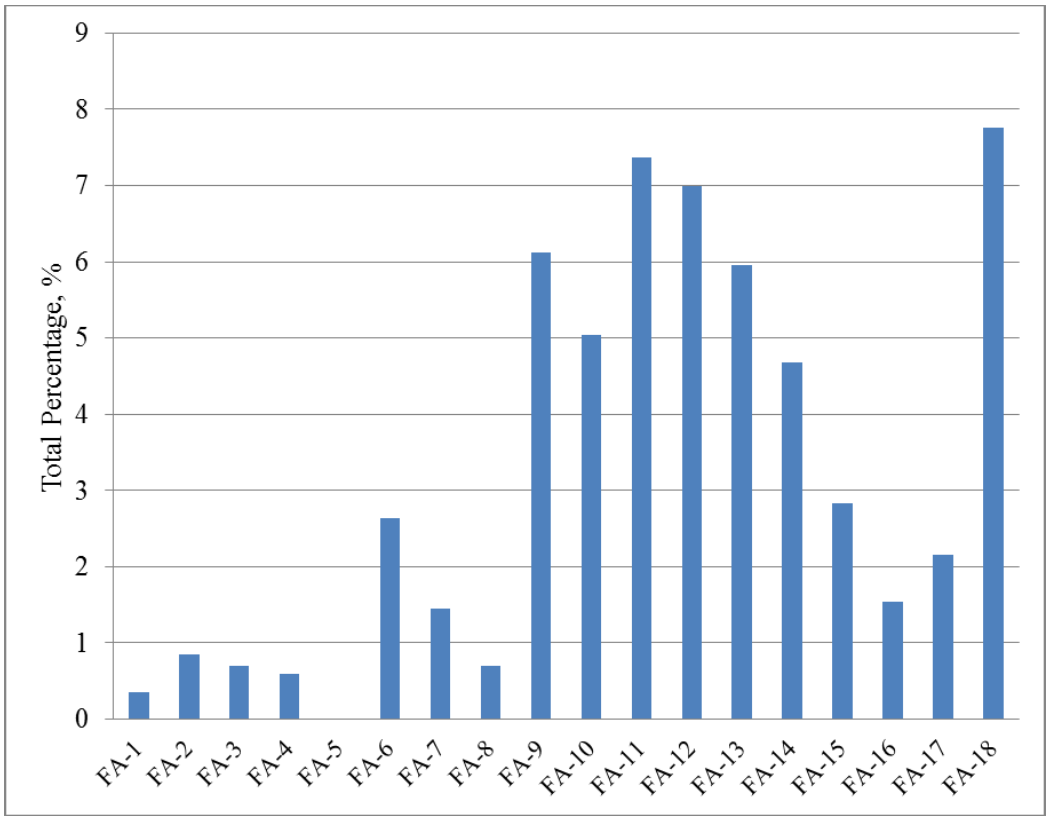

Figure 26: Crystalline C_3A Amount in Powder Fly Ash XRD

Dunstan also proposed that C_4AF along with C_3A contributed to the fly ashes sulfate resistance. C_4AF, also known as brownmillerite, forms ettringite when mixed

with water and calcium sulfates. The amount of C_4AF increased with increasing calcium content, which correlated to poor sulfate performance. See this relationship in Figure 27.

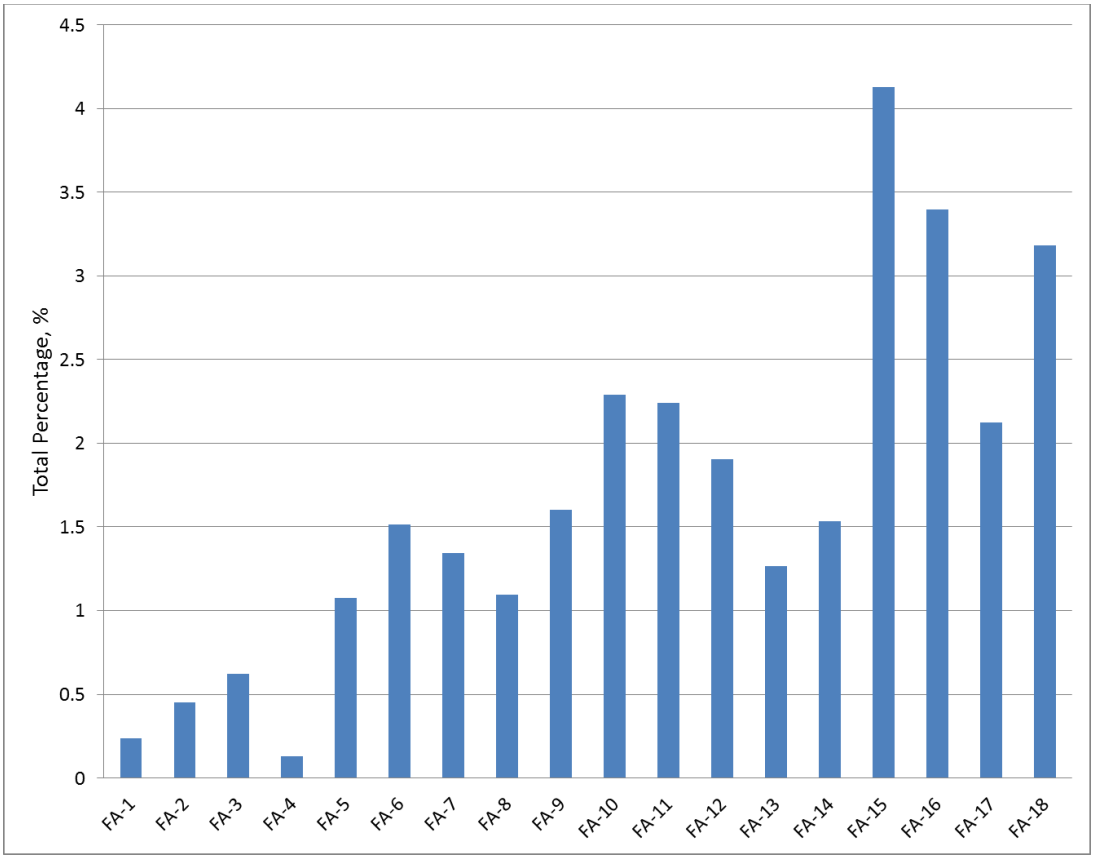

Figure 27: Crystalline Brownmillerite in Powder Fly Ash XRD

FA-11 and FA-13 had longer times to failure than FA-14 through FA-18. Analysis shows FA-11 and FA-13 had significantly lower amounts of periclase and lime, which are known reactive components. Periclase is limited to 5% due to potential soundness issues in fly ash. Periclase has a very small particle size, so if reactive periclase exists, it will hydrate early and not cause soundness issues (Tikalsky P. J., 1989). All of the fly ashes met this standard; however, the amount of periclase increased with increasing calcium content. See the periclase results in Figure 28.

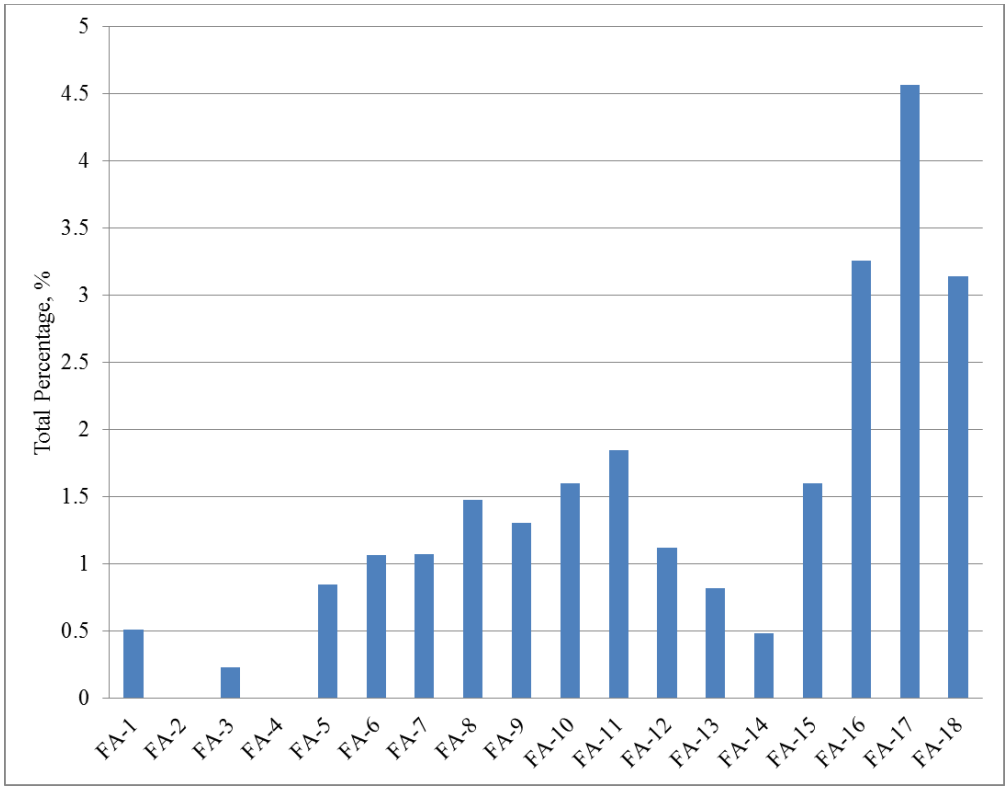

Figure 28: Crystalline Periclase Amount in Powder Fly Ash XRD

Lime is documented to be in all Class C ashes and some Class F ashes, which was observed in Figure 29. Lime is responsible for autoclave expansion, but depending on the form of the lime present it may or may not result in soundness issues. Free lime left over after the pozzolanic reaction is available for reaction with sulfates. The Class F lime percentages were mostly all consumed in this pozzolanic process and therefore not able to react with sulfates. Class C had a surplus of free lime, allowing for a reaction with sulfates and resulting poor sulfate performance.

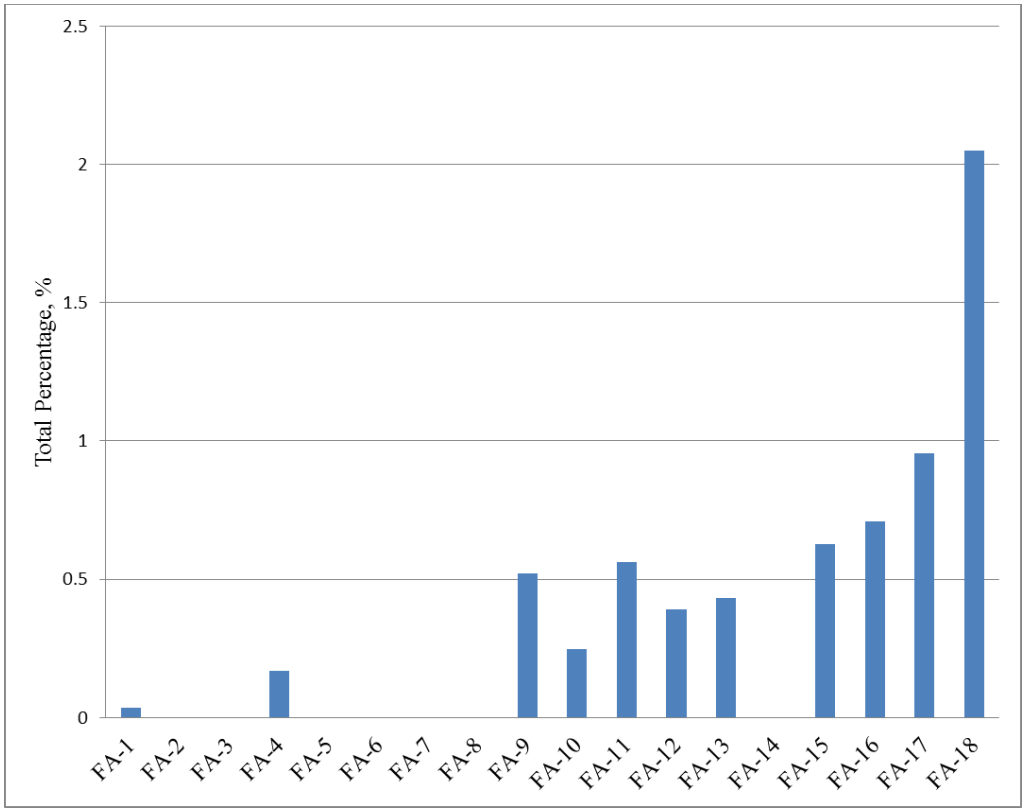

Figure 29: Crystalline Free Lime Amount in Powder Fly Ash XRD

5.2.2.3 Past Models

As for the model proposed by Dunstan, see Equation 6 in Section 2.3.4 for review, the results are presented in Figure 30. The correlation between the R-factor and sulfate resistance is indicated on the right side of the graph. As the calcium content of the ashes increased, the R-factor increased, which correlated to a decrease in sulfate resistance. FA-5 and FA-11had R-factors in the no change region, and these two ashes had similar time to failure performance. FA-6 did see reduced expansions when compared to FA-4 and FA-5. FA-12 thru FA-18 all had reduced resistance R-factors with FA-13 being right on the edge of the lower region. FA-13 had the longest time to failure of all of these higher calcium fly ashes. There did seem to be a correlation between the sulfate expansion data produced in this project and Dunstan's R-factor.

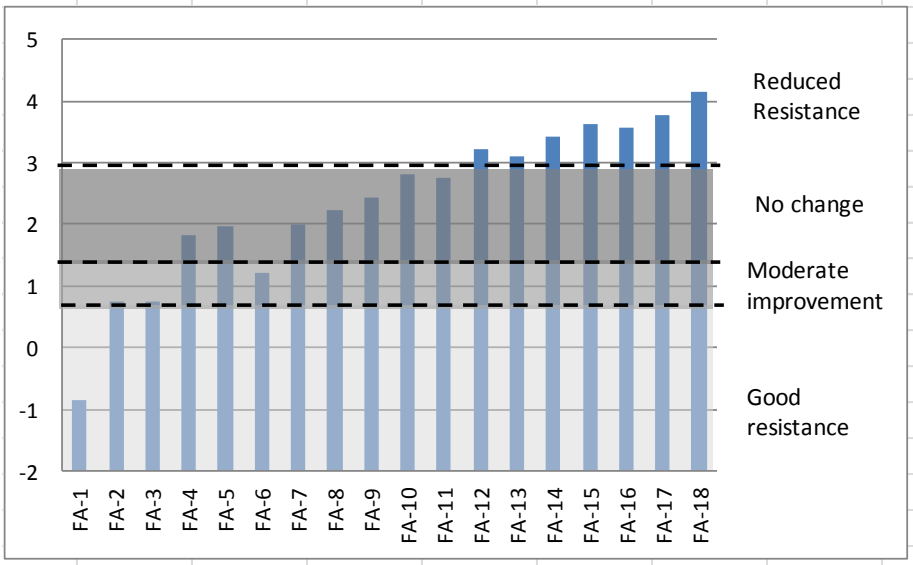

Figure 30: Dunstan's R-Factor

Manz also proposed a model correlating fly ash XRF oxide values and crystalline phases on sulfate resistance based on Dunstan's model. The results from these calculations are presented in Figure 31. The initial graph proposed plotted CSE on the x-axis and CAP on the y-axis, but this resulted in only FA-18 having acceptable performance, which is incorrect based on the time to failure and expansion data. However, when the regions of performance were flipped, the results were accurate with the expansions recorded. This flipped regions graph was presented below. The only incorrectly plotted point is FA-8, which has low expansions but would be deemed unsatisfactory with this revised model. Due to these findings, the model as proposed by Manz does not seem to accurately predict sulfate resistance, but the revised model with flipped regions accurately predicted performance with the observed expansions.

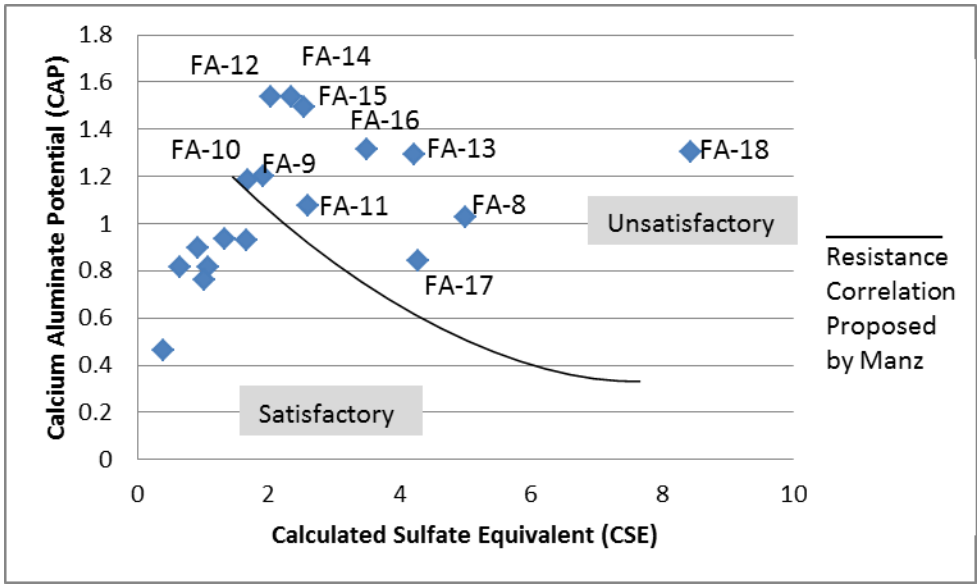

Figure 31: Manz Sulfate Resistance Parameters

Hartmann and Mangotich also presented a model for sulfate resistance based on Dunstan's original model. This calculation accounted for the composition of the fly ash and the cement used. The results from this model are presented in Figure 32, which also presents both cements used in this study. The blue bar is the fly ash mixed with C-1 and the red is missed with C-2. The cement lines refer to 100% cement. The lower ODF values correlate to greater sulfate resistance, but if the ODF is less than that of the cement then the sulfate resistance is improved. For the latter hypothesis, FA-18 was the only fly ash to decrease the sulfate resistance. From the time to failure data, FA-14 through FA-18 all had similar poor resistance, but the ODF values were significantly different for these ashes. The middle calcium ashes, FA-9 through FA-13, FA-1 and FA-4 should have had the greatest sulfate resistance based on the proposed ODF hypothesis. FA-1 and FA-4 had long times to failure, but FA-9 through FA-13 had moderate resistance. FA-6 had lower expansions than these moderate resistant ashes but a greater ODF. Due to these inconsistencies, this model did not correlate well with sulfate performance.

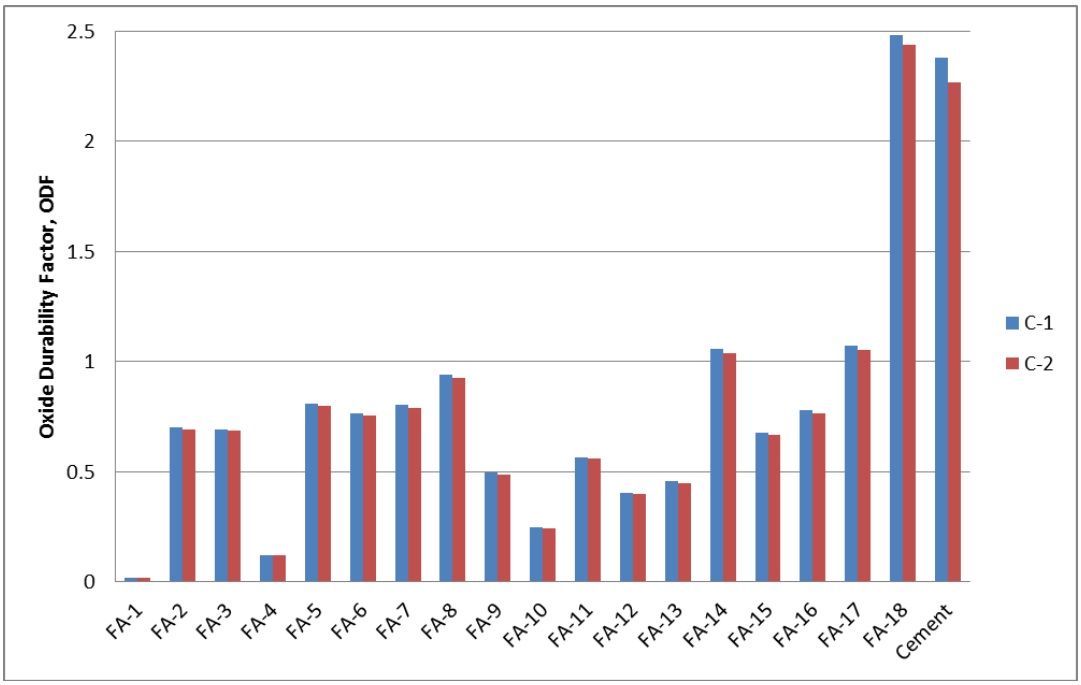

Figure 32: Hartmann and Mangotich Oxide Durability Factor

In general, the higher calcium ashes contained more reactive crystalline phases whereas the lower calcium ashes contained more non-reactive phases. The three models outlined in the literature review aim to correlate the effect of crystalline phases and XRF oxide values with sulfate resistance. Although the most scrutinized, Dunstan's R-factor appeared to be the most accurate with the testing results obtained from this thesis.

5.3 Amorphous Phase Composition

5.3.1 Testing

The amorphous content of the fly ashes were studied using a SEM. The machine used was a Quanta 650 SEM with a backscatter detector, 20 kV beam, 4.5 spot size and magnification around 5000x. Testing was performed on 14 of the 18 fly ashes under investigation. As mentioned previously, amorphous particles are 1-5 μm in diameter. In

order to obtain a representative sample for each fly ash, compositions of 150-200 amorphous particles were collected and analyzed. These compositions were converted into oxides based on conversion factors and molecular weights. The oxides for all data points were plotted on a series of conventional ternary diagrams by the use of a tri-plot spreadsheet (Graham & Midgley, 2000).

5.3.2 Results

5.3.2.1 CaO-Al_2O_3-Si_2O_3 Diagram

This ternary diagram is the most widely used diagram used to explain the glassy phases of fly ash as outlined in Section 2.3.3.2. This ternary diagram will be called diagram #1 in this thesis. On this diagram, mullite is alumina-silica oxide and anorthite and gehlenite are calcium alumina-silica oxides. Parent coal with higher levels of calcium resulted in fly ash with calcium aluminosilicate glass. Therefore, on this ternary diagram, one would have expected to see a shift from the mullite region to the gehlenite region when comparing low to high calcium oxide fly ashes. See this shift in a typical Class F ash in Figure 33 and with a typical Class C ash in Figure 34. The results confirmed that the higher calcium ashes contained more of the reactive calcium aluminosilicate glass. It is very important to note the regions discussed do not mean the amorphous content is gehlenite, but only that it performs like gehlenite or the other regions.

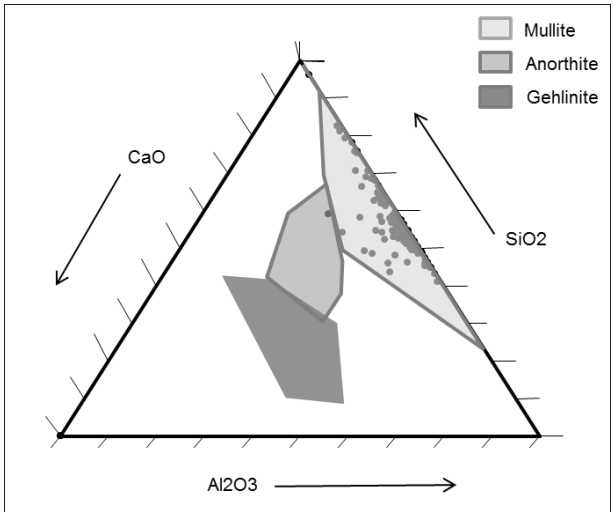

Figure 33: Typical Ternary Diagram #1 of Class F Fly Ash

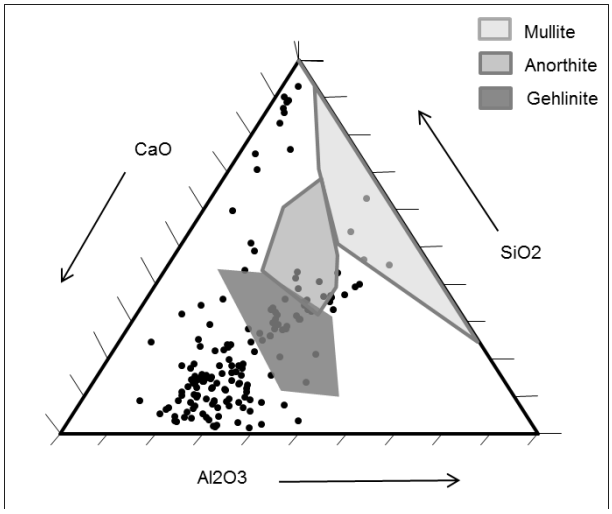

Figure 34: Typical Ternary Diagram #1 for Class C Fly Ash

The rest of these ternary diagrams are displayed in Appendix C. The numerical results of all the ternary diagrams are displayed in Figure 35. The relationship showing that higher calcium content ashes had less amorphous particles in the mullite region is shown here in the far right region of the graph. FA-9 and FA-13 had very different amounts of amorphous content in the gehlenite region; however, in the time to failure plot, the results were almost identical. It would be assumed that FA-13, which had more gehlenite amorphous content, would have more sulfate expansion. It is also interesting to note the behavior of FA-6. FA-6 had a very long time to failure, but it had mostly content in the gehlenite region. This contradicts what is expected. Looking at the XRF data for FA-6 though, this ash was classified as a Class F ash. This fly ash is an example of how plotting on the ternary diagram is not always accurate for individual fly ashes but seems to be accurate for the trend of a wide range of fly ashes. Looking at the high alkali ashes, FA-5 and FA-8, FA-8 had a greater percentage of amorphous content in the mullite region. This confirmed the sulfate expansion results presented previously that FA-8 had lower expansion than FA-5, which was not fully understood under examination of their

XRF results. FA-1, FA-3, and FA-4 fully proved the argument that ashes falling in the mullite field have good sulfate resistance. These three ashes have the highest amorphous content in the mullite region and have not failed the ASTM C1012 sulfate testing to date or have the maximum time to failure of 18 months depending on the replacement percentage.

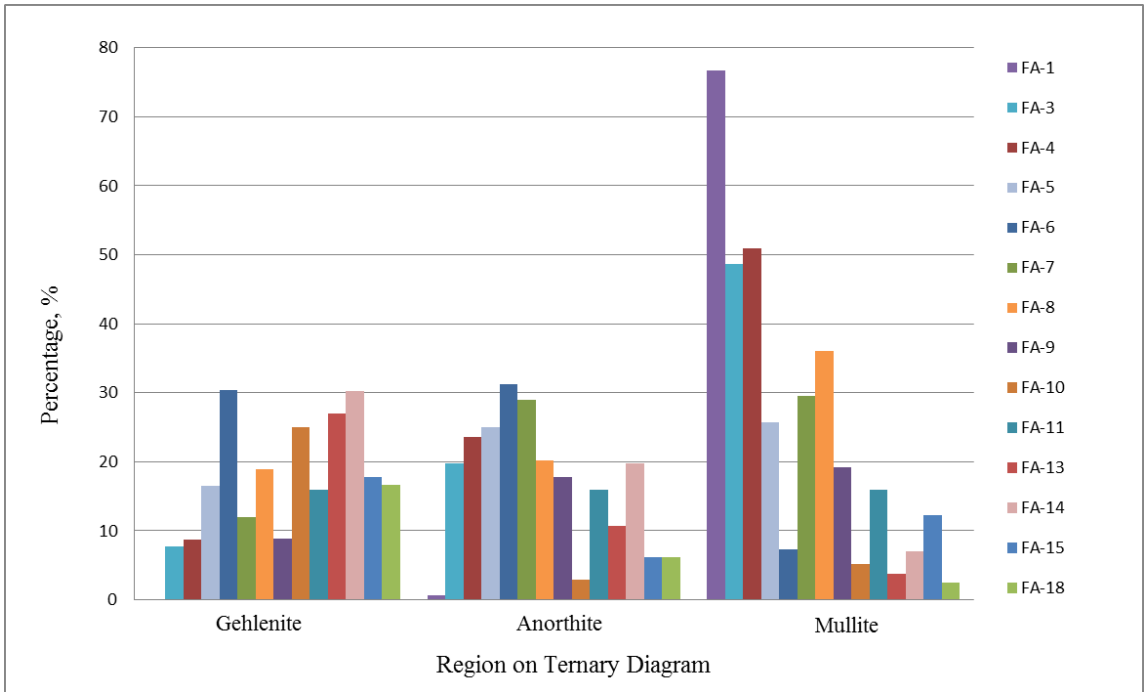

Figure 35: Amorphous Content on Ternary Diagram #1

FA-3 and FA-8 had a large cluster of points at the top point correlating to 100% SiO_2, shown in

Figure 36. These ashes had a long time to failure or low expansions. Stated in literature, if the SiO_2 content is in excess of 40%, the ash will improve the sulfate resistance, and as CaO content increases, there is a shift decreasing the percentage of SiO_2 amorphous points. FA-9 and FA-11 had similar plots on diagram #1, except that

FA-11 had a cluster at this 100% SiO_2 apex and more content in the gehlenite region. See these diagrams in Figure 37. Due to this observation of gehlenite content, FA-9 should have had better resistance; however, this was not the case. It appears this SiO_2 cluster is quite important. It seems for Class C ashes, sulfate resistance is improved if a cluster exists at 100% SiO_2.

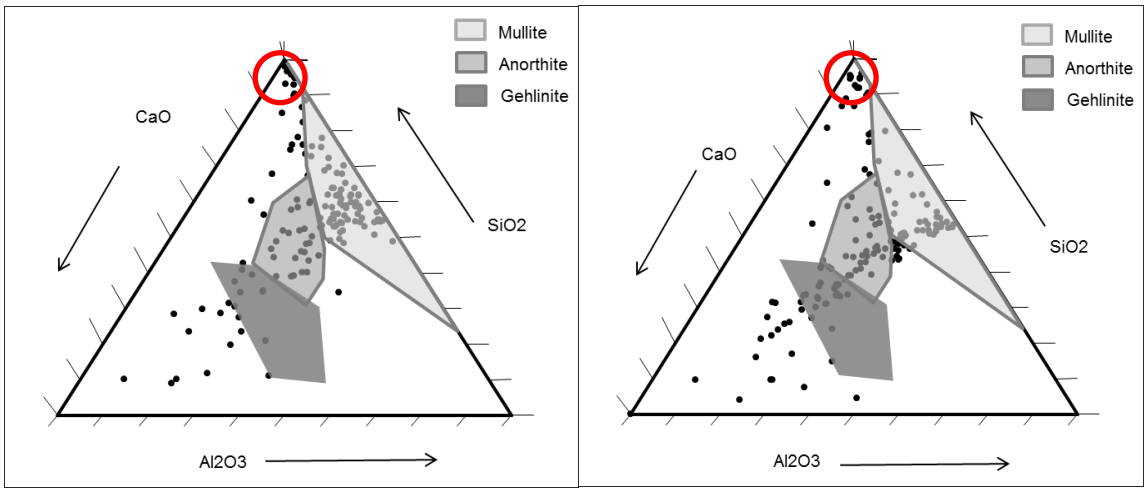

Figure 36: SiO_2 Clusters with FA-3 (left) and FA-8 (right)

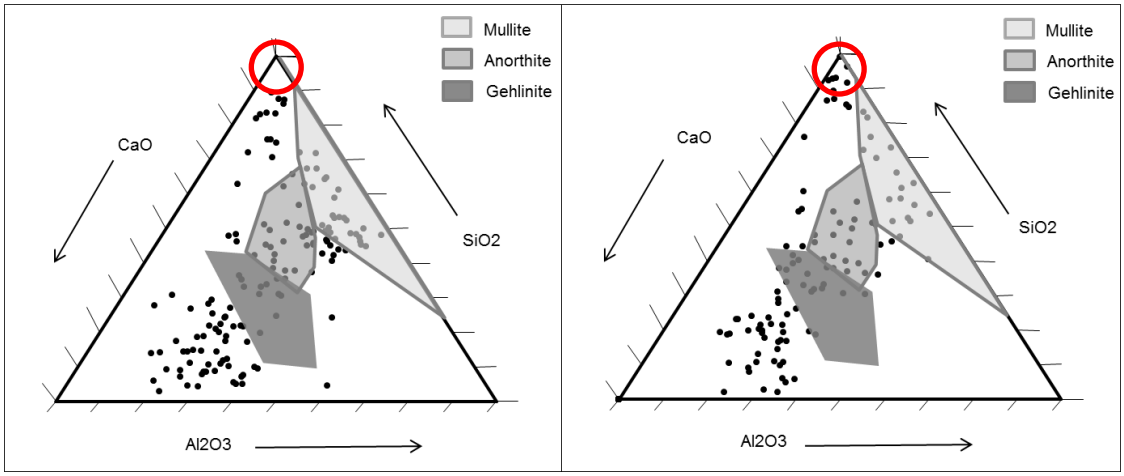

Figure 37: Difference in SiO_2 Clusters with FA-9 (left) and FA-11 (right)

5.3.2.2 $FeO{\cdot}Fe_2O_3$-Al_2O_3-SiO_2 Diagram

This ternary diagram was under investigation due to the argument that iron content plays a role in sulfate resistance as outlined in Section 2.3.4. An increase in iron relating to an increase in sulfate expansion was initially thought true; however, this was disproved in later research. This ternary diagram will be referred to as diagram #2. On this diagram, corundum is aluminum oxide, hematite is iron oxide, and spinel is magnetite or magnesium iron oxide with some aluminum substitutions. Again, the results presented are not the region they are plotted in but rather behave like that region.

The results of a typical Class F ash and typical Class C ash are presented in Figure 38 and Figure 39 respectively. The remaining ternary diagrams are presented in Appendix C. From solely observing this graph, there did not appear to be a trend involving iron. Analyzing the numerical results in Figure 40, there seemed to be a very slight linear relationship between increasing amorphous content in the spinel ss region and increasing calcium content, but this relationship did not have a high correlation coefficient. Ashes that had large amounts of spinel, such as FA-3 and FA-6, had good sulfate resistance. There existed a wider range of Al_2O_3 points plotted on this diagram; however, no correlation was found between this finding and sulfate expansion data.

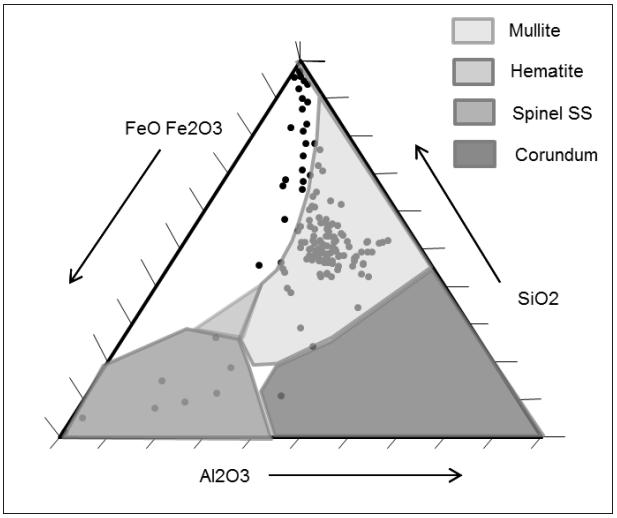

Figure 38: Typical Ternary Diagram #2 for Class F Fly Ash

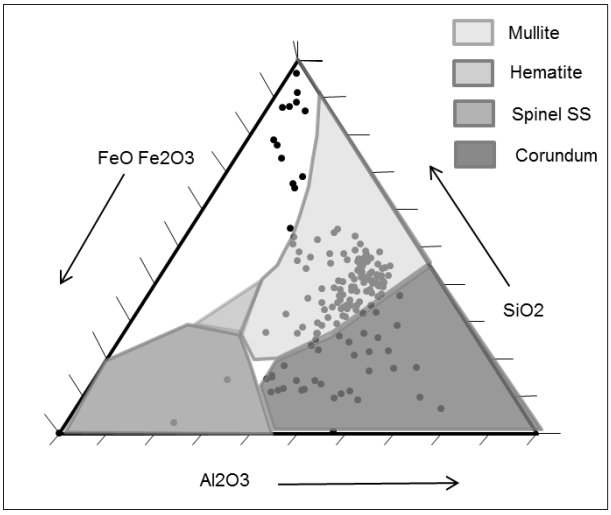

Figure 39: Typical Ternary Diagram #2 for Class C Fly Ash

The numerical results of the point count analysis are displayed in Figure 40. Again, there was a trend away from the mullite region as calcium content of the ashes increased as proved in ternary diagram #1. As for the iron content relating to sulfate performance, little amorphous content was observed even in the hematite region in this study. No correlation could be observed from the numerical analysis of hematite iron

content of the glassy phases. There was an increase in corundum with increasing calcium content. This increase in corundum correlated to a decrease in silica oxide content in ternary diagram #2. A decrease in SiO_2 below 40% relates to poor resistance based on fly ash ASTM classification. This relationship between CaO and SiO_2 is also observed from XRF data shown in Appendix A in Figure A-1. FA-7 had a very high corundum content compared to the other Class F ashes, noting that FA-5 was a Class C ash because of its sum of oxide content. FA-7 also had the poorest sulfate resistance, observed by the shortest time to failure, of all of the Class F ashes as well.

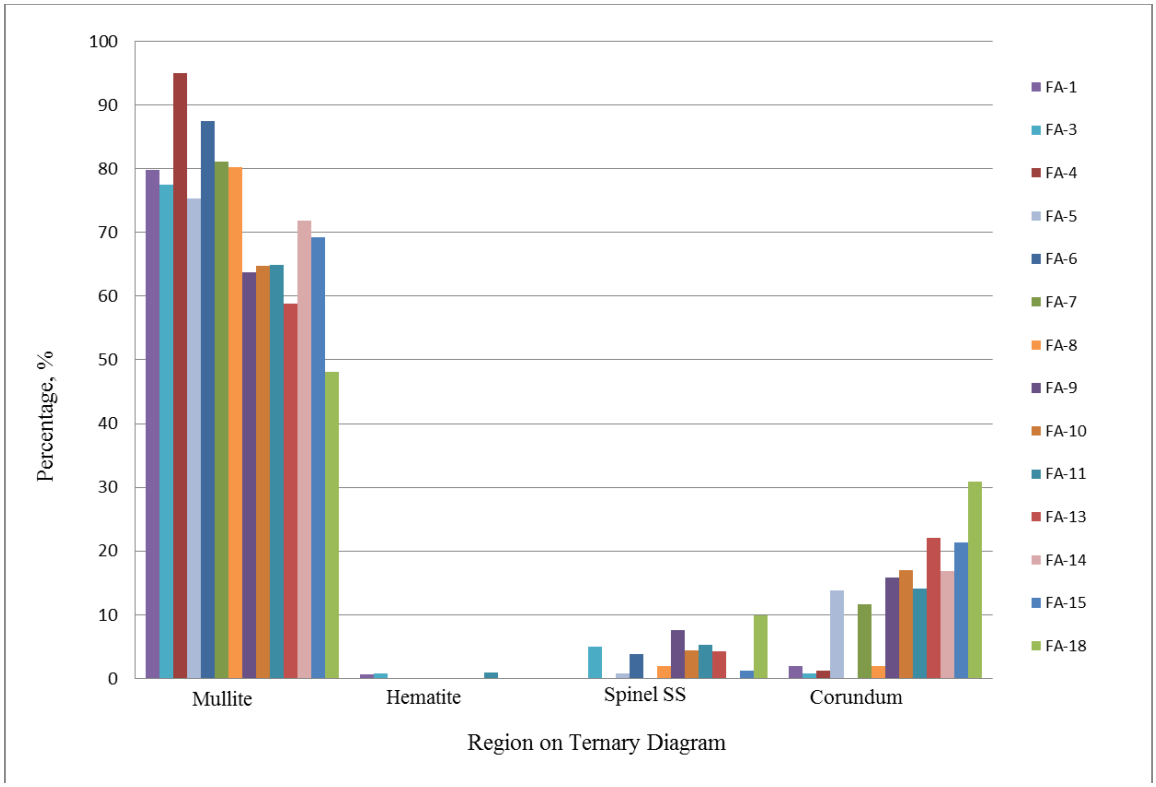

Figure 40: Amorphous Content on Ternary Diagram #2

FA-10 and FA-11 display the hypothesis that 100% amorphous SiO_2 helps sulfate resistance. FA-11 had a slight increase in SO_3 content, but otherwise these two ashes had

very similar XRF data. FA-11 had a cluster at the 100% SiO_2 apex and improved resistance, shown in Figure 41. This result was more pronounced for diagram #1 though.

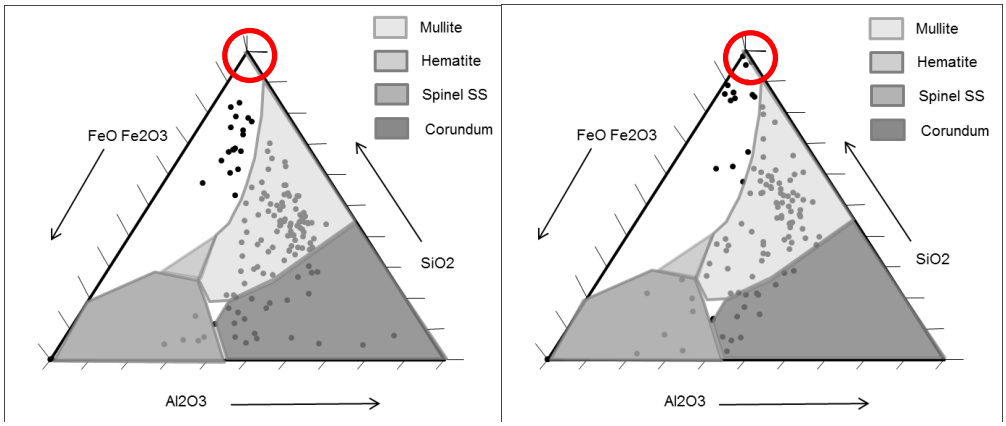

Figure 41: Difference in SiO_2 Clusters with FA-10 (left) and FA-11 (right)

5.4 REACTIVITY

5.4.1 Testing

This patent was discussed in Section 3.5, but the testing will be outlined more in depth in this section. The following procedure was performed for all 18 fly ashes under investigation. Approximately 20 g of fly ash was mixed with 250 mL of 5% tartaric acid solution. The mixture was placed over heat and boiled for 15 minutes with constant stirring. See the picture of the boiling mixture in Figure 42. The container was covered and allowed to cool for 3 hours. After this cooling period, the height of gel was measured and recorded.

Figure 42: Boiling during Reactivity Procedure

If the fly ash was reactive, the gel height would exceed 20 mm. A reactive fly ash had high early strength, which was the purpose of identifying fly ashes for which this test was created.

5.4.2 Results

The height of gel of all fly ashes studied is presented in Figure 43. A control, cement C-1, was also tested and is presented in the graph. The dashed line is the limit imposed by the reactivity test patented in the 1980's; however, a new proposed limit was suggested based on the results. This proposed limit increased the gel height to 30 mm for a fly ash to be considered reactive. All of the Class C ashes were labeled as reactive if this 30 mm gel height limit was used. Therefore, if the gel height exceeded 30 mm, the ash was considered reactive and would have poor sulfate resistance.

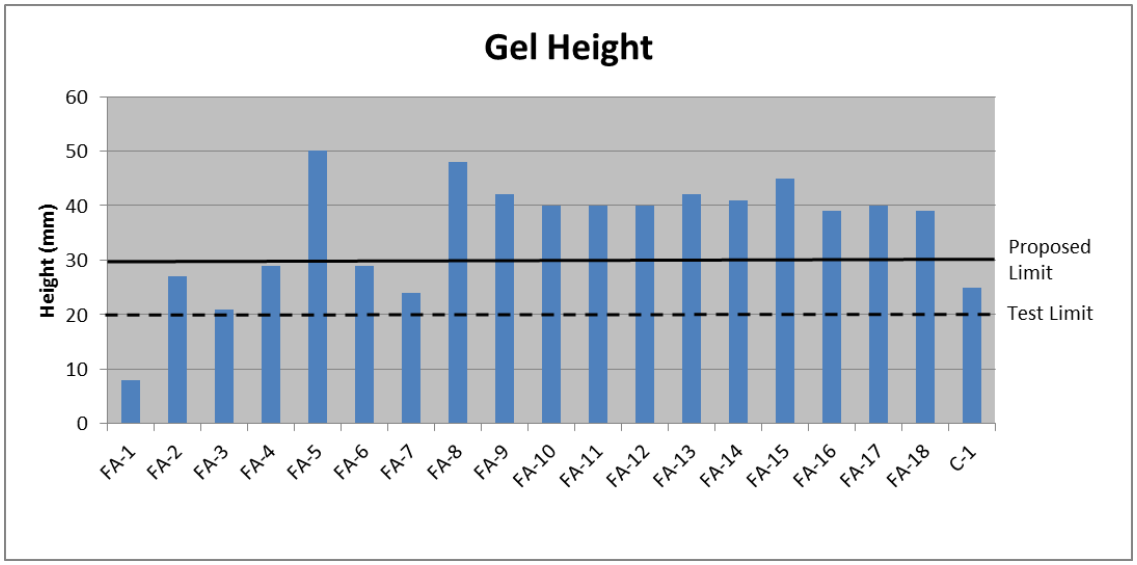

Figure 43: Reactivity Gel Heights

It is interesting to show the observed visual difference between gel products of the ashes. See Figure 44 for the relationship between a low, moderate, and a high calcium ash. FA-1 had the lowest gel height at 8.0 mm. This ash did fail but took a very long time to do so. FA-7 had the worst sulfate performance of all Class F ashes, but this fly ash did not have the highest gel height of Class F ashes.

Figure 44: Differences in Gel Heights of Low Calcium Ash (left), Moderate Calcium Ash (middle), and High Calcium Ash (right)

There did not appear to be a relationship between oxide values from XRF results and gel height except for SO_3 content and the alkali values. These relationships are presented in Figure 45, Figure 46, and Figure 47 respectively with increasing oxide contents on the x-axis. As SO_3 content increased, the gel height increased. Adding SO_3 will react and cause an expansion, which was observed here. As Na_2O content increased, the gel height increased greater than the proposed limit. As K_2O content increased though, the gel height decreased. When the equivalent alkali content was plotted though, not shown in this thesis, there did not appear to be a relationship. All of the ashes that had gel height under the proposed limit in these three figures, except for FA-6 and FA-7, had ASTM C1012 measurement bars that had not yet failed to date. All of these fly ashes were also classified as Class F ashes. Therefore this proposed height limit of 30 mm accurately predicted sulfate performance.

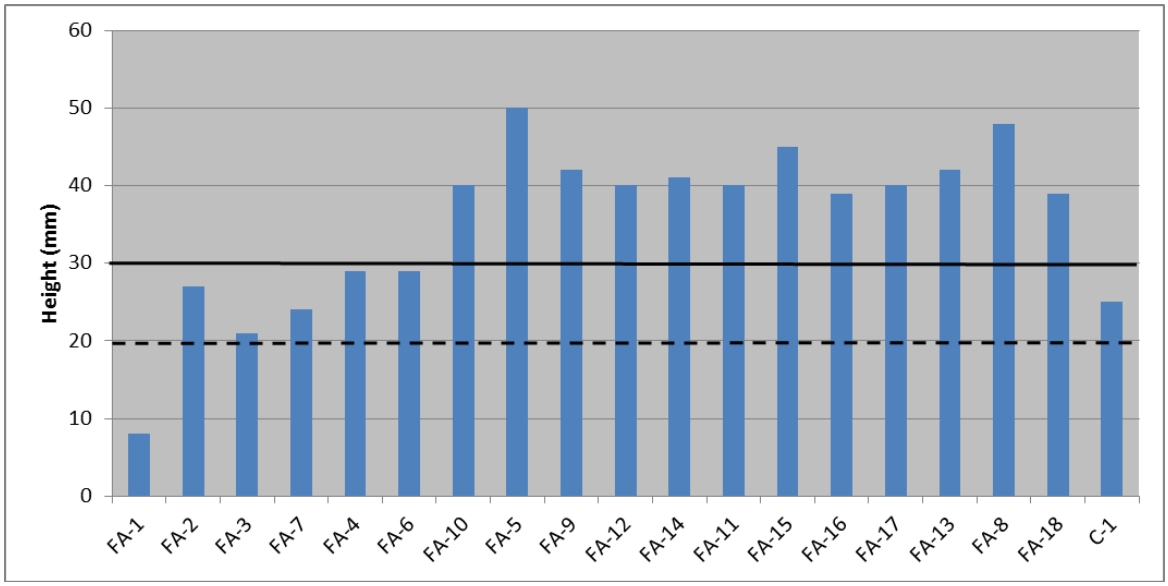

Figure 45: Relationship between SO_3 and Gel height

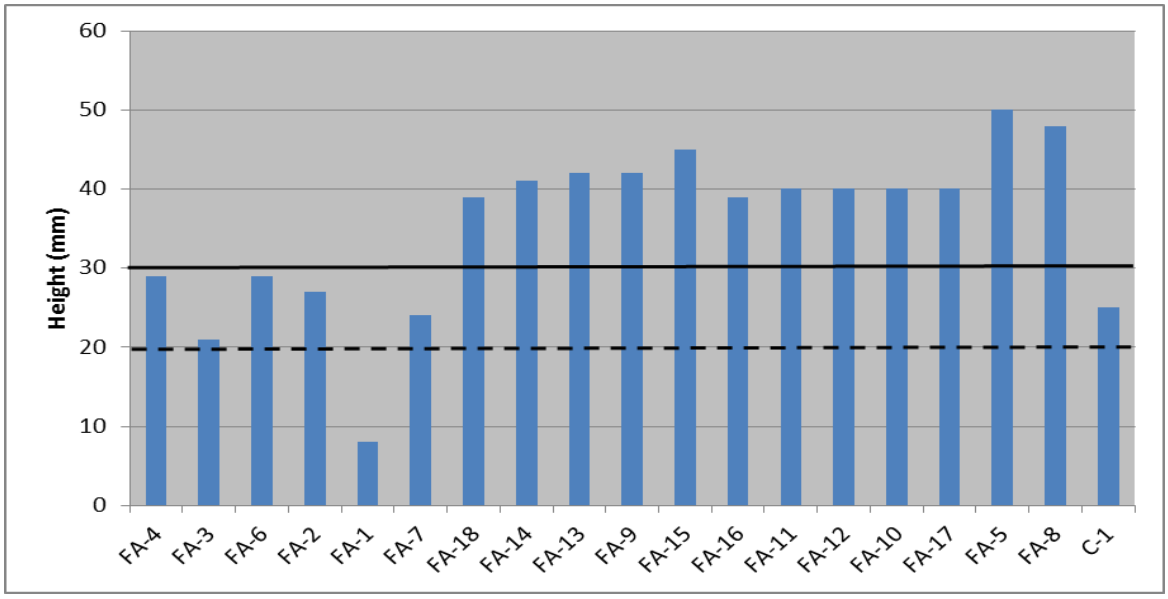

Figure 46: Relationship between Na_2O and Gel Height

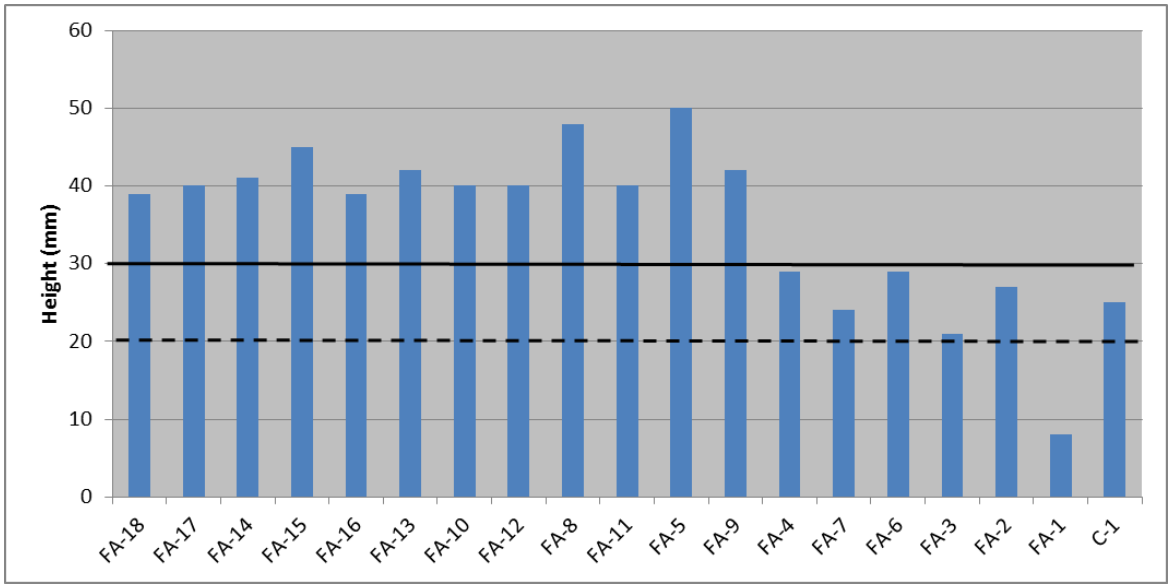

Figure 47: Relationship between K_2O and Gel Height

Chapter 6: Paste/Mortar Performance

This chapter contains testing results that describe the interaction of fly ash with cement during hydration.

6.1 Heat of Hydration

6.1.1 Testing

As discussed in Section 3.6, heat of hydration was measured using an isothermal calorimeter. All 18 fly ashes were analyzed at 20%, 30%, and 40% replacement percentages at temperatures of 5 °C, 23 °C, and 38 °C. These three different temperatures were used to mimic field performance in cold, moderate, and hot environments.

Three key items were used from calorimeter studies: heat of hydration graphs, cumulative heat graphs, and activation energy. The information obtained from the heat of hydration graphs were time and heat at the maximum peak, slope of the ascending line, and total heat generated. A cumulative heat graph was also useful for strength development. Activation energy was calculated to determine the amount of heat needed to start the reaction.

6.1.2 Results

All of the fly ashes studied showed the same general behavior on heat flow graphs. A heat flow graph showing the relationship between fly ash replacement percentages is displayed in Figure 48. As the replacement percentage increased, the total heat released decreased and the peak became narrower. Figure 49 shows the relationship between temperature and heat flow. As the temperature increased, the reaction proceeded at a faster rate, and the curve shifted to the left. The colder temperatures delayed the hydration reaction.

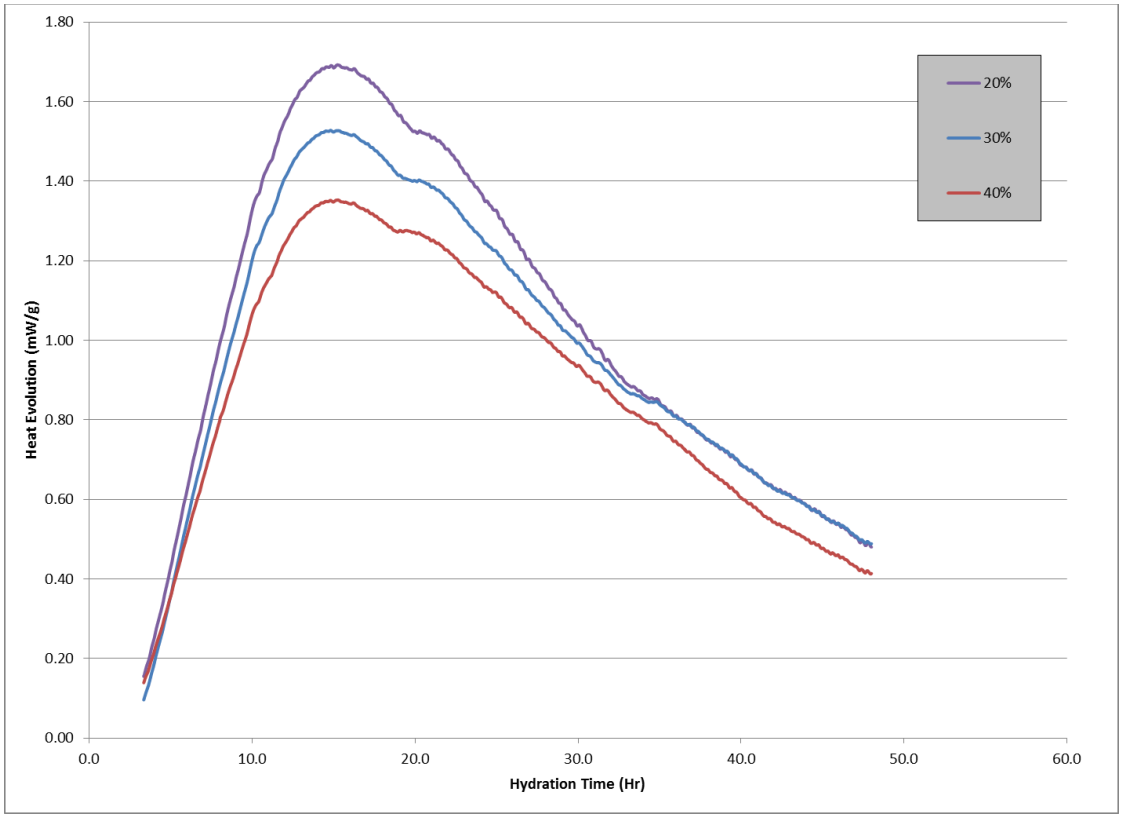

Figure 48: Typical Heat Flow Graph with Fly Ash Replacement Percentages

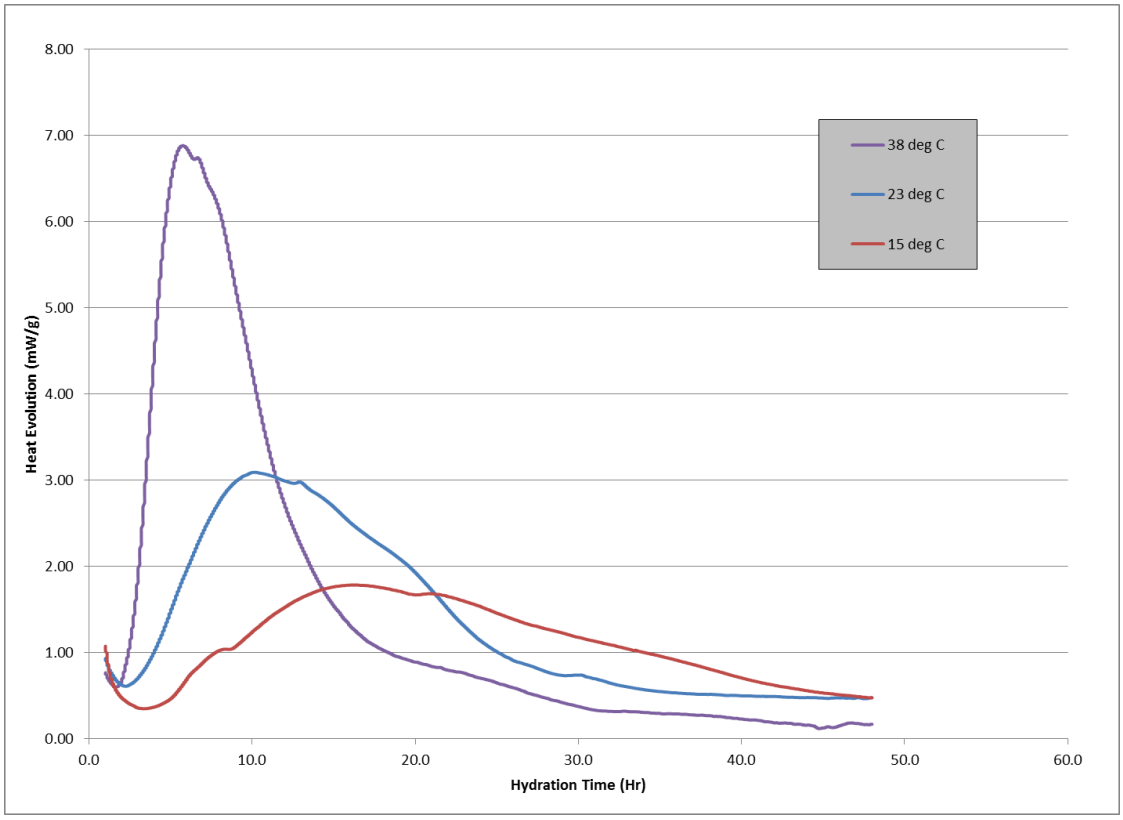

Figure 49: Typical Heat Flow Graph with Temperature Variations

The time of maximum peak was roughly the same for fly ash with similar calcium oxide contents at all replacement percentages for a given temperature. The results at 23 ºC are displayed in Figure 50. This time related to the length of the dormant period identified in Figure 13. Note the Class C ashes had increased times over Class F ashes for lower temperatures. Past research demonstrated that a longer dormant period results in improved sulfate resistance, but this was not observed here. As the temperature increased, the time to the maximum peak decreased. See this relationship in Figure 51.

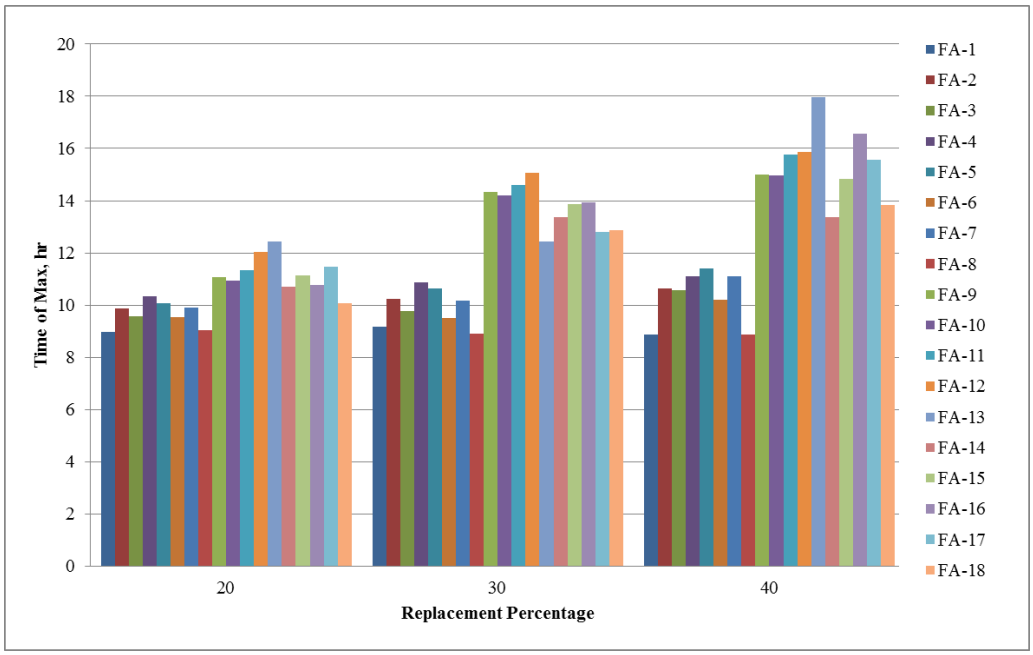

Figure 50: Time of Maximum Peak at 23 ºC

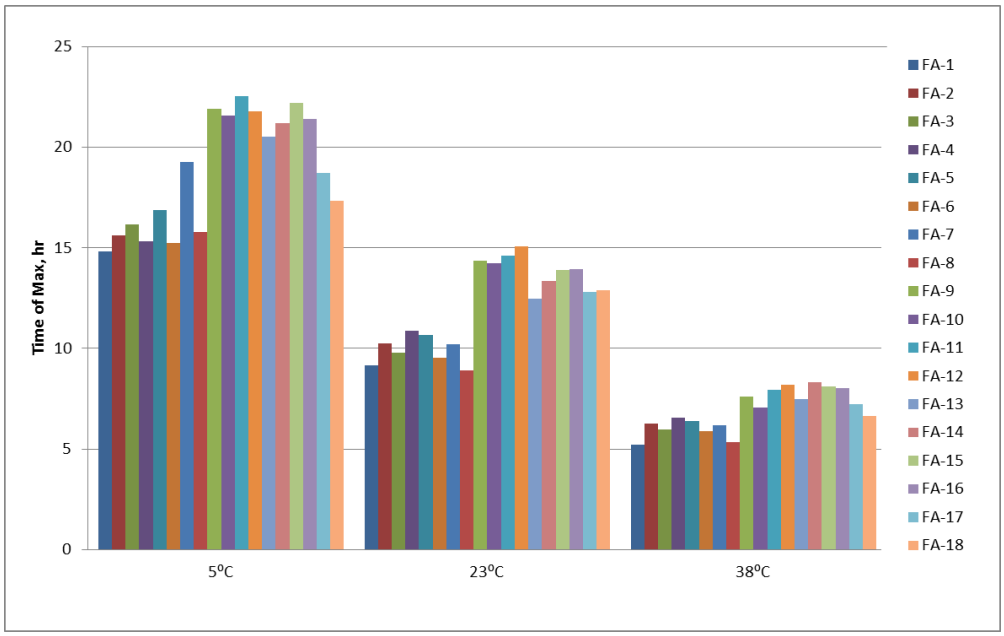

Figure 51: Time of Maximum Peak at 30% Fly Ash Replacement

The heat flow at this location of maximum peak was affected by the temperature. See this relationship in Figure 52. This graph was typical for all replacement percentages studied. The heat flow increased with rising temperature, but not with the class of the fly ash. FA-8 had the greatest heat flow at the maximum peak. FA-8 had good sulfate resistance due to ASTM C1012 specimens having either not yet failed or a long time to failure. This ash is one of high alkali; however, the other high alkali fly ash, FA-5, did not have high heat flow at the maximum peak. The heat flow at the maximum peak was greater for high calcium ashes than lower calcium ashes for ash replacement of 40%.

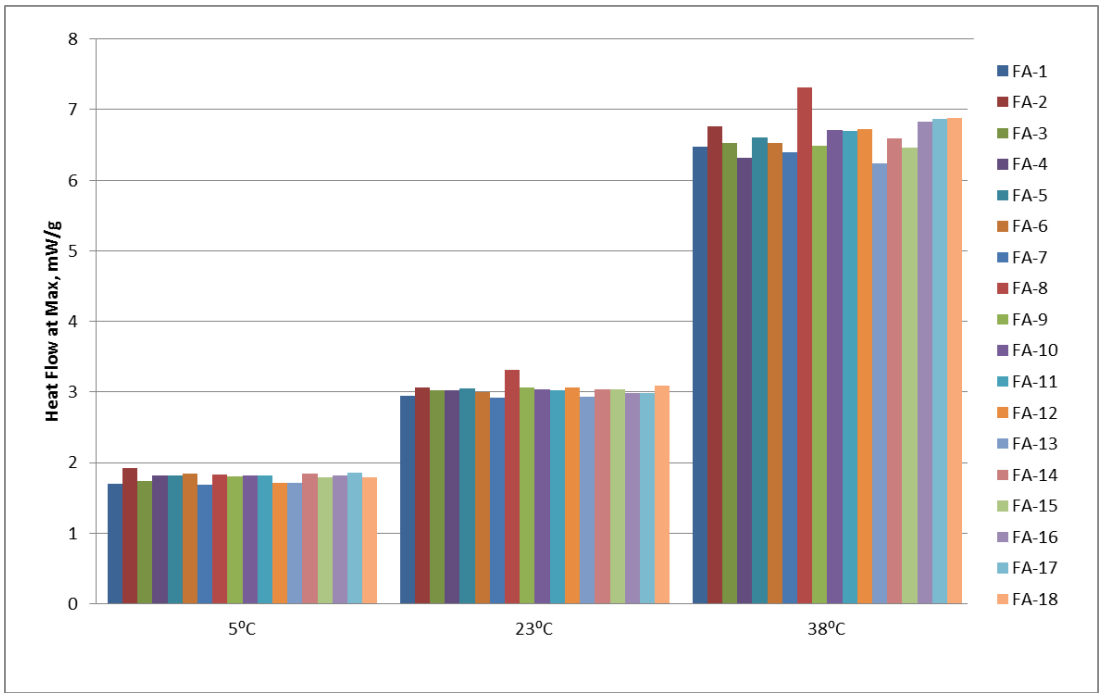

Figure 52: Heat Flow at Maximum Peak for 20% Fly Ash Replacement

The ascending slope of the heat flow plot, see Figure 49, was important in total heat generated during this reaction. As the slope increased, the peak became narrower, but the peak also increased as shown again in Figure 49. The slope increased with an

increase in temperature but did not change with replacement percentage at equal temperatures. This narrowing but higher curve related in roughly equal total cumulative heat generated for all fly ashes at all replacement percentages. Refer to Figure 53 for this relationship. At higher temperatures, there seemed to be a slight increase in total generated heat for the higher calcium ashes.

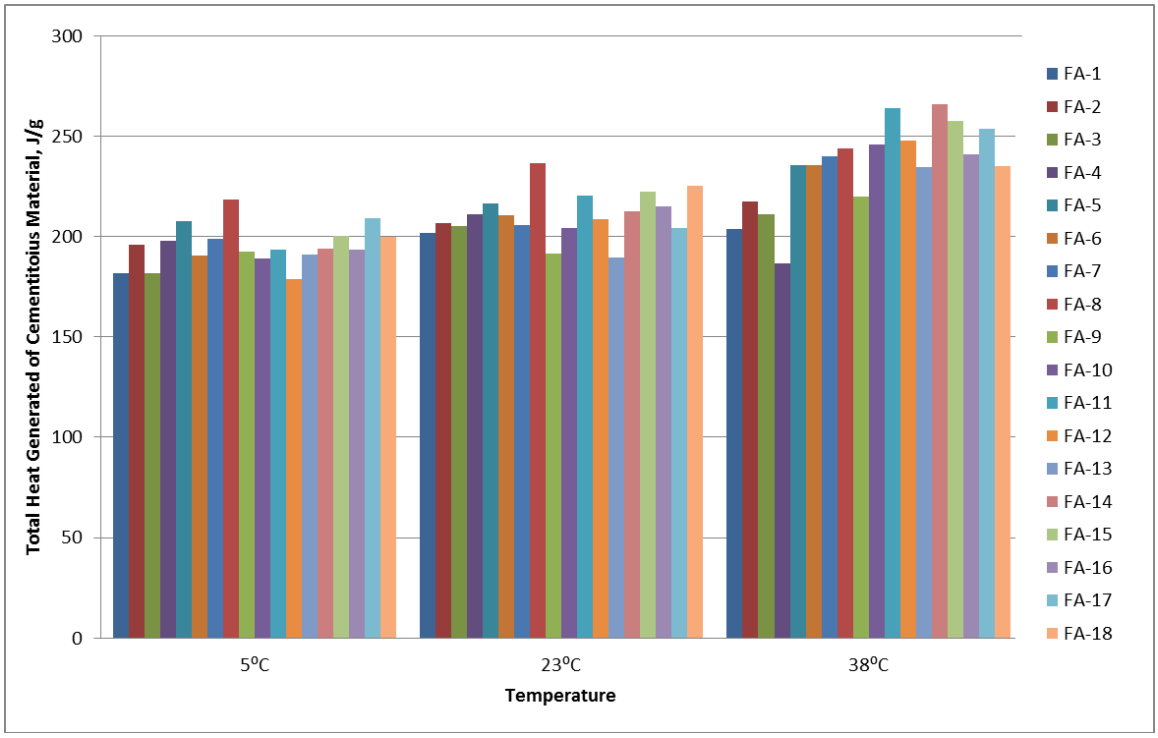

Figure 53: Total Heat Generated due to Cementitious Material

Activation energy did not seem to vary between all fly ashes under investigation until a later time of hydration, 48 hours for example. It is at this later hydration age that trends developed. Notice in Figure 54 the behavior of replacement percentage on a Class F fly ash. There was not a significant difference between the activation energies at the lower times of hydration; however, at the higher times, an increase in replacement

percentage resulted in a lower activation energy. See the opposite effect for Class C ashes in Figure 55. The trend showing an increase in ash replacement percentage resulting in higher activation energies was not observed until later hydration ages. Activation energy values at early hydration ages were comparable for Class F and Class C ashes. Class C ashes had greater activation energy values than Class F ashes for the three replacement percentages at later stages of hydration. See this general trend in Figure 56.

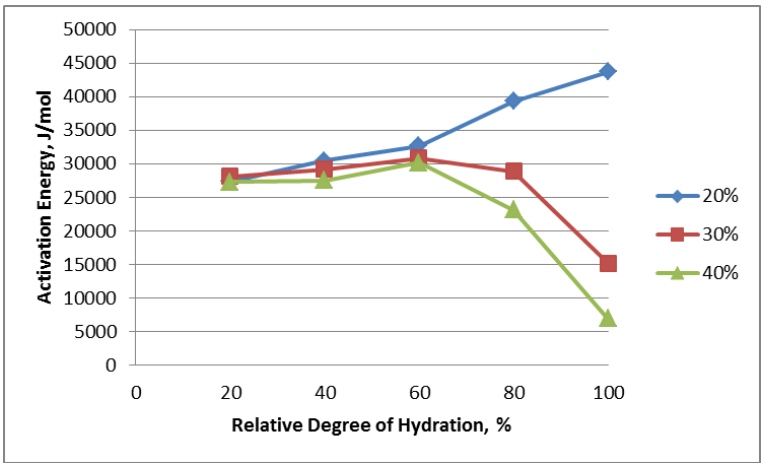

Figure 54: Typical Class F Ash Activation Energy vs. Time Plot

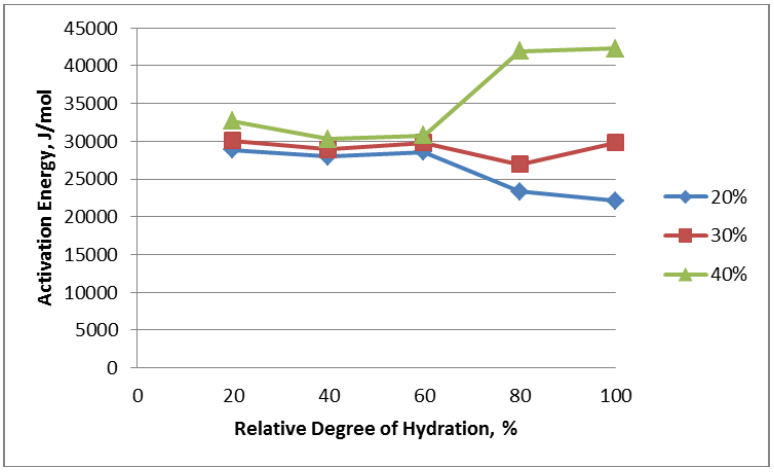

Figure 55: Typical Class C Ash Activation Energy vs. Time Plot

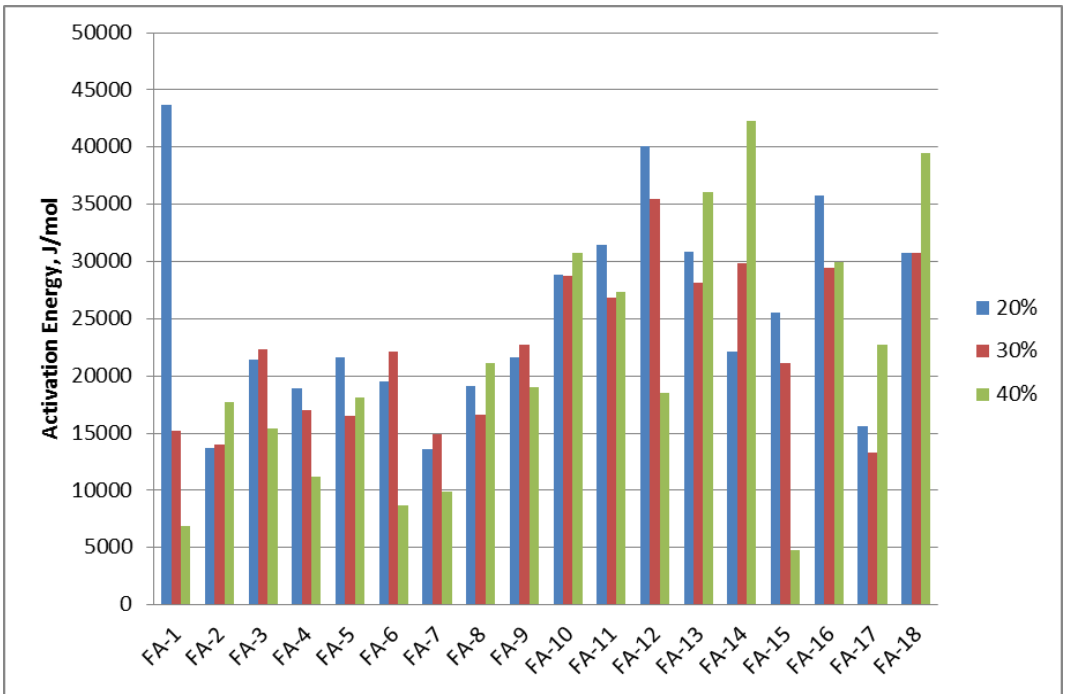

Figure 56: 48 Hour Hydration Activation Energy Values

The following graphs in Figure 57 show the relationship between XRF oxide values in ascending amounts on the x-axis with activation energies at 48 hours of hydration on the y-axis.

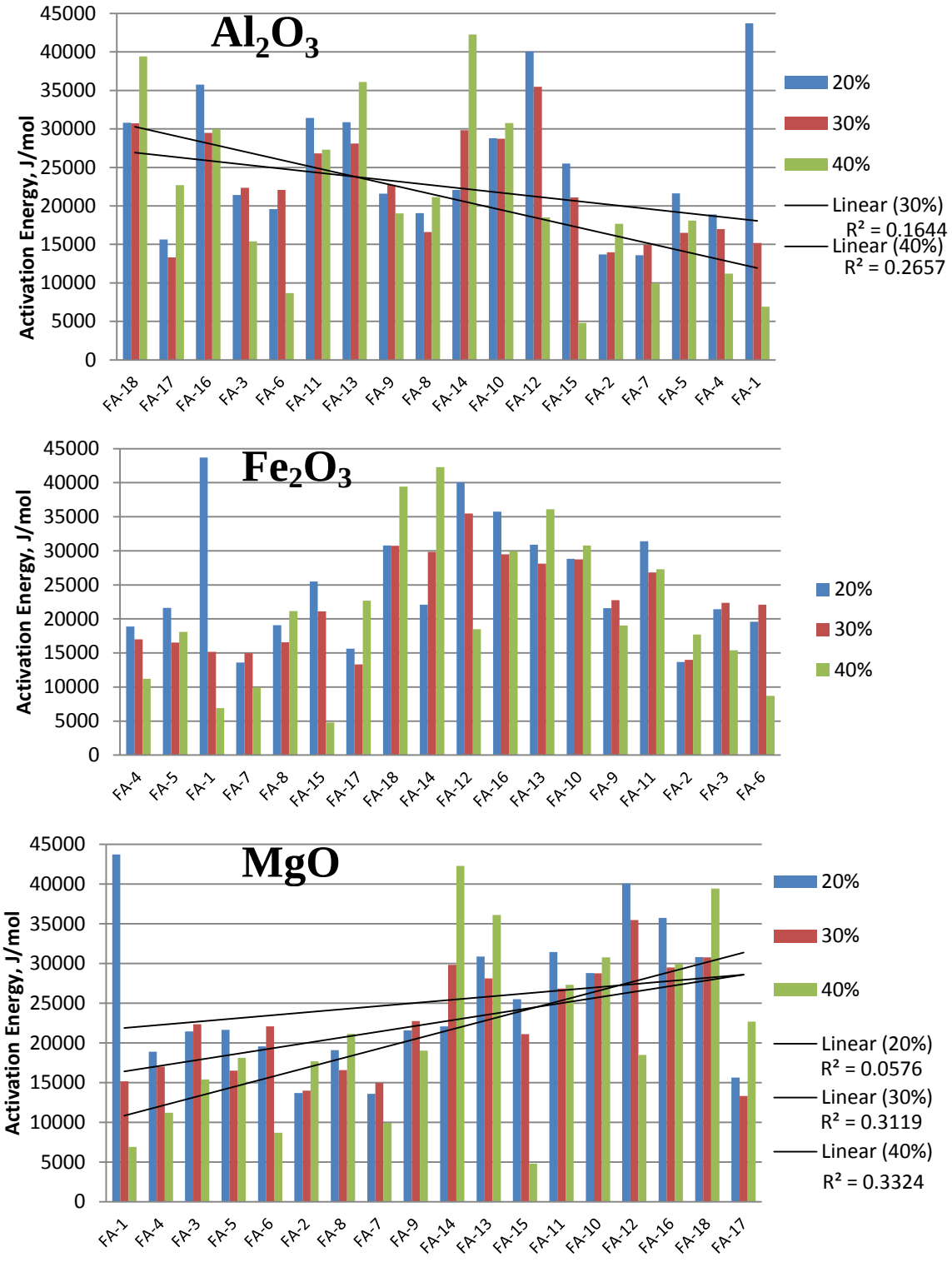

Figure 57: XRF Oxides versus Activation Energy at 48 hr Hydration Time

In comparing the activation energies of different replacement percentages of all fly ashes to XRF values in Figure 57, some trends were observed:

- Al_2O_3: An increase in Al_2O_3 corresponded with a decrease in activation energy, and this was more drastic as the replacement percentage increased. The ashes with lowest Al_2O_3 content did not have the greatest expansions.
- Fe_2O_3: The highest activation energies corresponded to the medium Fe_2O_3 values. Most of the mid-range Fe_3O_2 ashes had the highest sulfate expansions.
- CaO: The strongest correlation was the linear relationship between calcium content and activation energy shown in Figure 56. The highest calcium ashes had the poorest sulfate resistance.
- MgO: An increase in MgO content yielded a higher activation energy. This trend was better fit for the higher replacement percentages. This trend also held true for SO_3. Ashes with greater MgO and SO_3 contents did not necessarily have the greatest expansions.

Another interesting item noted included FA-1. This ash seemed to have very large values compared to the other Class F ashes, reference Figure 56. XRF values revealed this ash had the lowest calcium content and the highest sum of oxide percentage by a wide margin. From the sulfate testing results, this ash had the longest times to failure.

In general, for the factors of interest from heat flow graphs, the most important indicator of sulfate resistance seemed to be the time to the maximum peak. This correlated to the length of the dormant period or the reactivity of the ash. The more C_3A and calcium content of the ashes, the more reactive they were; this corresponded to the

Class C ashes which had a shorter time to failure in sulfate environments. This finding is contradictory to the findings published in literature. The higher activation energies tended to correspond to poor sulfate resistance. Class C ashes had greater activation energies than Class F ashes and the worst sulfate performance. At the longer hydration ages, an increase in replacement percentage resulted in lower activation energies for Class F ashes; the opposite effect happened for Class C ashes.

6.2 MICROSTRUCTURAL DEVELOPMENT

6.2.1 Testing

This testing section aimed to characterize sulfate resistance with the formation of hydration products over time. This study was performed on two machines. A Grace isothermal calorimeter was used to measure heat flow until a predetermined hydration age was reached. The samples were then removed and placed in acetone to stop hydration for 48 hours and ground for analysis in the XRD machine. Rietveld analysis was performed on these samples to identify hydration products. All samples were run at 23 °C, and the times of interest were 30 min, 1 hour, 2 hours, 4 hours, 8 hours, 24 hours, and 48 hours. Two replacement percentages of fly ash, 20% and 40%, were used. The XRD machine parameters used were a scan range of 5° to 70° 2θ degrees, step 0.02, and 4 sec dwell was employed for an average scan of 3.5 hours. The main products under investigation were portlandite, ettringite, monosulfate, and C_3A. This analysis was performed only on 7 of the 18 fly ashes. Cement C-2 was used in this testing regime.

6.2.2 Results

The same trends for the calorimeter heat flow data as presented in the previous section apply to this data. This section will only present the XRD data related to the hydration products.

Portlandite, or calcium hydroxide, was the primary phase attacked by sulfates. This phase was used during the pozzolanic reaction with fly ash to convert into beneficial calcium silica hydrate phases. The excess calcium was used in this reaction and led to ettringite formation. Portlandite was not detected at significant levels until 24 hours later for all ashes and continued to form at 48 hours. There were slightly higher amounts in the lower calcium ashes, especially at higher replacement percentages, see Figure 58. It was observed that the amount of portlandite formed would increase up to 28 days of hydration and then be used in the pozzolanic reaction, which would not be fully observed at normal fly ash replacement levels until around 90 days of hydration (Jozic, Zelic, & Janjatovic, 2010). The effect of portlandite on sulfate resistance could not be determined from this short hydration age.

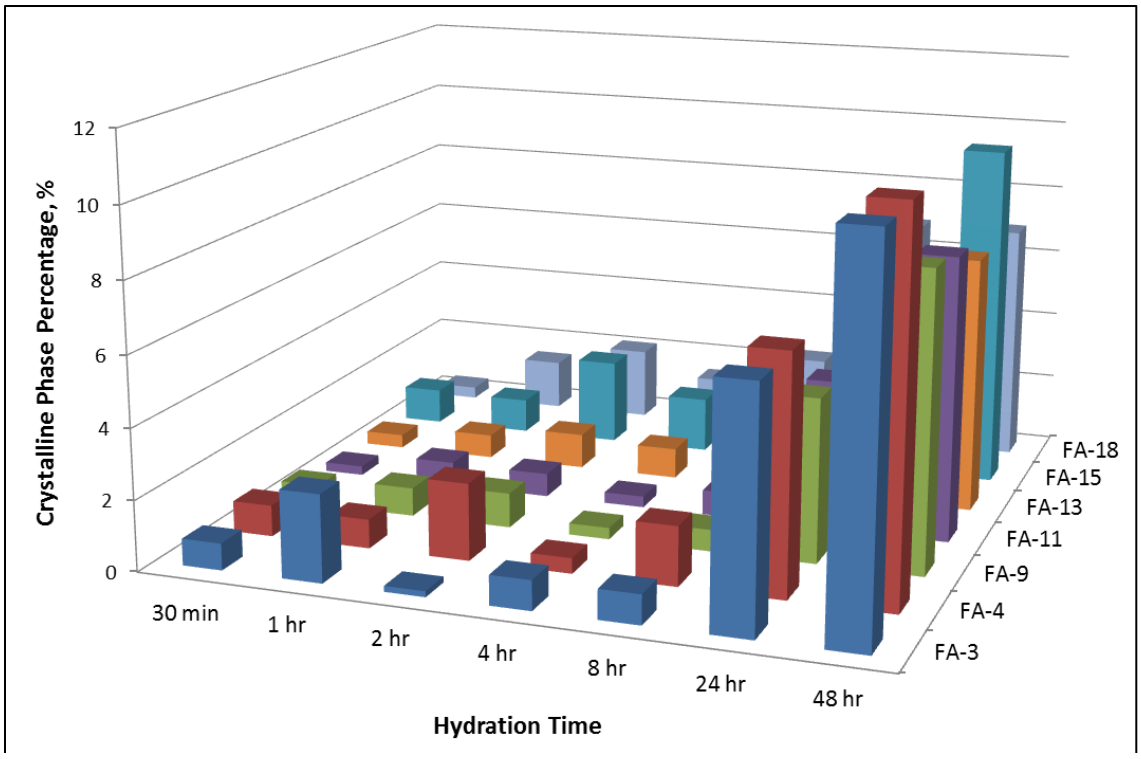

Figure 58: Portlandite Formation at 40% Fly Ash Replacement

The percentage of ettringite present increased with the hydration age. In general, as the calcium content increased, the amount of ettringite formed increased as well. There was also a decrease in ettringite as replacement percentage increased. See Figure 59 for the relationship between a Class F ash, FA-4, and a Class C ash, FA-18, and different replacement percentages. The higher calcium ash produced more ettringite at both replacement percentages for most of the hydration times under investigation. Figure 60 and Figure 61 show the ettringite formation over hydration time for all ashes studied. Note that most ettringite was formed from FA-15 and FA-18; however, FA-9 had a large amount at 20% replacement at 48 hours. FA-9 had a relatively short time to failure compared to FA-11 and FA-13, which had lower amounts of ettringite formation. It is interesting to note that at 40% ash replacement the amount of ettringite produced with FA-9 was 50% less, and the time to failure at 40% replacement lengthened by 3 months. There was a correlation between amount of ettringite produced and time to failure related to sulfate expansions: an increase in ettringite resulted in shorter time to failure.

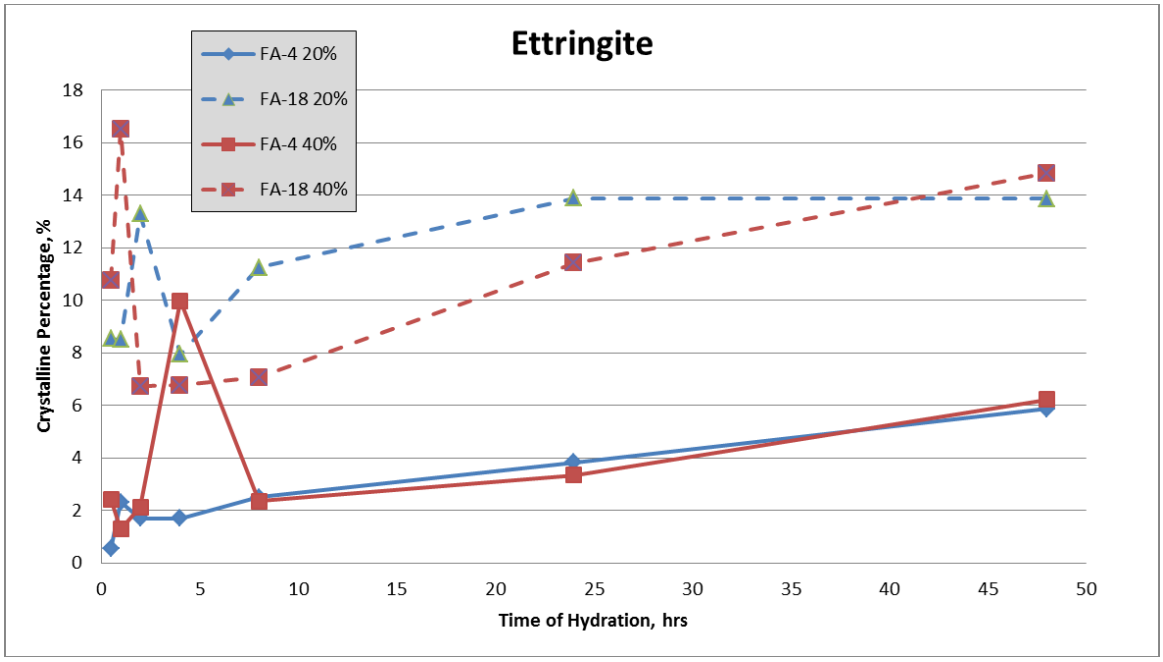

Figure 59: Ettringite Formation during Hydration of Two Fly Ashes

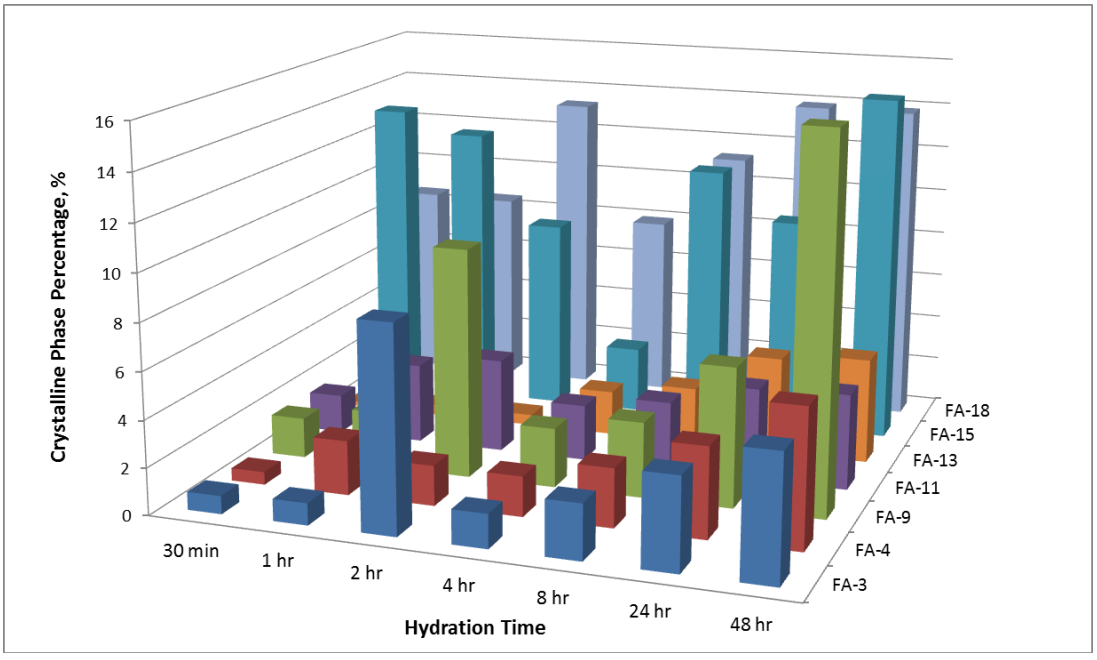

Figure 60: Ettringite Formation at 20% Fly Ash Replacement

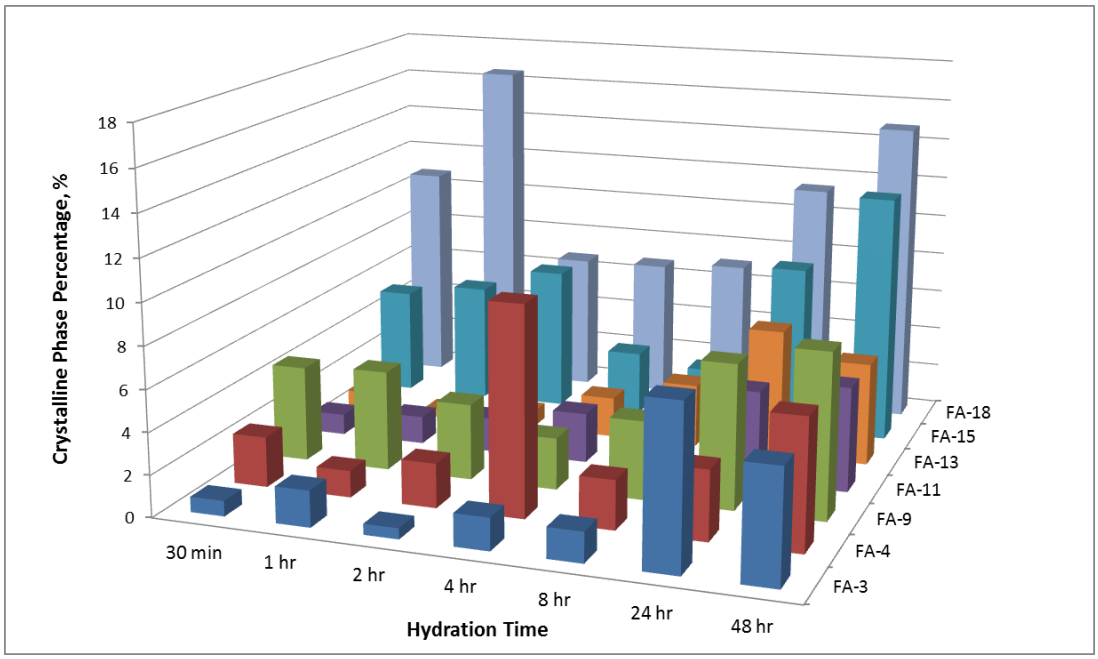

Figure 61: Ettringite Formation at 40% Fly Ash Replacement

Gypsum was another phase present during hydration. The formation of gypsum was another mechanism of sulfate attack; however, rather than causing expansion, it led to a loss of strength and cohesion. Anhydrite hydrated to gypsum as hydration continued; however, this process could take 30 days (Ubbriaco, Bruno, Traini, & Calabrese, 2001). In this study, the amount of gypsum identified was small, around 2-3% of crystalline phases. As hydration continued, the amount of gypsum decreased for both replacement percentages to almost negligible levels. See the higher levels at 48 hours for FA-3 and FA-13 in Figure 62. These two ashes had similar time to failure lengths, but ashes with lower amounts of gypsum at 48 hours had varying sulfate performance. Due to this finding, there did not appear to be a relationship between gypsum and sulfate expansion up to 48 hours of hydration evaluated in this study.

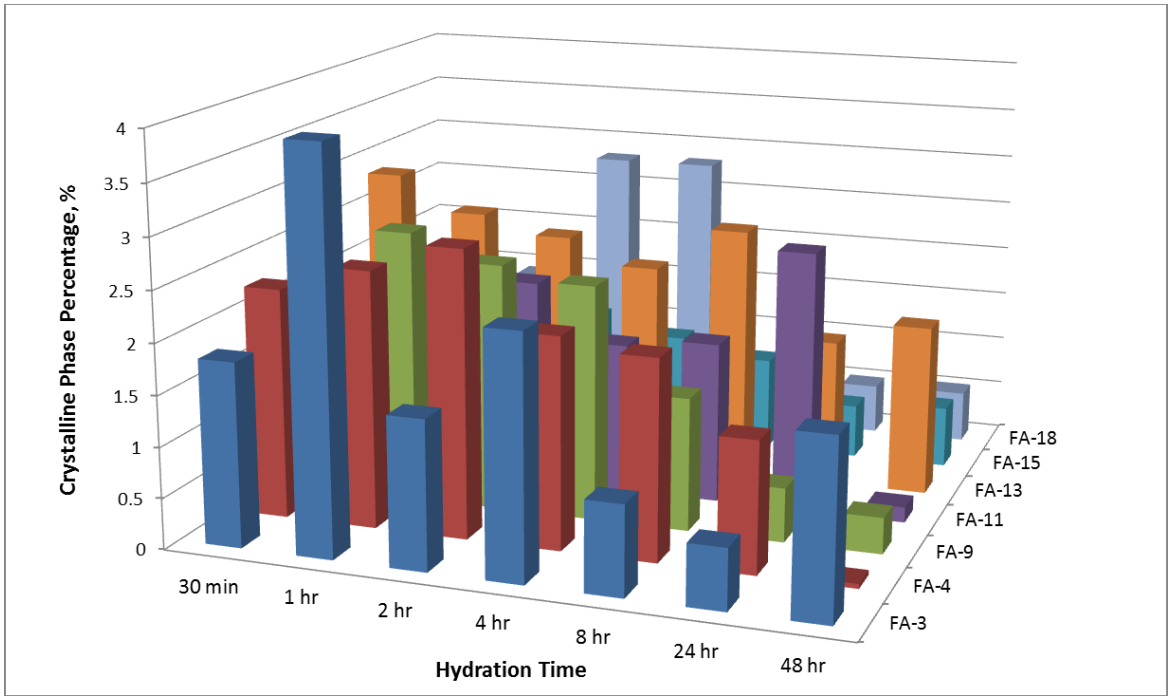

Figure 62: Gypsum Formation at 40% Fly Ash Replacement

Gypsum and ettringite formation is related due to setting and hardening of the fly ash-cement paste. Gypsum will form initially during hydration and then dissolve to form ettringite. This relationship is observed in the data previously presented. Gypsum content decreases as hydration continues, and ettringite content increases with aging hydration. The more ettringite that forms, the more strength gain. This is the mechanism responsible for higher calcium ashes having early strength gain than lower calcium fly ashes. This ettringite formation also leads to reduced sulfate resistance.

C_3A is the reactive aluminate component responsible for the expansions due to ettringite formation. C_3A content slightly decreased as hydration continued; however, the Class C ashes had much greater levels of C_3A at 48 hours than the Class F ashes. See Figure 63 for this relationship. The higher calcium ashes had worse sulfate resistance than Class F ashes, demonstrated by the C_3A formation during hydration.

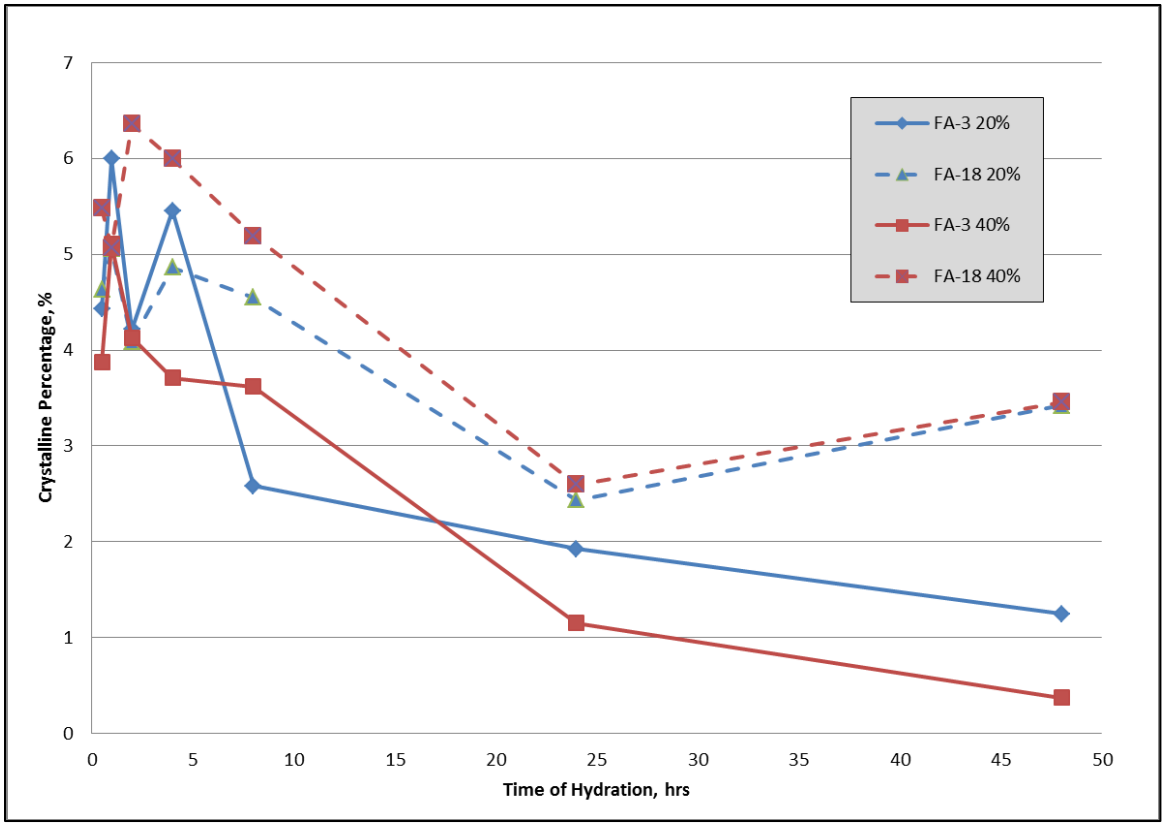

Figure 63: C_3A Formation at 40% Fly Ash Replacement

No monosulfate was observed in any fly ash up to 48 hours of hydration. The only trends observed were a function of calcium content of the ashes, which was also an inverse relationship with silica and potassium oxide values as well.

6.3 Sulfate Immersion

6.3.1 Testing

This testing was first conducted at the University of New Brunswick and will be repeated in this study in the same manner. A control of C-2 and 7 fly ashes were used in this study. The ashes used were: FA-3, FA-4, FA-8, FA-11, FA-13, FA-15, and FA-18. A 150 g sample of fly ash was mixed with 100 g of calcium hydroxide. These dry

materials were hand mixed until a uniform color was obtained. An alkaline solution was made consisting of 0.15 M NaOH and 0.35 M KOH, and 112.50 mL of this solution was added to the dry material mixture resulting in a w/c ratio of 0.45. This mixture was hand mixed for roughly 20 minutes when all materials were moved into a plastic container, sealed, and cured over water at 38 °C for 28 days.

Once curing was complete, the samples were removed from the plastic container. Samples were crushed into pieces and further ground until 50-75 g passed a No. 200 sieve. About 2 g of this finely ground sample was set aside for XRD analysis, and the remaining finely ground sample was kept for sulfate immersion.

Of the finely ground remaining sample, 15 g was immersed in sulfate solution. Two different sulfate solutions of calcium and sodium sulfate each at 5% were used for this test. The 15 g sample was mixed with 300 mL of each sulfate solution in a plastic bottle and sealed. All of the samples were continuously rotated on a mechanical rolling machine for 15 days. During the first month, the sodium sulfate solutions were changed weekly and then every 2 weeks thereafter, measuring the pH of the solutions at these times. This was done to control the pH of the solution to reduce the possibility that the reaction could reach equilibrium. The calcium sulfate solutions were not changed. To change the solution, the paste was filtered out of the sulfate solution. Then 300 mL of the sodium sulfate solution was added to the paste in a plastic bottle and resealed. The samples were immersed in these two sulfate solutions for 90 days. At the end of immersion, the bottles were vigorously shaken and the paste was filtered, washed with ethanol, and dried until a constant mass was obtained. A few grams were used for XRD analysis. For the pre- and post-sulfate immersion XRD, zincite was used as the internal standard. The scan parameters were a range of 5° to 70° 2θ degrees, step 0.02, 4 sec dwell. The average scan time was 3.5 hours per sample.

The study at the University of New Brunswick included a SEM and point count EDS analysis of mortar bars used in ASTM C1012 solution to study the effects of exposure to sulfate solution on CaO and SiO_2 content. This analysis was not conducted in this study due to time constraints.

6.3.2 Results

6.3.2.1 Pre-Sulfate Immersion

The pre-sulfate immersion XRD results are presented in Table 12 and Figure 64. The specimens had been curing for 28 days over water. The phases of interest were monosulfate, ettringite, and portlandite.

Table 12: Pre-Sulfate Immersion Phase Amounts

FA-ID	Monosulfate	Ettringite	Portlandite
C-2	0.500	2.584	47.450
FA-3	0.025	10.847	25.720
FA-4	0.292	4.589	22.393
FA-9	0.133	0.682	19.608
FA-11	0.786	1.445	16.415
FA-13	0.070	2.108	21.610
FA-15	0.011	2.580	20.670
FA-18	0.467	3.987	25.966

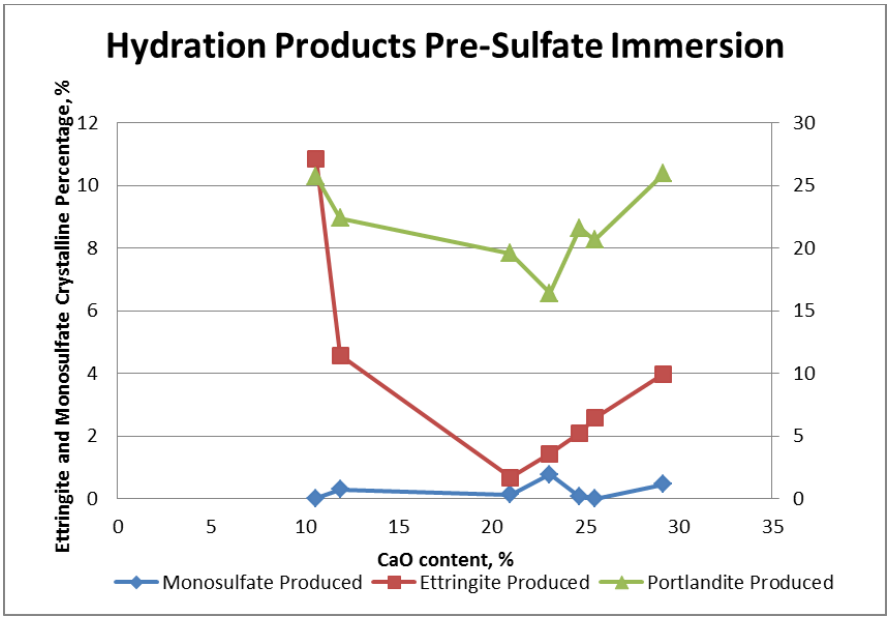

Figure 64: Quantities of Hydration Products Prior to Sulfate Immersion

On average, the Class F ashes, FA-3 and FA-4, had less monosulfate than Class C ashes and more ettringite after 28 days of curing. According to Mehta, if ettringite was formed initially, the phase would be stable and not cause expansion. If monosulfate was formed though, it would convert over time to form ettringite and would cause expansions (Mehta, 1986). These statements confirm the findings presented in Table 12. The Class C ashes, which had poor sulfate resistance, had more monosulfate formed prior to sulfate immersion, and the Class F ashes, which had good sulfate resistance, formed more ettringite initially.

The reference cement had a large amount of portlandite. The fly ash samples had significantly less portlandite after 28 days of curing. This suggests that the portlandite was consumed during fly ash reactions in this period of time, which was also observed by Raj Dhole in his work (Dhole, 2008). The Class F ashes in this study consumed more

portlandite on average than the Class C ashes. The Class F ashes are more pozzolanic fly ashes and would consume portlandite (CH) in the pozzolanic reaction.

6.3.2.2 Post-Sulfate Immersion

The hydration product intensities formed during the sodium and calcium sulfate immersion were very different. See this relationship between FA-4 and FA-18 in Figure 65 and Figure 66, respectively. The numerical results from the post-sulfate immersion studies are presented in Table 13.

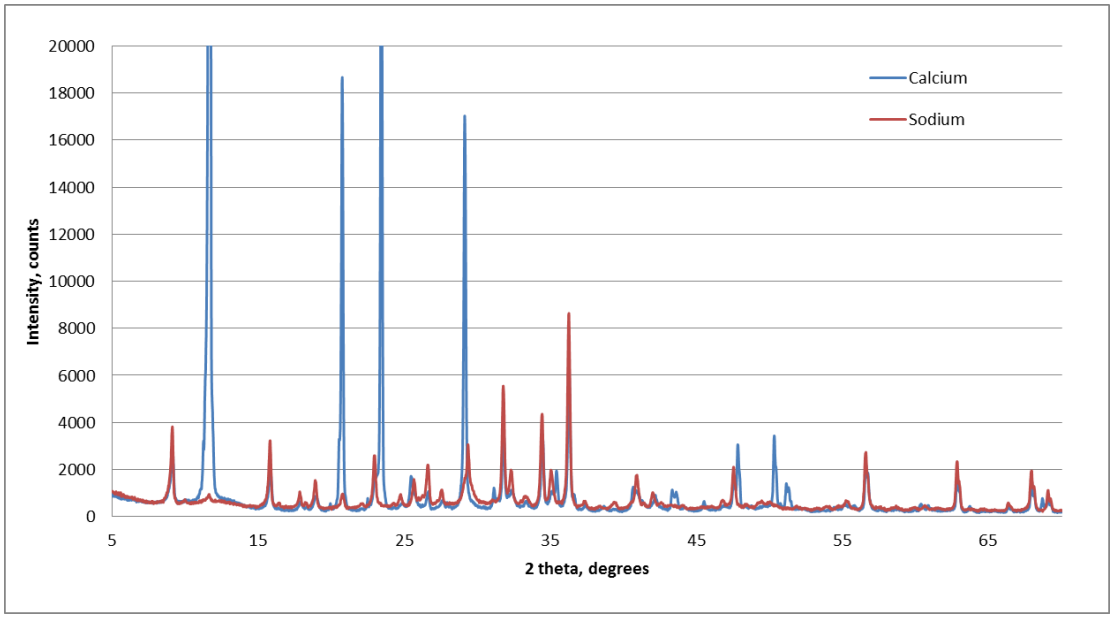

Figure 65: Comparison of Post-Sulfate Solution RQXRD of FA-4

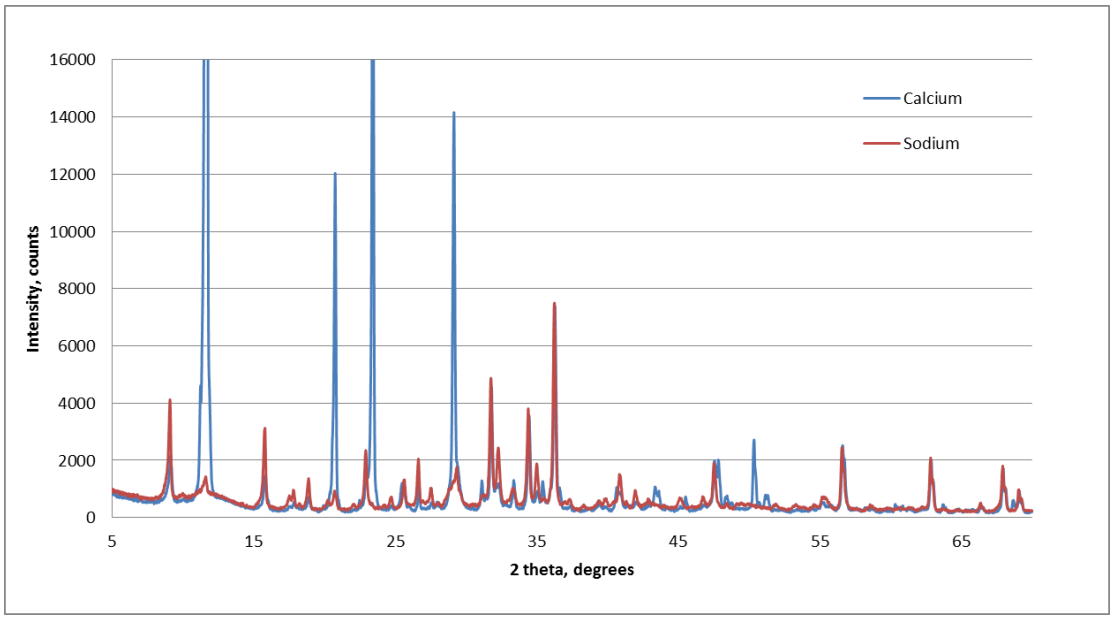

Figure 66: Comparison of Post-Sulfate Solution RQXRD of FA-18

Table 13: Post-Sulfate Immersion Phase Amounts

FA-ID	FA Source	Sulfate Solution	Gypsum	Ettringite	Portlandite
C-2	Alamo	5% Sodium	14.89	9.21	22.43
		5% Calcium	22.60	5.22	23.28
FA-3	LEGS	5% Sodium	25.51	25.59	0.42
		5% Calcium	67.23	17.03	0.73
FA-4	Rockdale	5% Sodium	19.11	28.30	0.59
		5% Calcium	71.72	24.11	0.07
FA-9	Harington	5% Sodium	9.53	27.38	0.61
		5% Calcium	68.58	17.15	0.73
FA-11	Tolk	5% Sodium	13.33	21.44	0.40
		5% Calcium	70.58	15.49	0.78
FA-13	Parish	5% Sodium	5.44	28.78	0.42
		5% Calcium	70.61	19.26	0.71
FA-15	Deely	5% Sodium	7.30	23.70	0.85
		5% Calcium	69.83	17.33	0.27
FA-18	Welsh	5% Sodium	8.11	25.37	0.26
		5% Calcium	73.25	15.00	0.27

The ashes immersed in the calcium sulfate solution formed substantialy more gypsum than those ashes immersed in the sodium sulfate soltuions. As noted in Dhole's dissertation, this gypsum formation was not solely from reactions with sulfate solutions (Dhole, 2008). More ettringite was produced for ashes submersed in sodium sulfate solutions. No monosulfate was identified in any of the samples for either solution.

The relationships between hydration product content and cakium oxide content of the ashes are presented in Figure 67 and Figure 68 for 5% calcium sulfate and 5% sodium sulfate soltuions. There did not appear to be a relationship between ettringite formation and calcium content of the ashes for either sulfate solution. This is contradictory to what would be assumed and Dhole's findings. A larger amount of ettringite at a later age, significantly after final set and curing, could potentially cause severe cracking and poor sulfate resistance. This expected result was confirmed in Dhole's disseration, so repeat testing is recommended for a comprehensive analysis. This relationship is highlighted in Figure 69. Figure 67 above shows an increase in gypsum formation for higher calcium ashes immersed in a calcium sulfate solution. This increase in gypsum may have been produced from the sulfate solution rather than the fly ashes (Dhole, 2008). The amount of portlandite identified was very small compared to the other products of interest. Most likely, the portlandite was consumed in the pozzolanic reactions. On average, the amount of portlandite identified was greater for Class C ashes than Class F ashes because they are less pozzolanic.

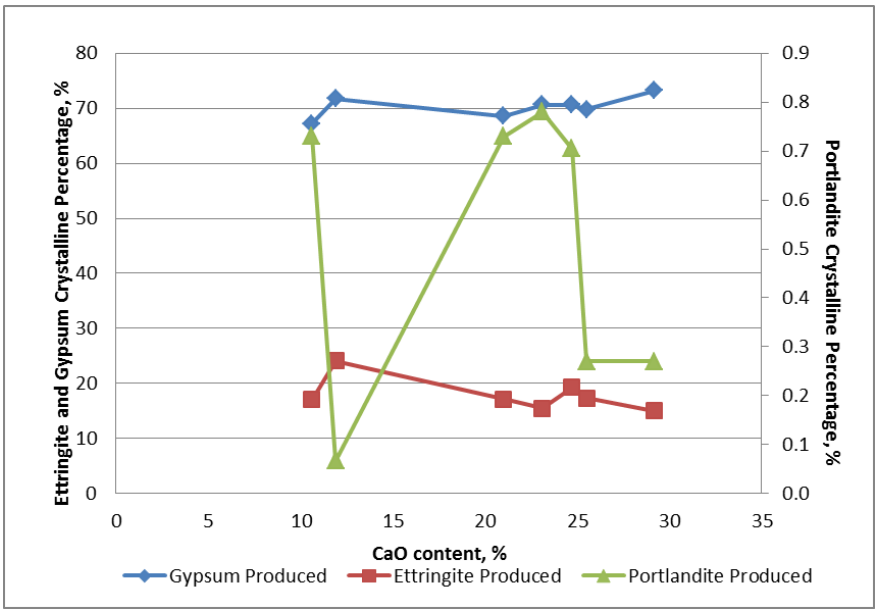

Figure 67: Hydration Products from 5% Calcium Sulfate Immersion

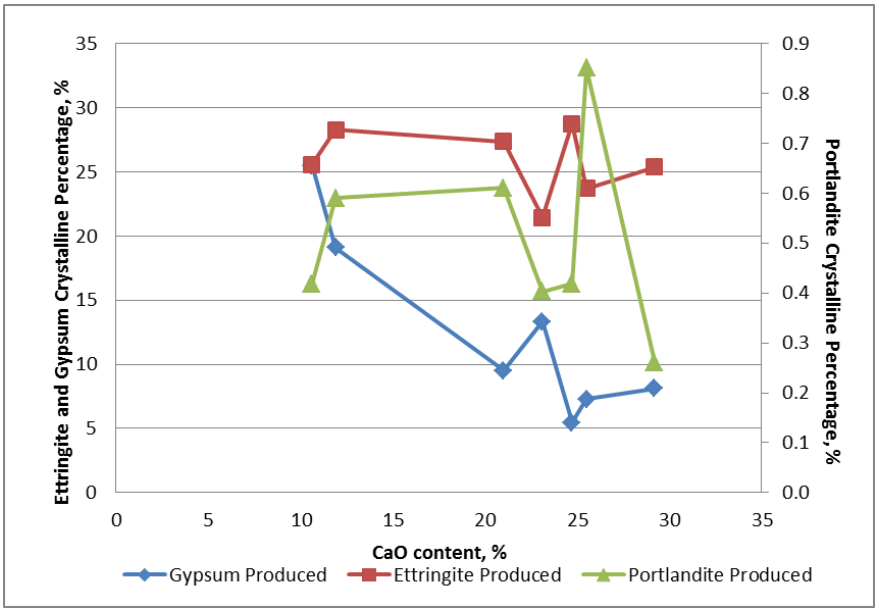

Figure 68: Hydration Products from 5% Sodium Sulfate Immersion

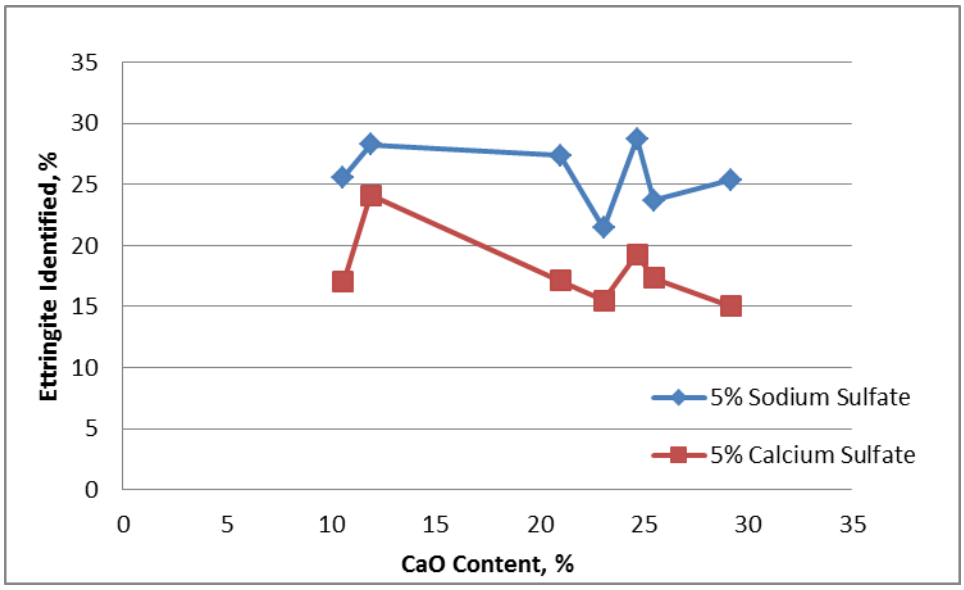

Figure 69: Comparison of Ettringite Formation in Different Sodium Solutions

In general, the results obtained in similar testing by Dhole did not agree with the testing results presented above. There appeared to be no correlation between the calcium content of fly ash and ettringite formation after sulfate immersion. One would have expected for the reactive calcium aluminosilica glass found in the higher calcium fly ashes to react with the sulfate solutions and formed more ettringite. No correlation was observed between time to failure and ettringite formation to explain the poor sulfate resistance by the higher calcium ashes. The pre-sulfate immersion results were agreeable with those found by Dhole and past literature. The better sulfate performing ashes formed more ettringite and less monosulfate early in the hydration process. One potential factor that may have led to the results of this study varying from those of Dhole was the chemistry of the cement used in the immersion studies. Additional work is needed to better elucidate the effects of fly ash chemistry and mineralogy on hydration products prior to sulfate exposure and reaction products after sulfate exposure.

Chapter 7: Discussion

This chapter presents a summary of the key testing results presented in the previous two chapters. This chapter aims to relate or correlate some or all of the findings to sulfate attack and present recommendations based on these findings.

The following tables identify a trend of sulfate results with probable reasons for these results. If a test is not listed, no strong correlations could be drawn from the data. Table 14 lists possible explanations for higher calcium ashes performing worse than lower calcium ashes in sulfate environments.

Table 14: Possible Explanations for Increased Expansions for Class C Ashes

Test	Findings
XRF	Increased CaO
	Decreased SiO_2
	Decreased sum of oxides
	Mid-range Fe_2O_3 (~6.0%)
	Increased SO_3
PSD	Smaller D(50)
XRD - more reactive phases	Decreased SiO_2
	Decreased Al_2O_3
	Mid-range Fe_2O_3 (~6.0%)
	Increased CaO
	Increased MgO
	Increased SO_3
	Mid-range Na_2O_e
XRD - more crystalline phases	Increased C_3A (~>2.7%)
	Increased brownmillerite (~>1.5%)
	Increased periclase
	Increased free lime
Previous Models	R-factor > 2.4 (Dunstan)
	Unacceptable region (revised Manz model)
SEM - diagram #1	lack of 100% SiO_2 cluster for Class C ashes
	More points in gehlenite region
	Fewer points in mullite region
Reactivity	Gel height > 30mm
Activation Energy	AE>22500
Calorimetry	Longer time to maximum peak
Timed Calorimetry	Increased ettringite formation
	Increased C3A formation

Table 15 explains reasons that an increase in Class C replacement led to increased sulfate expansions, whereas an increase in Class F replacement led to decreased

sulfate expansions. The primary reason for this finding was the increased amount of reactive phases introduced into the concrete mix.

Table 15: Possible Explanations for Increased Expansions with Increased Class C Replacement Percentage

Test	Findings
PSD	Increased amount of smaller, reactive particles
XRD	Increased amount of reactive phases, such as C_3A

Table 16 lists possible mechanisms to explain the behavior of the two high alkali fly ashes, FA-5 and FA-8. The behavior of the ashes is illustrated in the first row of the table. The results stated were from an analysis of testing from just these two ashes independent from the other ashes studied unless otherwise noted. The results stated also do not necessarily correlate to the other findings listed in the other tables in this chapter; they only apply to the high alkali ashes.

Table 16: Possible Explanations for Different High Alkali Fly Ash Sulfate Performance

Test	FA-5	FA-8
ASTM C1012 expansion	12 months to failure	Bars still readable
XRF of solely these two ashes	Increased SiO2	Increased Fe_2O_3
	Increased Al2O3	Increased CaO
	Increased sum of oxides	Increased MgO
	-	Increased LOI
	-	Increased SO_3
XRF of all the ashes	Second lowest Fe2O3	Third highest LOI
		Highest SO_3
PSD	-	Slightly larger D(50)
SEM - diagram #1	More points in gehlenite region	100% SiO_2 cluster
		More points in mullite region
Reactivity of all ashes	Highest gel height	Second highest gel height
Calorimetry	-	More total heat released for all replacement percentages

Table 17 lists possibilities for large 15 week expansions. These sulfate testing results did not seem to correlate to long-term performance though, so these conclusions are just stated to link to the conclusions drawn in Chapter 4 results section and may have limited applicability herein.

Table 17: Possible Explanations for Large 15 week Expansions

Test	FA-6	FA-15	FA-18
XRF of these three ashes	Highest SiO_2	Highest Al_2O_3	Highest CaO
	Highest Fe_2O_3	Highest Na_2O_e	Highest MgO
	Highest sum of oxides	-	Highest SO_3
XRF of all the ashes	Highest Fe_2O_3	-	Lowest SiO_2
	Second lowest Na_2O	-	Lowest Al_2O_3
	Second lowest Na_2O_e	-	Lowest sum of oxides
	-	-	Lowest SO_3
	-	-	Lowest K_2O
	-	-	Second highest MgO
PSD	Very high D(50)	Small D(50)	Small D(50)
XRD	High C3A for Class F Ash	Roughly same C3A content as FA-6	Increase in reactive content
		Highest brownmillerite	Most C3A content

The following are a series of hypotheses that were created to help propose a model to identify a fly ash's sulfate resistance more accurately. The results are discussed in the following chapter.

Looking individually at 20%, 30%, 40% fly ash replacement, and an average of all replacement percentages, a chart was created to identify if the fly ash passed or failed a test. Criteria used were proposed in the literature review or specifically developed/refined for the data presented. The graphs used to correlate testing to time to failure are shown below in Figure 70, Figure 71, Figure 72, and Figure 73. If an ash has yet to fail, the time to failure was plotted at 999 months for simplicity.

																		20%	30%	40%	Avg	20%	40%	20%	40%
	Test:	**XRF - CaO**	**XRF - sum of oxides**	**XRF-Fe2O3**	**XRF - SO3**	**PSD**	**XRD - reactive amts**	**XRD crystalline phases**				**Models**			**SEM**		**Reactivity**	**Calorimetry- Activation Energy**				**Timed Cal at 48 hours**			
	Criteria:	Class F (< 20%) is good	sum > 70% good	iron ~6% bad	increase is bad	small is bad	more reactive bad	C_3A bad	brownmillerite bad	periclase bad	free lime bad	Dunstan > 3 bad	Manz in region	ODF high bad	mullite good	100% SiO_2 cluster good for Class C ashes	Gel height bad	High AE bad				C_3A bad		Ettringite bad	
FA-ID	**20% Time to Failure**				SO_3 >1%	D(50) < 10	Total react > 15%	C_3A> 2.7%	brown >1.52%	peric >1.5%	lime > 0.2%	R > 2.3	flipped unaccep table	ODF > 0.9	gehlentite > 16.5%	cluster?	height > 30 mm	AE > 22000	AE> 22500	AE> 22500	AE> 25000	C_3A> 1.5%	C_3A>2 %	Ett>6 %	Ett>7 %
FA-18	3 months	fail	fail	fail	fail	fail	fail	fail	fail	fail	fail	fail	fail	fail	fail	fail	fail	fail	fail	fail	fail	fail	fail	fail	fail
FA-14	4 months	fail	fail	fail	fail	pass	fail	fail	fail	pass	pass	fail	fail	fail	fail	fail	fail	fail	fail	fail	fail	-	-	-	-
FA-4	6 months	pass	pass	pass	pass	pass	pass	pass	pass	pass	pass	pass	pass	pass	pass	-	pass	pass	pass	pass	pass	pass	pass	pass	pass
FA-7	6 months	pass	pass	pass	pass	fail	pass	pass	pass	pass	pass	pass	pass	pass	fail	-	pass	pass	pass	pass	pass	-	-	-	-
FA-9	6 months	fail	fail	pass	fail	fail	fail	fail	fail	pass	fail	fail	fail	pass	pass	fail	fail	pass	fail	pass	pass	fail	fail	fail	fail
FA-10	6 months	fail	fail	pass	pass	fail	fail	fail	fail	fail	fail	fail	fail	pass	fail	fail	fail	fail	fail	fail	fail	-	-	-	-
FA-15	6 months	fail	fail	fail	fail	fail	fail	fail	fail	fail	fail	fail	fail	pass	fail	fail	fail	fail	pass	pass	pass	fail	fail	fail	fail
FA-16	6 months	fail	fail	fail	fail	pass	fail	pass	fail	fail	fail	fail	fail	pass	-	-	fail	fail	fail	fail	fail	-	-	-	-
FA-1	9 months	pass	pass	pass	pass	pass	pass	pass	pass	pass	pass	pass	pass	pass	pass	-	pass	pass	pass	pass	pass	-	-	-	-
FA-3	9 months	pass	pass	pass	pass	pass	pass	pass	pass	pass	pass	pass	pass	pass	pass	-	pass	pass	pass	pass	pass	pass	pass	pass	pass
FA-13	9 months	fail	fail	pass	fail	fail	fail	fail	pass	pass	fail	fail	fail	pass	fail	pass	fail	fail	fail	fail	fail	fail	fail	pass	pass
FA-5	12 months	pass	fail	pass	pass	pass	pass	pass	pass	pass	pass	pass	pass	pass	fail	-	fail	pass	pass	pass	pass	-	-	-	-
FA-6	12 months	pass	pass	pass	pass	pass	pass	pass	pass	pass	pass	pass	pass	pass	pass	-		pass	pass	pass	pass	-	-	-	-
FA-11	12 months	fail	fail	pass	fail	fail	fail	fail	fail	fail	fail	fail	fail	pass	pass	pass	fail	fail	fail	fail	fail	fail	fail	pass	pass
FA-8	15 months	pass	fail	pass	fail	pass	pass	pass	pass	pass	pass	pass	fail	fail	pass	-	fail	pass	pass	pass	pass	-	-	-	-
FA-2	999 months	pass	pass	pass	pass	pass	pass	pass	pass	pass	pass	pass	pass	pass	-	-	pass	pass	pass	pass	pass	-	-	-	-

Figure 70: Proposal Criteria for 20% Fly Ash Replacement

																			20%	30%	40%	Avg	20%	40%	20%	40%
	Test:	**XRF - CaO**	**XRF - sum of oxides**	**XRF- Fe2O3**	**XRF - SO3**	**PSD**	**XRD - reactive amts**	**XRD crystalline phases**				**Models**			**SEM**		**Reactivity**	**Calorimetry- Activation Energy**				**Timed Cal at 48 hours**			
	Criteria:	Class F (< 20%) is good	sum > 70% good	iron ~6% bad	increase is bad	small is bad	more reactive bad	C_3A bad	brown bad	periclase bad	free lime bad	Dunstan > 3 bad	Manz in region	ODF high bad	mullite good	100% SiO_2 cluster good for Class C ashes	Gel height bad	High AE bad				C3A bad		Ettringite bad	
FA-ID	**30% Time to Failure**				SO_3 >1%	D(50) < 10	Total react > 15%	C_3A> 2.7%	brown >1.2%	peric >1.5%	lime > 0.2%	R > 2.3	flipped unacceptable	ODF > 0.9	gehlentite > 16.5%	cluster?	height > 30 mm	AE > 22000	AE> 22500	AE> 22500	AE> 25000	C_3A> 1.5%	C_3A>2 %	Ett>6 %	Ett>7 %
FA-14	2 months	fail	fail	fail	fail	pass	fail	fail	fail	pass	pass	fail	fail	fail	fail	fail	fail	fail	fail	fail	fail	-	-	-	-
FA-15	3 months	fail	fail	fail	fail	fail	fail	fail	fail	fail	fail	fail	fail	pass	fail	fail	fail	fail	pass	pass	pass	fail	fail	fail	fail
FA-18	3 months	fail	fail	fail	fail	fail	fail	fail	fail	fail	fail	fail	fail	fail	fail	fail	fail	fail	fail	fail	fail	fail	fail	fail	fail
FA-16	4 months	fail	fail	fail	fail	pass	fail	pass	fail	fail	fail	fail	fail	pass	-	-	fail	fail	fail	fail	fail	-	-	-	-
FA-7	6 months	pass	pass	pass	pass	fail	pass	pass	fail	pass	pass	pass	pass	pass	fail	-	pass	pass	pass	pass	pass	-	-	-	-
FA-2	9 months	pass	pass	pass	pass	pass	pass	pass	pass	pass	pass	pass	pass	pass	-	-	pass	pass	pass	pass	pass	-	-	-	-
FA-3	9 months	pass	pass	pass	pass	pass	pass	pass	pass	pass	pass	pass	pass	pass	pass	-	pass	pass	pass	pass	pass	pass	pass	pass	pass
FA-9	9 months	fail	fail	pass	fail	fail	fail	fail	fail	pass	fail	fail	fail	pass	pass	fail	fail	pass	fail	pass	pass	fail	fail	fail	fail
FA-10	9 months	fail	fail	pass	pass	fail	fail	fail	fail	fail	fail	fail	fail	pass	fail	fail	fail	fail	fail	fail	fail	-	-	-	-
FA-5	12 months	pass	fail	pass	pass	pass	pass	pass	pass	pass	pass	pass	pass	pass	fail	-	fail	pass	pass	pass	pass	-	-	-	-
FA-11	12 months	fail	fail	pass	fail	fail	fail	fail	fail	fail	fail	fail	fail	pass	pass	pass	fail	fail	fail	fail	fail	fail	fail	pass	pass
FA-13	12 months	fail	fail	pass	fail	fail	fail	fail	fail	pass	fail	fail	fail	pass	fail	pass	fail	fail	fail	fail	fail	fail	fail	pass	pass
FA-8	999 months	pass	fail	pass	fail	pass	pass	pass	pass	pass	pass	pass	fail	fail	pass	-	fail	pass	pass	pass	pass	-	-	-	-

Figure 71: Proposal Criteria for 30% Fly Ash Replacement

																			20%	30%	40%	Avg	20%	40%	20%	40%
	Test:	**XRF - CaO**	**XRF - sum of oxides**	**XRF-Fe2O3**	**XRF - SO3**	**PSD**	**XRD - reactive amts**	**XRD crystalline phases**				**Models**			**SEM**		**Reactivity**	**Calorimetry- Activation Energy**				**Timed Cal at 48 hours**			
	Criteria:	Class F (< 20%) is good	sum > 70% good	iron ~6% bad	increase is bad	small is bad	more reactive bad	C_3A bad	brown bad	periclase bad	free lime bad	Dunstan > 3 bad	Manz in region	ODF high bad	mullite good	100% SiO_2 cluster good for Class C ashes	Gel height bad	High AE bad				C3A bad		Ettringite bad	
FA-ID	**40% Time to Failure**				SO_3 >1%	D(50) < 10	Total react > 15%	C_3A> 2.7%	brown >1.2%	peric >1.5%	lime > 0.2%	R > 2.3	flipped unacceptable	ODF > 0.9	gehlentite > 16.5%	cluster?	height > 30 mm	AE > 22000	AE> 22500	AE> 22500	AE> 25000	C_3A> 1.5%	C_3A>2 %	Ett>6 %	Ett>7 %
FA-18	2 months	fail	fail	fail	fail	fail	fail	fail	fail	fail	fail	fail	fail	fail	fail	fail	fail	fail	fail	fail	fail	fail	fail	fail	fail
FA-15	4 months	fail	fail	fail	fail	fail	fail	fail	fail	fail	fail	fail	fail	pass	fail	fail	fail	fail	pass	pass	pass	fail	fail	fail	fail
FA-16	4 months	fail	fail	fail	fail	pass	fail	pass	fail	fail	fail	fail	fail	pass	-	-	fail	fail	fail	fail	fail	-	-	-	-
FA-10	6 months	fail	fail	pass	pass	fail	fail	fail	fail	fail	fail	fail	fail	pass	fail	fail	fail	fail	fail	fail	fail	-	-	-	-
FA-11	6 months	fail	fail	pass	fail	fail	fail	fail	fail	fail	fail	fail	fail	pass	pass	pass	fail	fail	fail	fail	fail	fail	fail	pass	pass
FA-14	6 months	fail	fail	fail	fail	pass	fail	fail	fail	pass	pass	fail	fail	fail	fail	fail	fail	fail	fail	fail	fail	-	-	-	-
FA-9	9 months	fail	fail	pass	fail	fail	fail	fail	fail	pass	fail	fail	fail	pass	pass	fail	fail	pass	fail	pass	pass	fail	fail	fail	fail
FA-13	9 months	fail	fail	pass	fail	fail	fail	fail	pass	pass	fail	fail	fail	pass	fail	pass	fail	fail	fail	fail	fail	fail	fail	pass	pass
FA-5	12 months	pass	fail	pass	pass	pass	pass	pass	pass	pass	pass	pass	pass	pass	fail	-	fail	pass	pass	pass	pass	-	-	-	-
FA-2	999 months	pass	pass	pass	pass	pass	pass	pass	pass	pass	pass	pass	pass	pass	-	-	pass	pass	pass	pass	pass	-	-	-	-
FA-7	999 months	pass	pass	pass	pass	fail	pass	pass	pass	pass	pass	pass	pass	pass	fail	-	pass	pass	pass	pass	pass	-	-	-	-
FA-8	999 months	pass	fail	pass	fail	pass	pass	pass	pass	pass	pass	pass	fail	fail	pass	-	fail	pass	pass	pass	pass	-	-	-	-

Figure 72: Proposal Criteria for 40% Fly Ash Replacement

																		20%	30%	40%	Avg	20%	40%	20%	40%
	Test:	**XRF - CaO**	**XRF - sum of oxides**	**XRF- Fe2O3**	**XRF - SO3**	**PSD**	**XRD - reactive amts**	**XRD crystalline phases**				**Models**			**SEM**		**Reactivity**	**Calorimetry- Activation Energy**				**Timed Cal at 48 hours**			
	Criteria:	Class F (< 20%) is good	sum > 70% good	iron ~6% bad	increase is bad	small is bad	more reactive bad	C_3A bad	brown bad	periclase bad	free lime bad	Dunstan > 3 bad	Manz in region	ODF high bad	mullite good	100% SiO_2 cluster good for Class C ashes	Gel height bad	High AE bad				C3A bad		Ettringite bad	
FA-ID	**Avg. Time to Failure**				SO_3 >1%	D(50) < 10	Total react > 15%	C_3A> 2.7%	brown >1.2%	peric >1.5%	lime > 0.2%	R > 2.3	flipped unacceptable	ODF > 0.9	gehlentite > 16.5%	cluster?	height > 30 mm	AE > 22000	AE> 22500	AE> 22500	AE> 25000	C_3A> 1.5%	C_3A>2 %	Ett>6 %	Ett>7 %
FA-18	2.8 months	fail	fail	fail	fail	fail	fail	fail	fail	fail	fail	fail	fail	fail	fail	fail	fail	fail	fail	fail	fail	fail	fail	fail	fail
FA-16	4.0 months	fail	fail	fail	fail	pass	fail	pass	fail	fail	fail	fail	fail	pass	-	-	fail	fail	fail	fail	fail	-	-	-	-
FA-14	4.0 months	fail	fail	fail	fail	pass	fail	fail	fail	pass	pass	fail	fail	fail	fail	fail	fail	fail	fail	fail	fail	-	-	-	-
FA-15	4.5 months	fail	fail	fail	fail	fail	fail	fail	fail	fail	fail	fail	fail	pass	fail	fail	fail	fail	pass	pass	pass	fail	fail	fail	fail
FA-7	5.3 months	pass	pass	pass	pass	fail	pass	pass	pass	pass	pass	pass	pass	pass	fail	-	pass	pass	pass	pass	pass	-	-	-	-
FA-9	7.2 months	fail	fail	pass	fail	fail	fail	fail	fail	pass	fail	fail	fail	pass	pass	fail	fail	pass	fail	pass	pass	fail	fail	fail	fail
FA-10	9.0 months	fail	fail	pass	pass	fail	fail	fail	fail	fail	fail	fail	fail	pass	fail	fail	fail	fail	fail	fail	fail	-	-	-	-
FA-11	9.6 months	fail	fail	pass	fail	fail	fail	fail	fail	fail	fail	fail	fail	pass	pass	pass	fail	fail	fail	fail	fail	fail	fail	pass	pass
FA-13	10.2 months	fail	fail	pass	fail	fail	fail	fail	pass	pass	fail	fail	fail	pass	fail	pass	fail	fail	fail	fail	fail	fail	fail	pass	pass
FA-4	12.0 months	pass	pass	pass	pass	pass	pass	pass	pass	pass	pass	pass	pass	pass	pass	-	pass	pass	pass	pass	pass	pass	pass	pass	pass
FA-5	12.0 months	pass	fail	pass	pass	pass	pass	pass	pass	pass	pass	pass	pass	pass	fail	-	fail	pass	pass	pass	pass	-	-	-	-
FA-1	13.5 months	pass	pass	pass	pass	pass	pass	pass	pass	pass	pass	pass	pass	pass	pass	-	pass	pass	pass	pass	pass	-	-	-	-
FA-6	15.0 months	pass	pass	pass	pass	pass	pass	pass	pass	pass	pass	pass	pass	pass	pass	-		pass	pass	pass	pass	-	-	-	-
FA-3	339.0 months	pass	pass	pass	pass	pass	pass	pass	pass	pass	pass	pass	pass	pass	pass	-	pass	pass	pass	pass	pass	pass	pass	pass	pass
FA-2	669.0 months	pass	pass	pass	pass	pass	pass	pass	pass	pass	pass	pass	pass	pass	-	-	pass	pass	pass	pass	pass	-	-	-	-
FA-8	671.0 months	pass	fail	pass	fail	pass	pass	pass	pass	pass	pass	pass	fail	fail	pass	-	fail	pass	pass	pass	pass	-	-	-	-

Figure 73: Proposal Criteria for Average of 20%, 30%, and 40% Fly Ash Replacement

Looking through these charts with the time to failure data, tests were eliminated that produced an inaccurate outcome or were approved if a test accurately predicted sulfate performance. Based on this method, the following steps are proposed to identify a fly ash's acceptable or unacceptable use in a sulfate environment:

1. Find the sum of the oxide (SiO_2 + Al_2O_3 + Fe_2O_3) content. If this sum is greater than 70%, the ash will have good sulfate resistance. If the sum is less than 70%, the ash has poor sulfate resistance. This step essentially groups the ashes in the Class F or Class C groups.
2. Of the remaining unacceptable ashes, calculate Dunstan's R-factor. If the R-factor is greater than 2.3, the ash will have poor performance. If the R-factor is less than 2.3, it is acceptable for use in a sulfate performance. The total reactive percentage from Rietveld XRD can also be used in this step instead of Dunstan's R-factor. If the total reactive percentage is greater than 15%, the ash will have poor sulfate performance. If the reactive components are less than 15%, the ash will have good resistance to sulfate attack.
3. For the remaining Class C ashes deemed unacceptable for use in a sulfate environment, plot the amorphous phases identified through SEM on ternary diagram #1. If any Class C ashes have a cluster of amorphous particles at 100% SiO_2 apex, they will have good resistance. The remaining Class C ashes with no cluster at this location will have poor performance.

This combination of three tests most accurately covers the performance of a wide range of ashes. The sum of oxide step referenced above was included because it generally does an accurate job of combing through the majority of ashes and

determining their acceptability in a sulfate environment. This test does not accurately predict the behavior of high alkali fly ashes though, so step two was introduced. Both Dunstan's R-factor with a revised limit of 2.3 rather than the initially proposed 3 and the total crystalline reactive amount calculation limit predict the performance of high alkali ashes. These two tests had the exact same outcome for all ashes studied and for all replacement percentages. The third step was introduced because there were some Class C ashes in this study that had acceptable expansion limits and a cluster of 100% SiO_2 amorphous particles. These three tests address the chemical make-up of the ash itself with XRF analysis, reactive crystalline phases in the fly ash through Rietveld XRD, and amorphous content of the ash. Dunstan's model was initially criticized for lacking phases responsible for ettringite formation, so this model includes the role of those reactive phases. Other critics stated the glassy phase was responsible for sulfate resistance, so amorphous content was included in this model as well.

The tests not included were the timed calorimeter microstructural development studies specifically related to ettringite formation at 48 hours. These results accurately predicted performance for 20% and 40% replacement; however, these tests were only run on a select number of samples and cannot be correlated with all of the sulfate data. In addition, the inclusions of XRD phase percentages alone as a screening tool were deemed unacceptable for use in these steps because the error in the Rietveld analysis, from 4-6%, was larger than most of the phase amounts identified. Dunstan's R-factor and the sum of total crystalline reactive percentage are calculated by using crystalline phase amounts, but many phases are included and error would be diminished. The sulfate immersion studies were not included in this model either due to the inconclusive findings of the post-sulfate

immersion results with those of Dhole and the University of New Brunswick. The pre-sulfate immersion results seemed to be an indicator of sulfate performance, but more work is needed to fully comprehend and rely on the results.

Chapter 8: Conclusion

8.1 Summary of Project

It is widely understood that the addition of some fly ashes improve the sulfate resistance of the concrete, but some fly ash additions actually reduce the sulfate resistance. This project aimed to understand this relationship between fly ash and sulfate resistance. Using sulfate testing results previously performed at The University of Texas at Austin, a wide variety of physical and advanced chemical characterization techniques were performed in order to understand the role of fly ash in the sulfate resistance of concrete.

8.2 Conclusions

The most important conclusions from the testing program are presented below:

- A greater percentage of reactive crystalline phases lead to poor sulfate resistance after RQXRD analysis.
- It was found in SEM testing that reactive calcium aluminosilicate glass was responsible for poor sulfate resistance.
- For Class C ashes, the presence of a cluster at the 100% SiO_2 apex of ternary diagram #1 improved the ash's sulfate resistance.
- In the reactivity test, if the gel height exceeded 30 mm, the ash was considered reactive and would have poor sulfate resistance.
- The higher activation energies tended to correspond to poor sulfate resistance from calorimeter studies.
- An increase in ettringite and C_3A formation resulted in shorter time to failure in microstructural development studies.

- In the sulfate immersion studies, the Class C ashes, which had poor sulfate resistance, had more monosulfate formed prior to sulfate immersion, and the Class F ashes, which had good sulfate resistance, formed more ettringite initially.

Overall, the chemistry of the ash, the reactive crystalline phases, and the amorphous content must be considered in order to most accurately predict the sulfate resistance of a fly ash. A three step process was proposed in Chapter 7 outlying the necessary steps to properly predict the performance of all ashes, including high alkali and Class C ashes. These steps are as follows:

1. Find the sum of the oxide (SiO_2 + Al_2O_3 + Fe_2O_3) content. If this sum is greater than 70%, the ash will have good sulfate resistance.
2. Of the remaining unacceptable ashes, calculate Dunstan's R-factor. If the R-factor is less than 2.3, it is acceptable for use in a sulfate performance. The total reactive percentage from Rietveld XRD can also be used in this step instead of Dunstan's R-factor. If the reactive components are less than 15%, the ash will have good resistance to sulfate attack.
3. For the remaining Class C ashes deemed unacceptable for use in a sulfate environment, plot the amorphous phases identified through SEM on ternary diagram #1. If any Class C ashes have a cluster of amorphous particles at 100% SiO_2 apex, they will have good resistance.

8.3 FUTURE WORK

The work performed in this thesis was limited to a year duration, limiting the analysis needed for full understanding of fly ash and sulfate attack. The following work

is recommended to increase knowledge on fly ash and its effects on sulfate resistance and to fill in missing gaps in existing understandings:

1. Continue this analysis on more fly ashes with a wide range of compositions, including other high alkali ashes.
2. Perform all of the testing for a sulfate solution other than sodium sulfate. Re-run ASTM C1012 expansions tests and compare the different sulfate solution results with the sodium sulfate results presented in this thesis.
3. Perform more detailed SEM analysis including elemental maps for multi-spectral image analysis (MSIA). This data can be used for better understanding of the glassy phases.
4. Re-analyze hydration products after immersion to different sulfate immersion. Focus specifically on the formation of ettringite after immersion to sulfates to either confirm or refute the findings of Dhole and this research.
5. Continue refining previously proposed models and the steps presented in this thesis to more accurately predict a fly ash's sulfate resistance.

Appendix A: XRF Trends

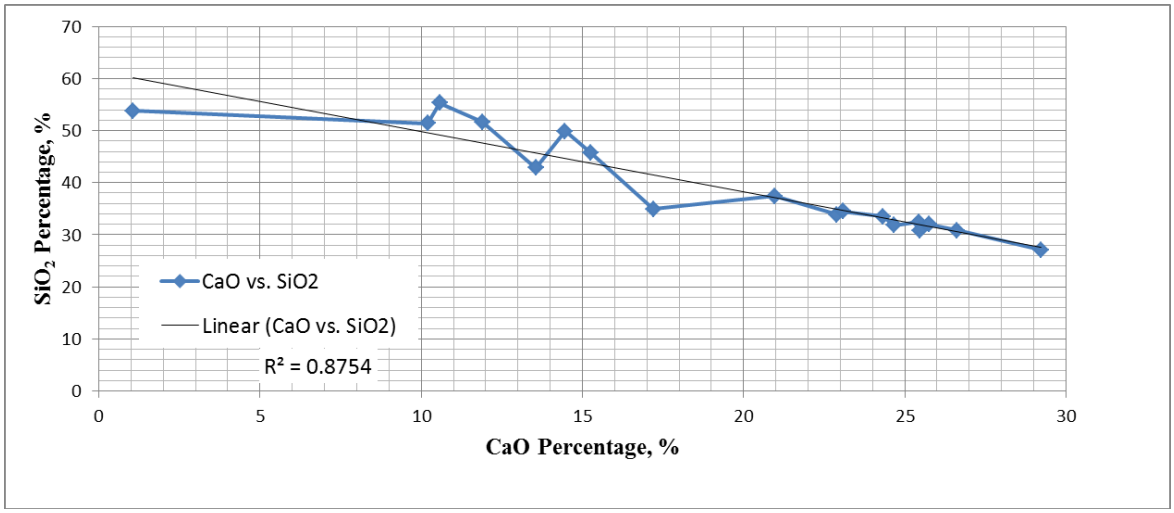

Figure A-1: CaO vs. SiO_2 Relationship

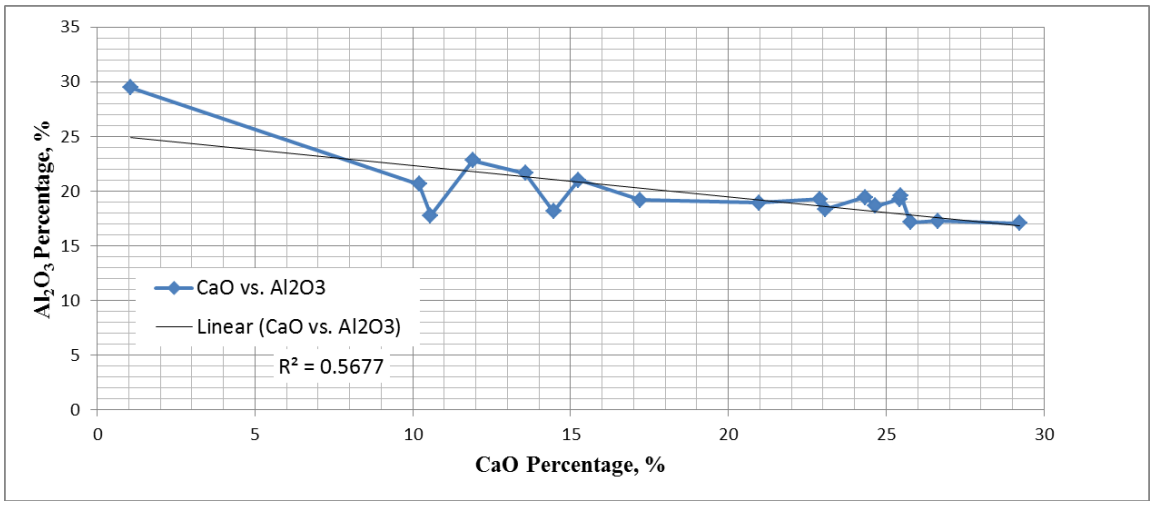

Figure A-2: CaO vs. Al_2O_3 Relationship

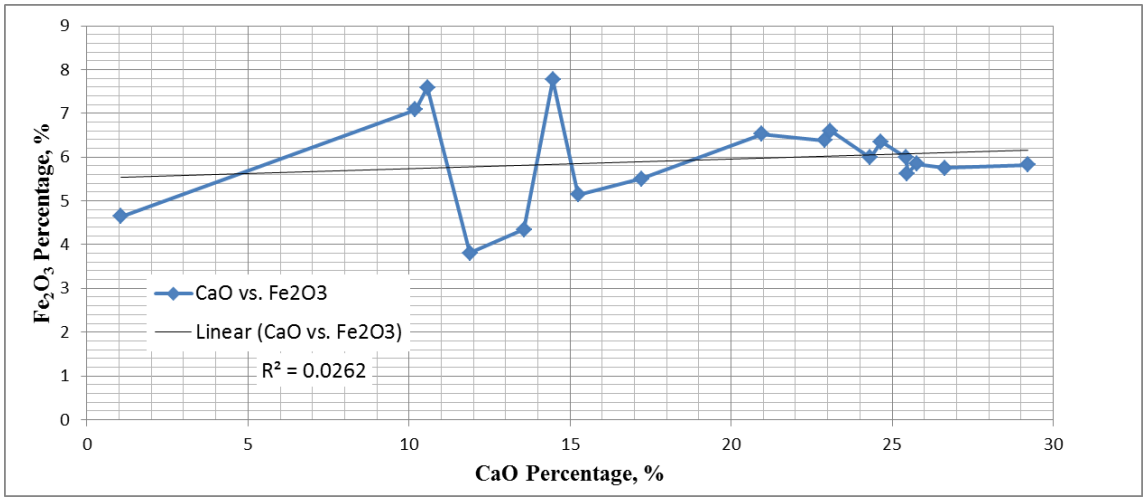

Figure A-3: CaO vs. Fe_2O_3 Relationship

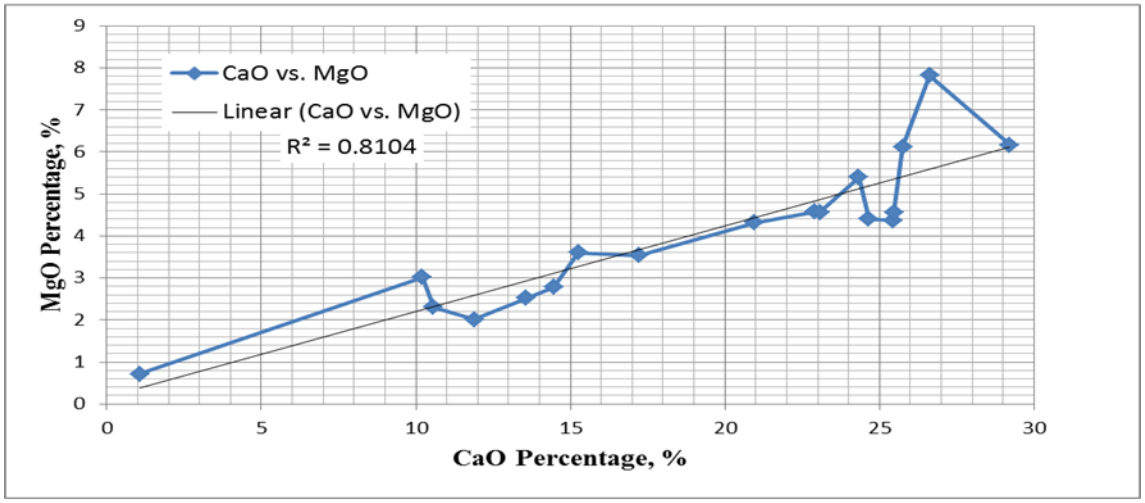

Figure A-4: CaO vs. MgO Relationship

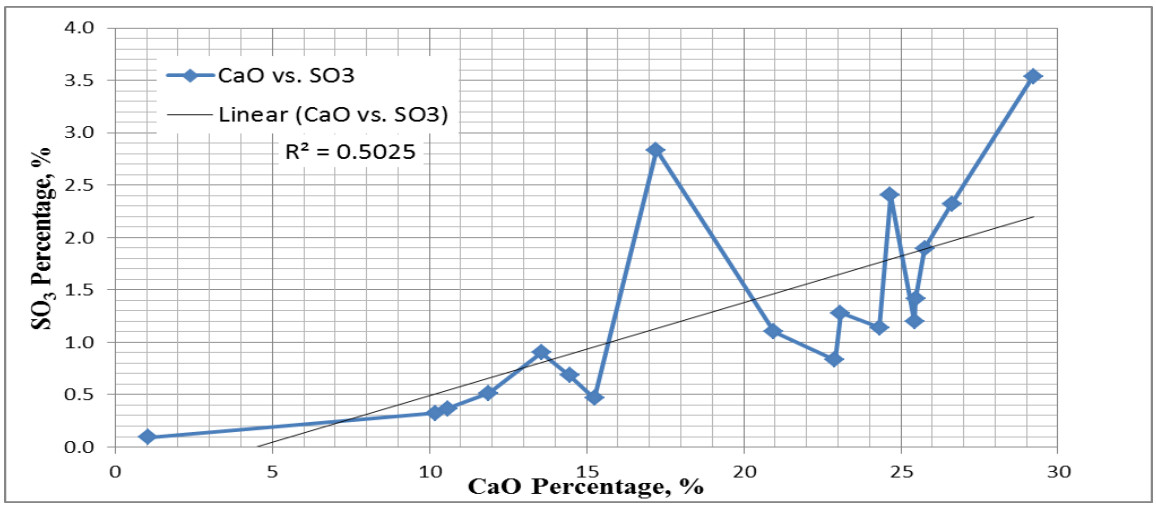

Figure A-5: CaO vs. SO_3 Relationship

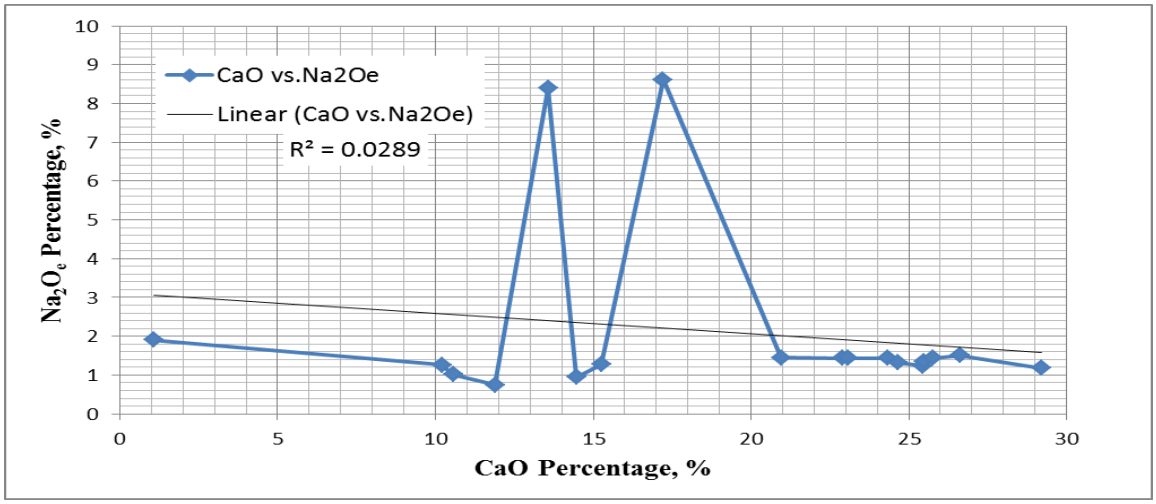

Figure A-6: CaO vs. Na_2O_e Relationship

Appendix B: ASTM C1012 Testing Results

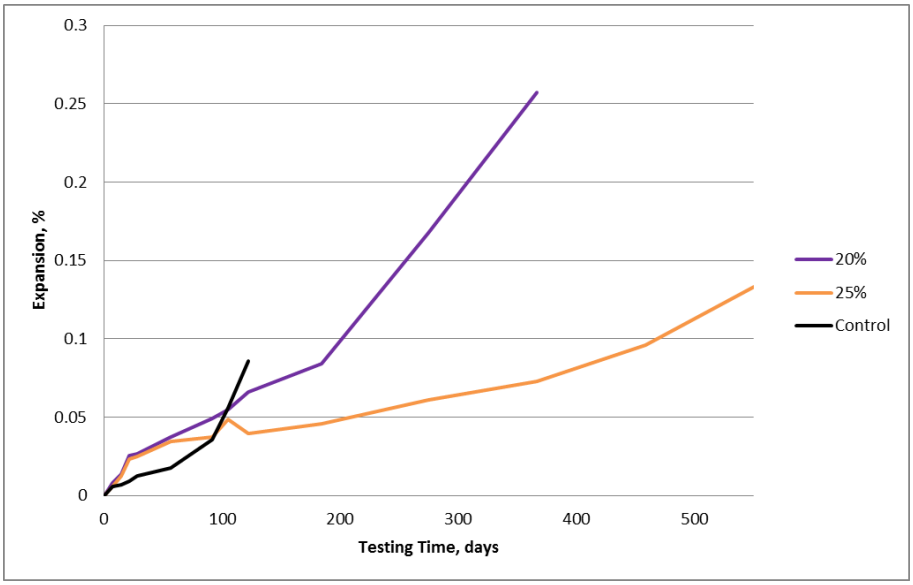

Figure B-1: FA-1 ASTM C1012 Expansions

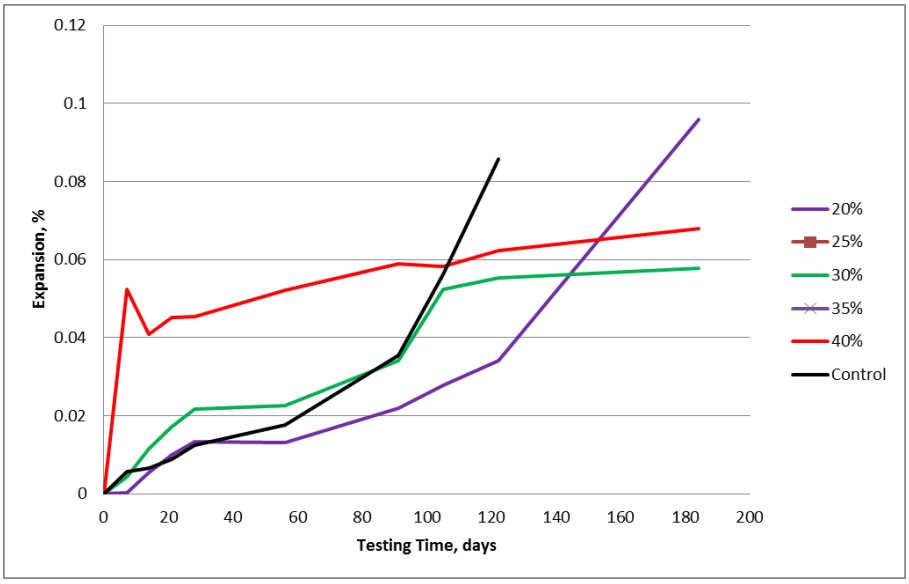

Figure B-2: FA-2 ASTM C1012 Expansions

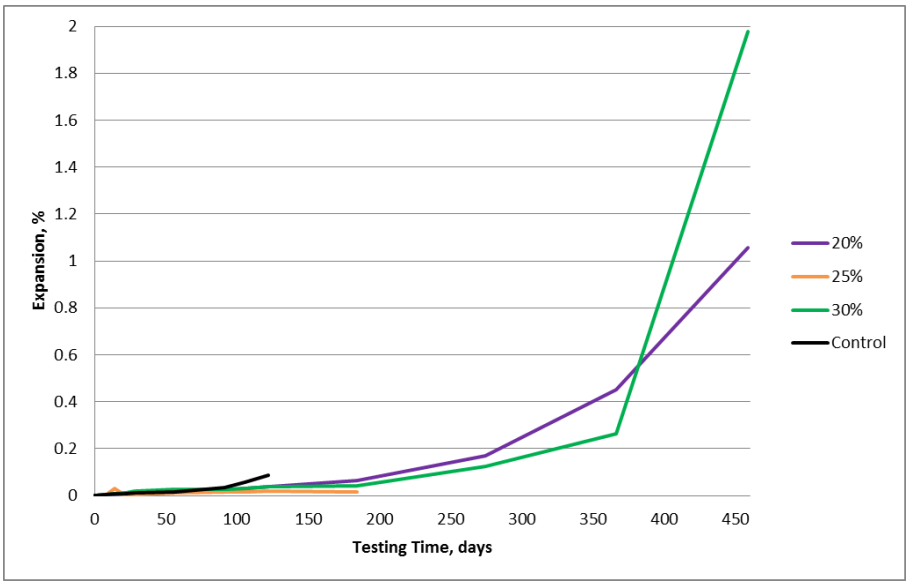

Figure B-3: FA-3 ASTM C1012 Expansions

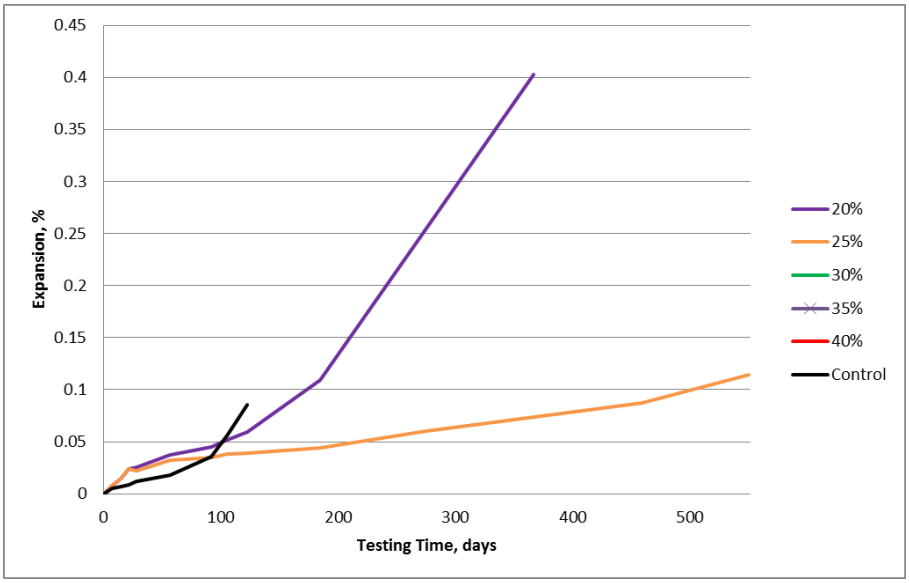

Figure B-4: FA-4 ASTM C1012 Expansions

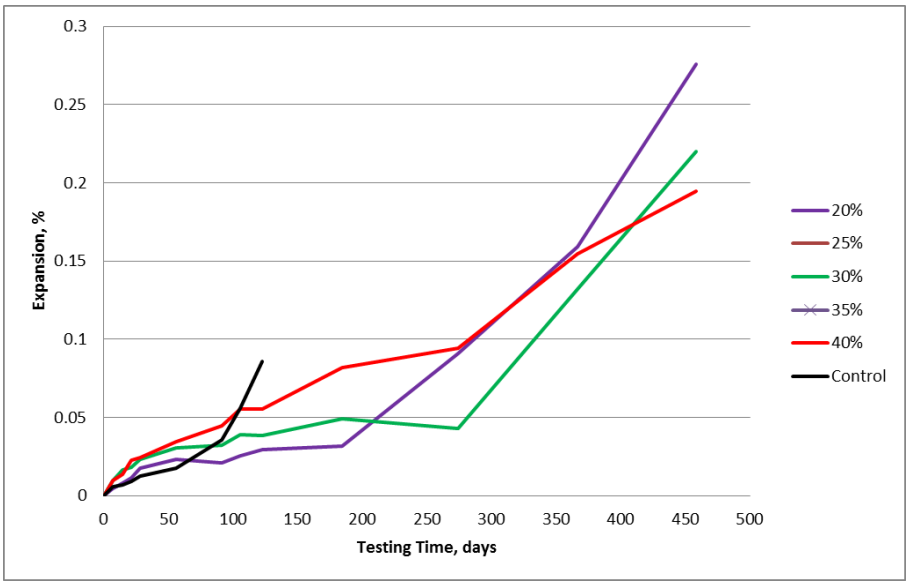

Figure B-5: FA-5 ASTM C1012 Expansions

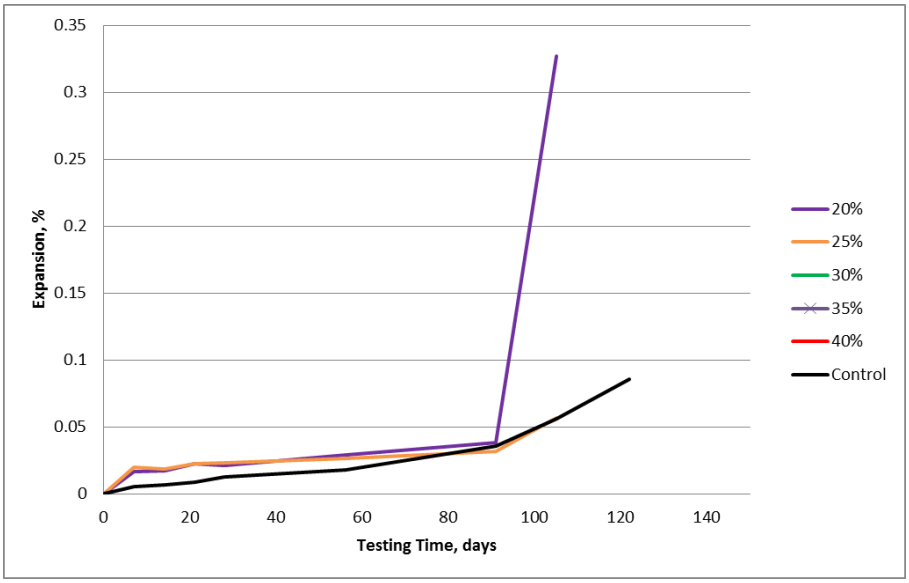

Figure B-6: FA-6 ASTM C1012 Expansions

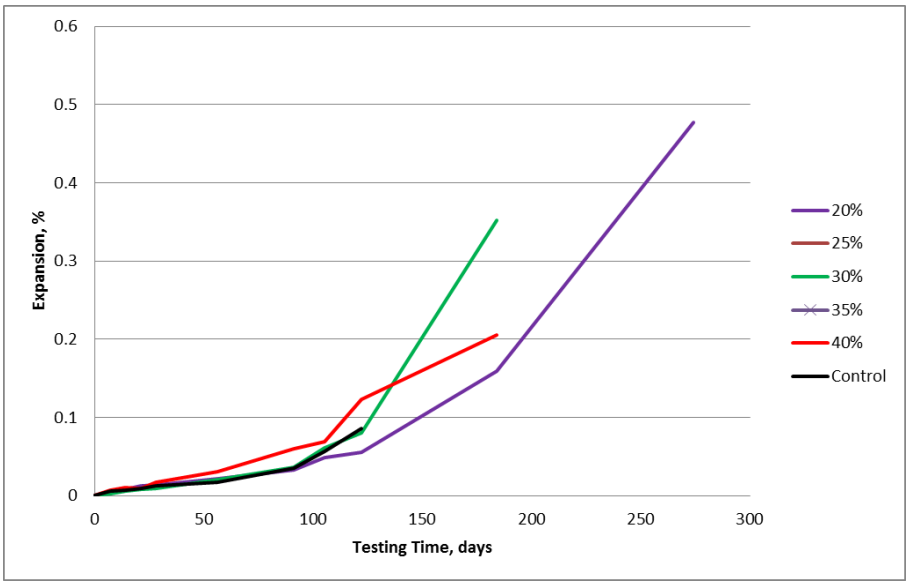

Figure B-7: FA-7 ASTM C1012 Expansions

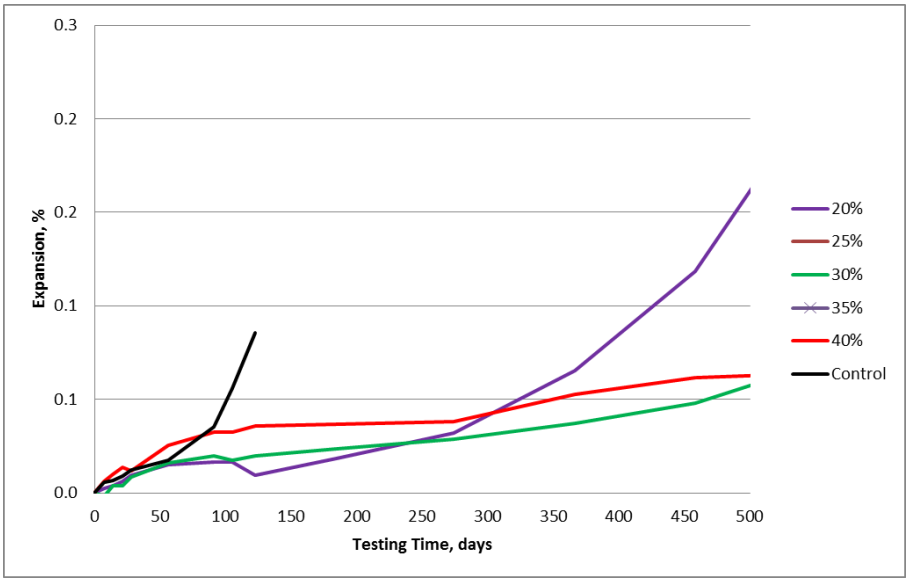

Figure B-8: FA-8 ASTM C1012 Expansions

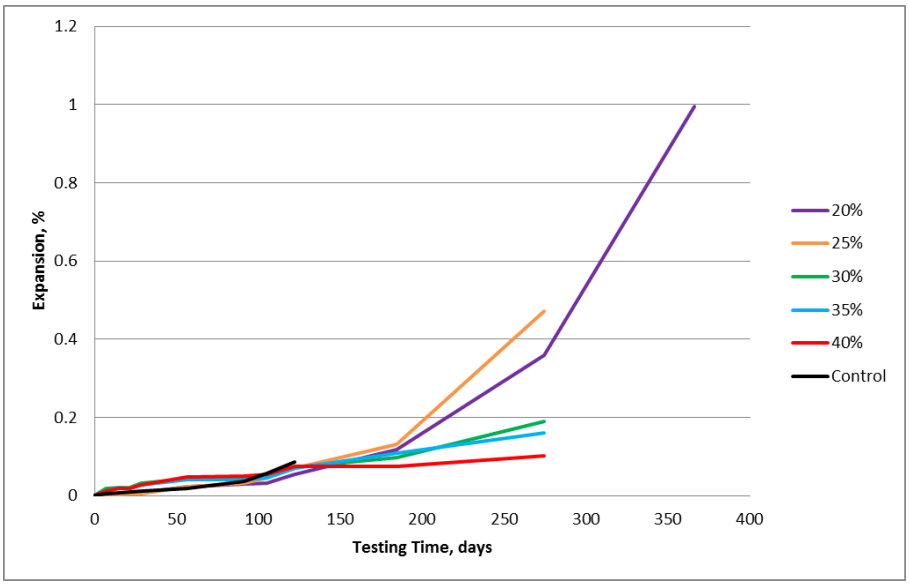

Figure B-9: FA-9 ASTM C1012 Expansions

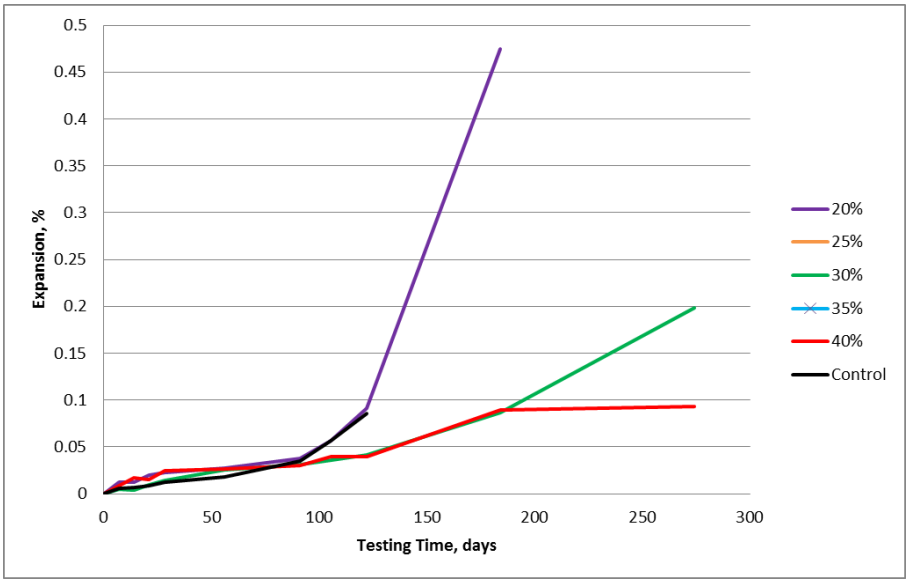

Figure B-10: FA-10 ASTM C1012 Expansions

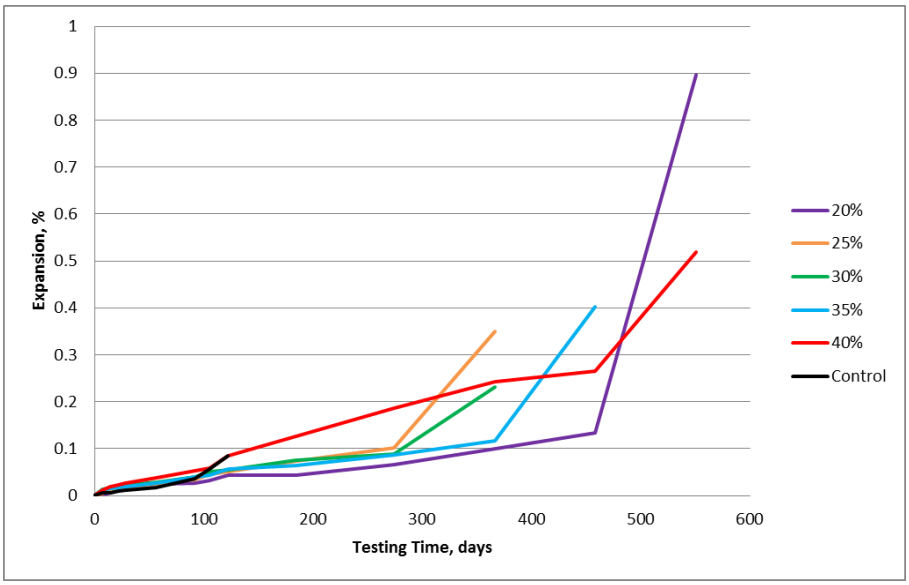

Figure B-11: FA-11 ASTM C1012 Expansions

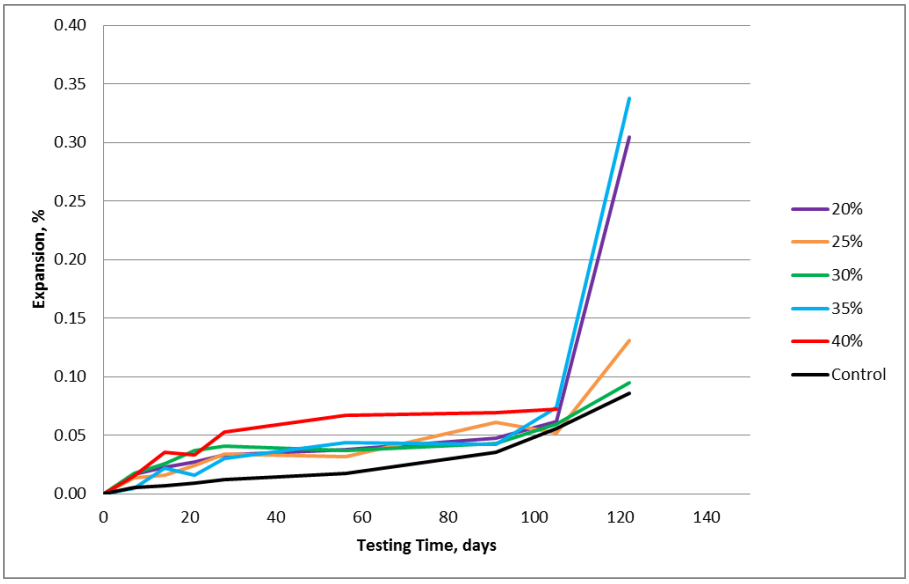

Figure B-12: FA-13 ASTM C1012 Expansions

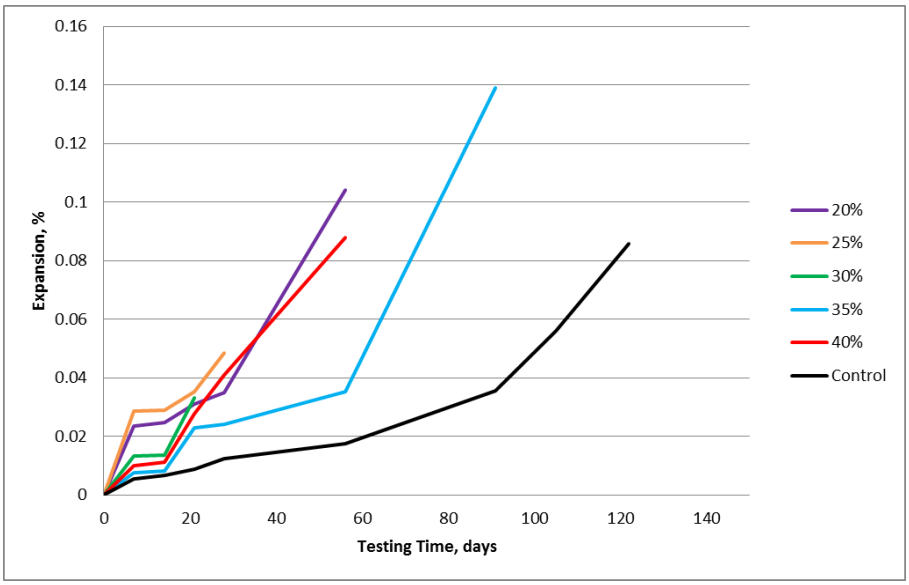

Figure B-13: FA-14 ASTM C1012 Expansions

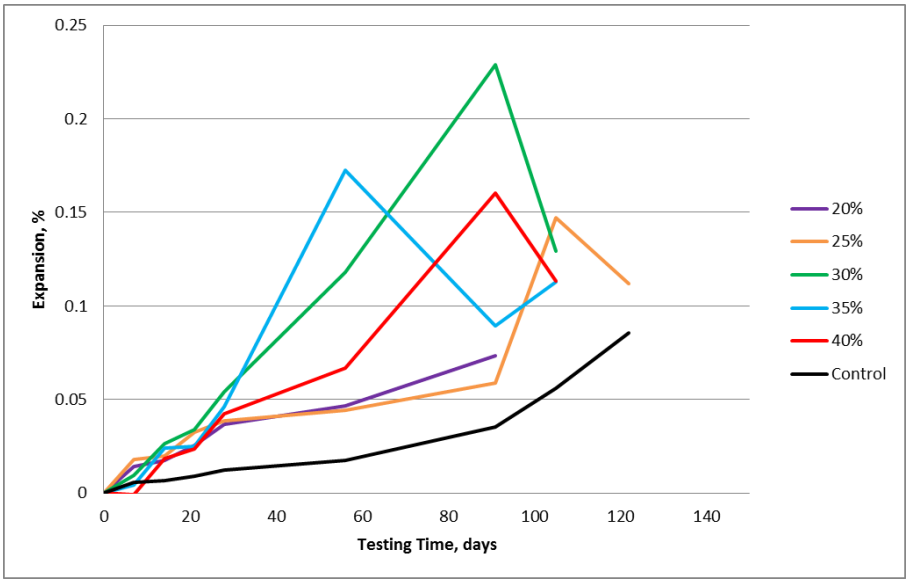

Figure B-14: FA-15 ASTM C1012 Expansions

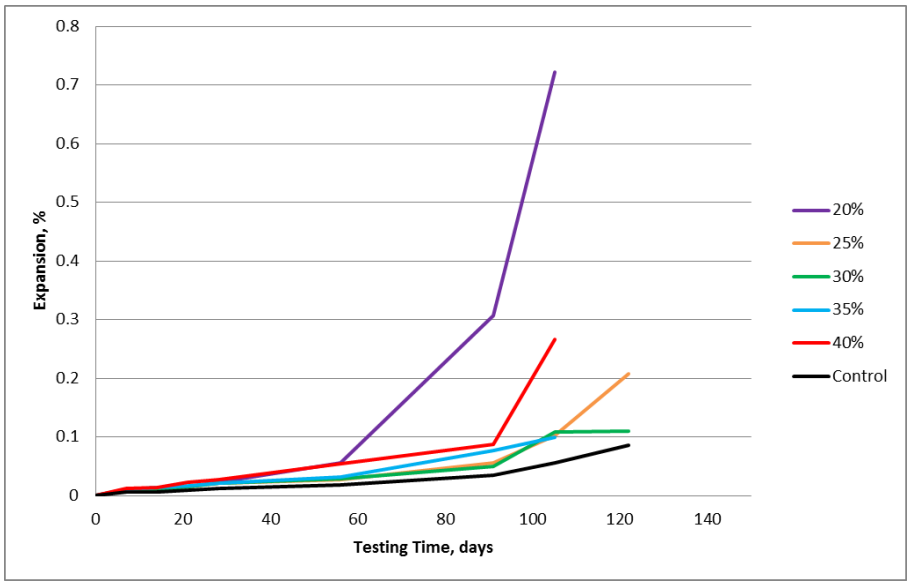

Figure B-15: FA-16 ASTM C1012 Expansions

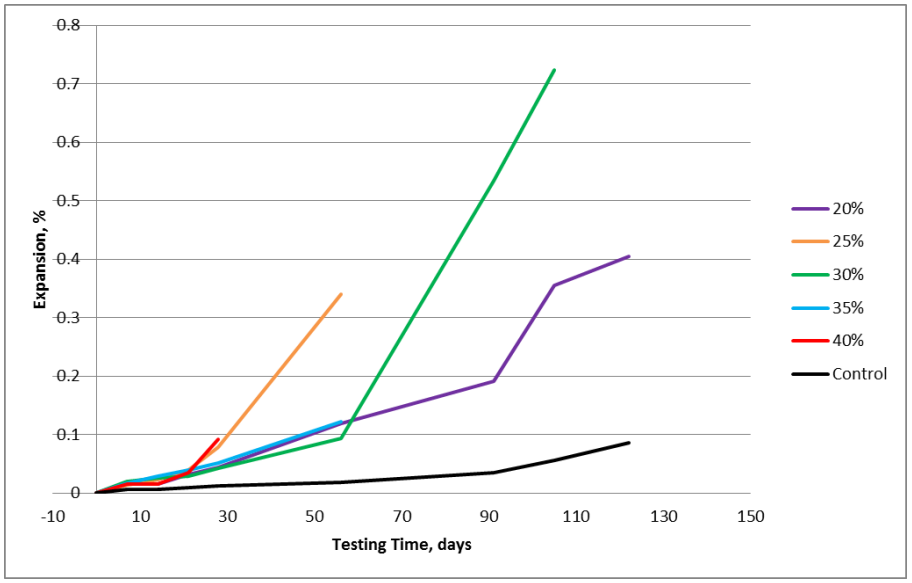

Figure B-16: FA-18 ASTM C1012 Expansions

Appendix C: Fly Ash Ternary Diagrams

Ternary diagrams #1 and #2 are presented in this appendix for all fly ashes investigated. The left diagram is diagram #1, and the right diagram is diagram #2.

- FA-1

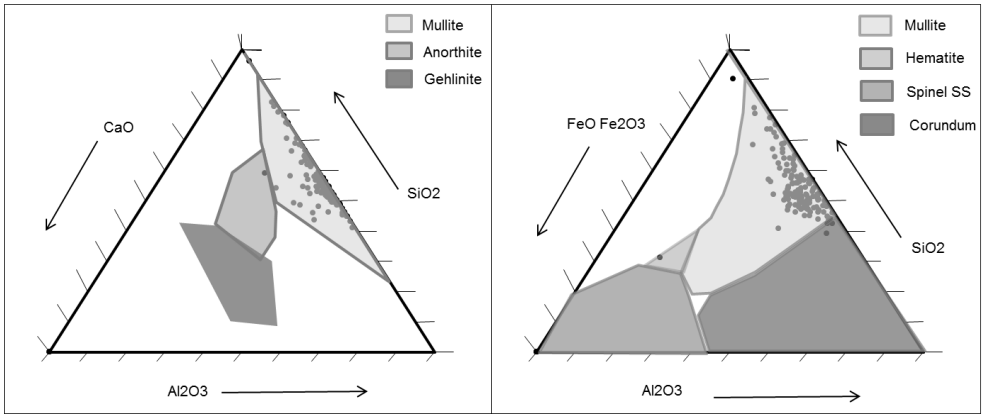

Figure C-1: FA-1 Ternary Diagrams

- FA-3

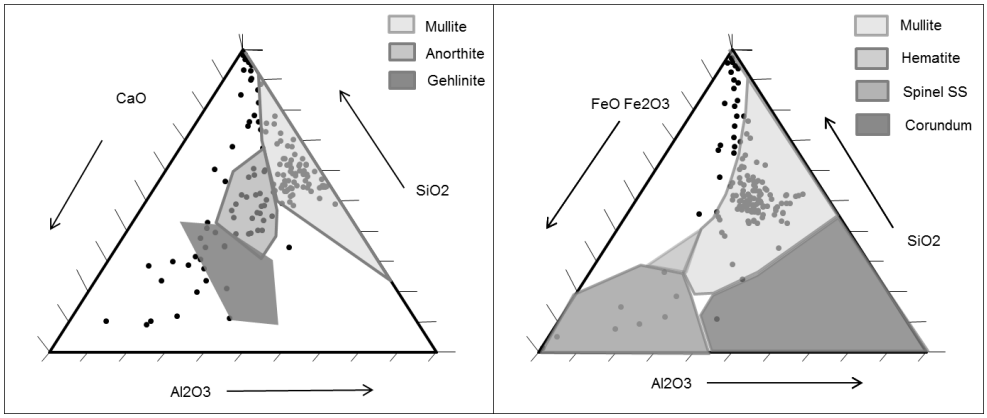

Figure C-2: FA-3 Ternary Diagrams

- FA-4

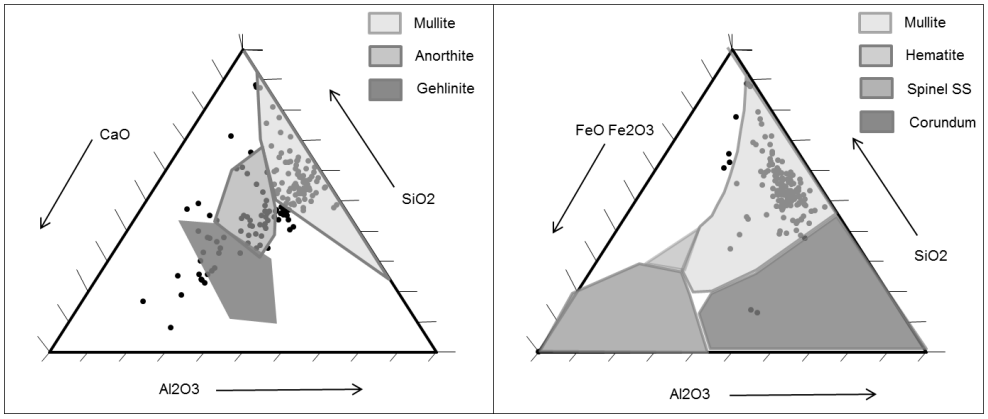

Figure C-3: FA-4 Ternary Diagrams

- FA-5

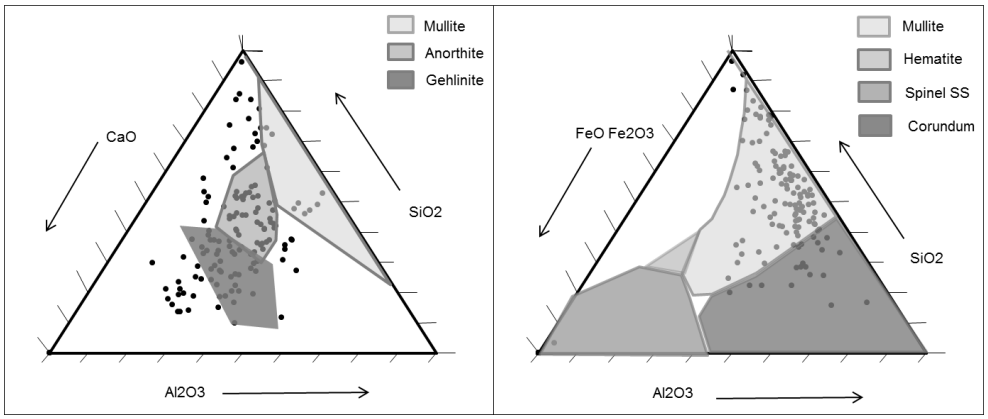

Figure C-4: FA-5 Ternary Diagrams

- FA-6

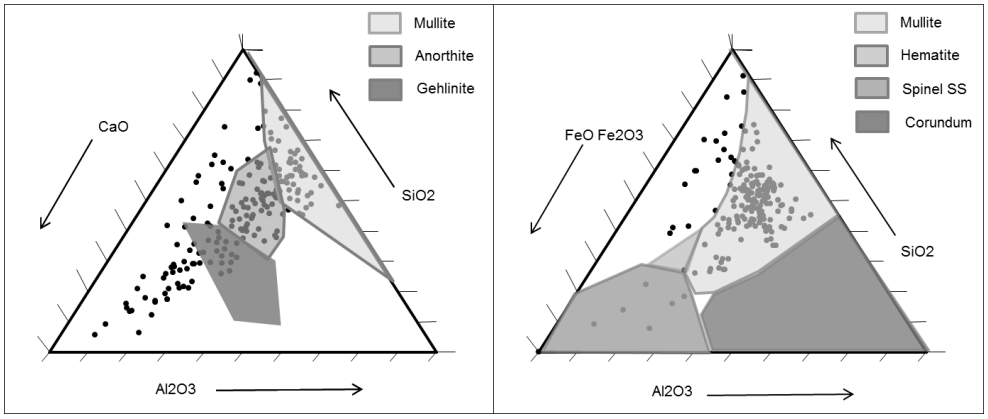

Figure C-5: FA-6 Ternary Diagrams

- FA-7

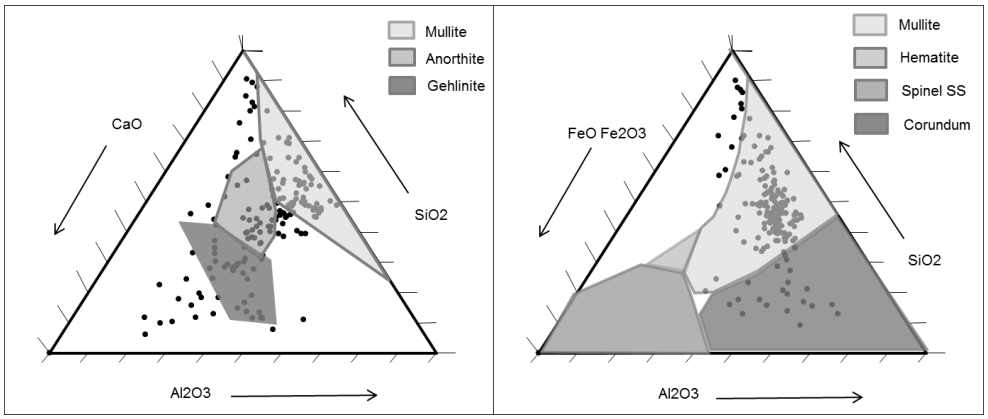

Figure C-6: FA-7 Ternary Diagrams

- FA-8

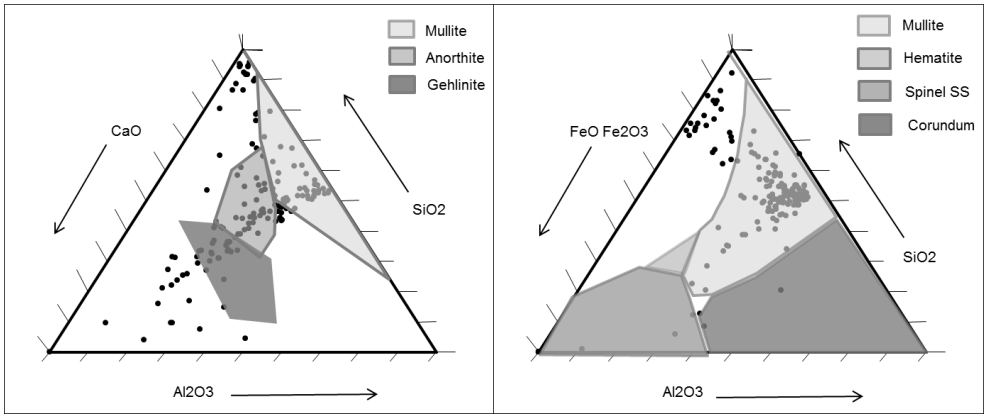

Figure C-7: FA-8 Ternary Diagrams

- FA-9

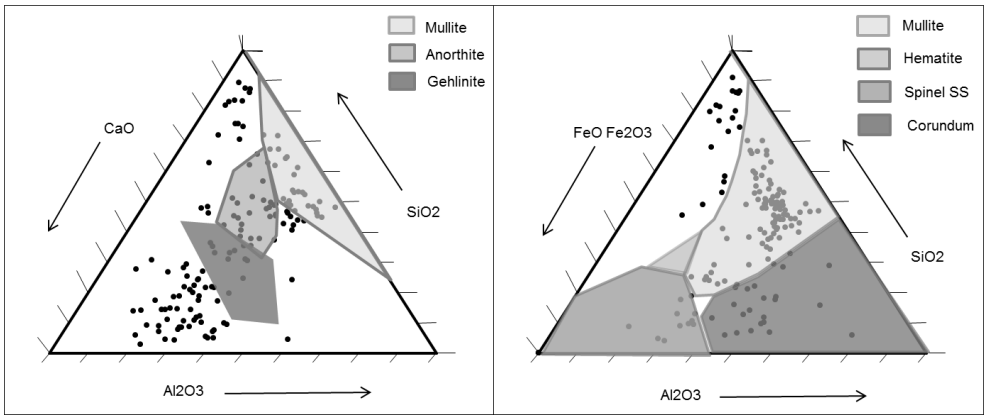

Figure C-8: FA-9 Ternary Diagrams

- FA-10

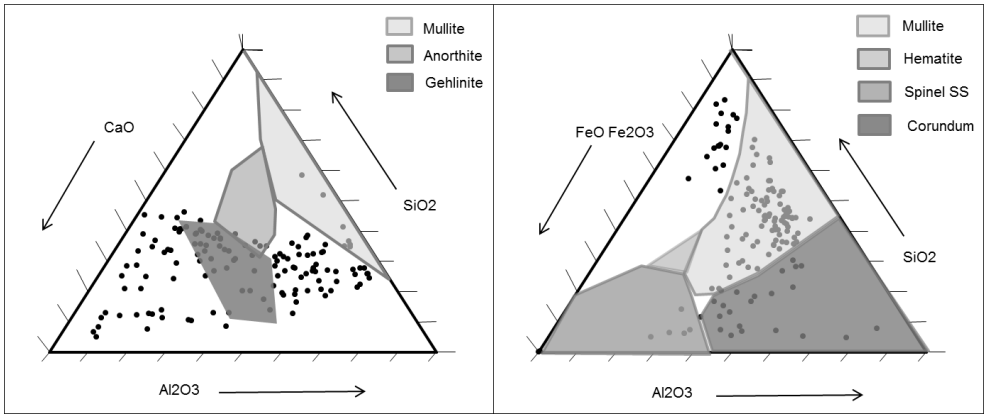

Figure C-9: FA-10 Ternary Diagrams

- FA-11

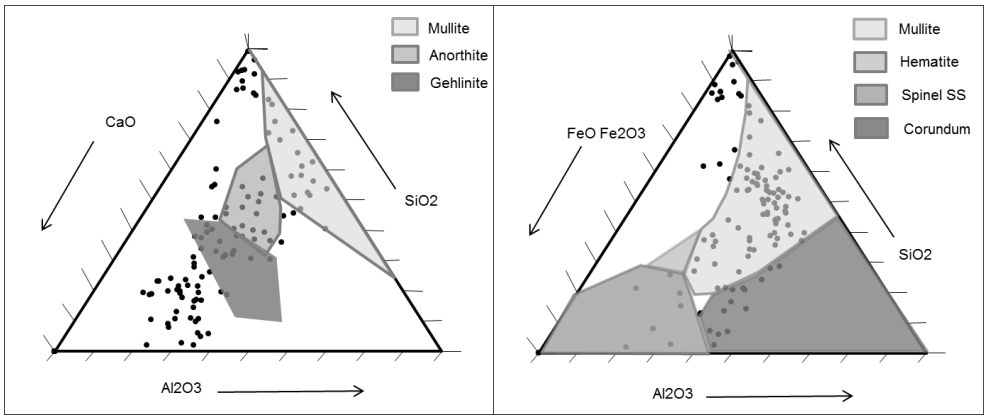

Figure C-10: FA-11 Ternary Diagrams

- FA-13

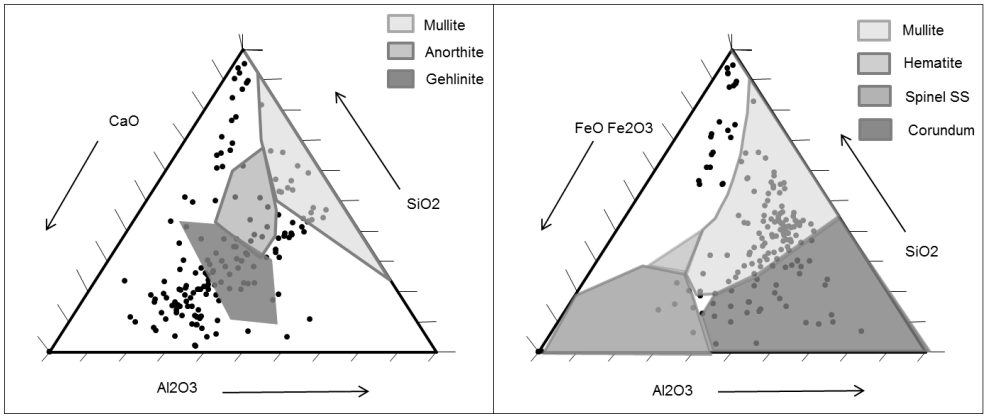

Figure C-11: FA-13 Ternary Diagrams

- FA-14

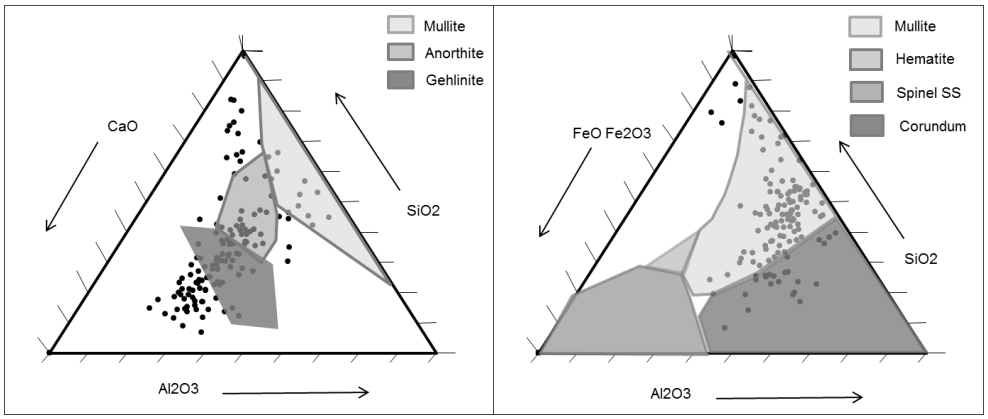

Figure C-12: FA-14 Ternary Diagrams

- FA-15

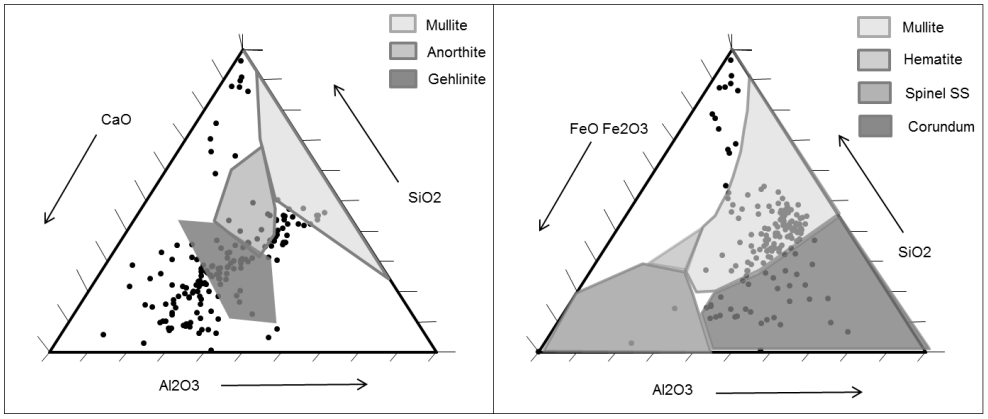

Figure C-13: FA-15 Ternary Diagrams

- FA-18

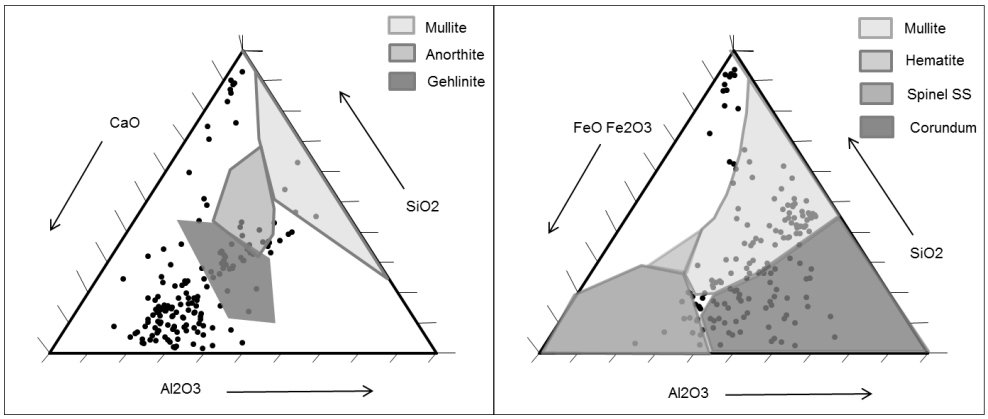

Figure C-14: FA-18 Ternary Diagrams

References

Abdallah, I., Mahmoud, E., Nazarian, S., & Masad, E. (2008). *Quantifying the Role of Coarse Aggregate Strength on Resistance to Load in HMA for Blended Aggregates.* El Paso, Texas: Center for Transportation Infrastructure Systems.

ACI 232.R-96. (1996). Use of Fly Ash in Concrete. *ACI Committee 232*.

ACI201.2R-01. (2001). Guide to Durable Concrete.

ASTM C 618. (2008). Standard Specification for Coal Fly Ash and Raw or Calcined Natural Pozzolan for Use in Concrete. *ASTM International*.

ASTM International. (2011). C125-11b: Standard Terminology Relating to Concrete and Concrete Aggregates. *ASTM International*.

Bensted, J. (1999). Thaumasite - background and nature in deterioration of cements, mortars and concretes. *Cement & Concrete Composites Vol. 21*, 117-121.

Bhatty, J. I., & Taylor, P. C. (2006). Sulfate Resistance of Concrete Using Blended Cements or Supplementary Cementitious Materials. *PCA Research & Development Information*.

Carrasquillo, R. L., & Tikalsky, P. J. (1992). Influence of Fly Ash on the Sulfate Resistance of Concrete. *ACI Structural Journal*, 69-75.

Carrasquillo, R. L., & Tikalsky, P. J. (1993). Fly Ash Evaluation and Selection for Use in Sulfate-Resistant Concrete. *ACI Materials Journal*, 545-551.

Chancey, R. (2008). *Characterization of Crystalline and Amorphous Phases and Respective Reactivities in a Class F Fly Ash.* Austin: The University of Texas at Austin.

Chindaprasirt, P., Homwuttiwong, S., & Sirivivatnanon, V. (2004). Influence of fly ash fineness on strength, drying shrinkage and sulfate resistance of blended cement mortar. *Cement and Concrete Reserach Vol. 34*, 1087-1092.

Cyr, M., & Tagnit-Hamou, A. (2001). Particle size distribution of fine powders by LASER diffractino spectrometry. Cas of cementitious materials. *Materials and Structures Vol. 34*, 342-350.

Day, R. L. (2000). Development of Performance Tests for Sulfate Attack on Cementitious. *Cement, Concrete and Aggregates: Vol. 22, No.2*, 169-176.

De La Torre, A., Bruque, S., & Arand, M. (2001). Rietveld quantitative amorphous content analysis. *Journal of Applied Crystallography*, 196-202.

Dhole, R. (2008). *Sulfate Resistance of High Calcium Fly Ash Concrete.* University of New Brunswick.

Dodson, V. H., & Roberts, L. R. (1980). *Patent No. 4,210,457.* United States.

Drimalas, T. (2007). *Laboratory and Field Evaluations of External Sulfate Attack.* Austin: University of Texas at Austin.

Dunstan, J. E. (1980). A Possible Method for Identifying Fly Ashes That Will Improve the Sulfate Resistance of Concretes. *Cement, Concrete and Aggregates* , 20-30.

Ferraris, C., Bullard, J., & Hackley, V. (n.d.). *Particle size distribution by LASER diffraction spectrometry: application to cementitous powers.* Gaithersburg: National Institute of Standard and Technology (NIST).

Flatt, R. J., & Scherer, G. W. (2002). Hydration and Crystallization Pressure of Sodium Sulfate: a Critical Review. *Mat. Res. Soc. Symp. Proc. Vol. 712*.

Folliard, K. (2010, Fall). Sulfate Attack. *Advanced Concrete Materials class, University of Texas at Austin*.

Folliard, K. J. (2006). Preventing ASR/DEF in New Concrete: Final Report, Technical Report 0-4085-5. *Center for Transportation Research*.

Folliard, K. J., & Sandberg, P. (1994). Mechanisms of Concrete Deterioration by Sodium Sulfate Crystallization. *Special Publication (SP-145), Third International ACI/CANMET Conference on Concrete Durability*, 933-946.

Graham, D., & Midgley, N. (2000). Triangular Diagram Plotting Spreadsheet.

Haynes, H., & Bassuoni, M. (2011). Physical Salt Attack on Concrete. *Concrete International*.

Hemmings, R. T., & Berry, E. E. (1988). On the glass in coal fly ashes: Recent advances. *Materials Research Society Symposium Proceedings Vol 113*.

Joshi, Natt, Day, & Tillerman. (1985). Scanning Electron Microscopy and X-ray Diffraction Analysis of Various Size Fractions of Fly Ash. *Materials Research Society Symposium Proceedings Vol. 43*, 31-39.

Jozic, D., Zelic, J., & Janjatovic, I. (2010). Influence of the Coarse Fly Ash on the Mechanical Properties of Cement Mortars. *Ceramics-Silikáty* , 144-151.

Kalousek, G., & Benton, E. (1970). Mechanisms of Sea Water Attack on Cement Pastes. *ACI Proceedings Vol. 67*, 187-192.

Kosmatka, S. H., & Panarese, W. C. (1994). *Design and Control of Concrete Mixtures.* Skokie: Portland Cement Association.

McCarthy, G., Solem, J., Manz, O., & Hassett, D. (1190). Use of a database of chemical, mineralogical and physical properties of North American fly ash to study the nature of fly ash and its utilization as a mineral admixture in concrete. *Materials Research Society*.

Mehta, P. K. (1986). Effect of Fly Ash Compositions on Sulfate Resistance of Cement. *ACI Materials Journal*, 994-1000.

Mindess, S., & Young, J. (1981). *Concrete.* Englewood Cliffs, N.J.: Prentice Hall.

Neville, A. M. (1996). *Properties of Concrete: Fourth and Final Edition.* Wiley.

Riding, K., Poole, J., Folliard, K., Juenger, M., & Schindler, A. (2011). New Model for Estimating Apparent Activation Energy of Cementitous Systems. *ACI Materials Journal*, 550-557.

Roy, D., Luke, K., & Diamond, S. (1985). Characterization of fly ash and its reactions in concrete. *Materials Research Society Vol 43*, 3-20.

Scrivener, K. L., & Nonat, A. (2011). Hydration of cementitious materials, present and future. *Cement and Concrete Research 41*, 651-665.

Skalny, J., Marchand, J., & Odler, I. (2002). *Sulfate Attack on Concrete.* London: Spon Press.

Stephens, J. B., & Carrasquillo, R. L. (2000). *Evaluating Performace-Based Test and Specifications for Sulfate Resistance in Concrete.* Austin: Center for Transportation Research.

Tikalsky, P. J. (1989). The Effects of Fly Ash on the Sulfate Resistance of Concrete. *Ph.D. dissertation*. University of Texas at Austin.

Tikalsky, P., & Carrasquillo, R. (1992). Influence of Fly Ash on the Sulfate Resistance of Concrete. *ACI Materials Journal Vol. 89*, 69-75.

Tikalsky, P., & Carrasquillo, R. (1993). Fly Ash Evaluation and Selection for use in Sulfate-Resistant Concrete. *ACI Materials Journal Vol. 90*, 545-551.

Tishmack, J., Olek, J., & Diamond, S. (1999). Characterization of High-Calcium Fly Ashes and Their Potential Influence on Ettringite Formation in Cementitious Systems. *Cement, Concrete and Aggregates*, 82-92.

Tokyay, M., & Hubbard, H. (1992). Minerological Investigations of High Lime Fly Ashes. *ACI Special Publication Vol 132*, 65-77.

Ubbriaco, P., Bruno, P., Traini, A., & Calabrese, D. (2001). Fly Ash Reactivity: Formation of hydrate phases. *Journal of Thermal Analysis and Calorimetry Vol 66*, 293-305.

Vassilev, S. V., & Vassileva, C. G. (2007). A new approach for the classification of coal fly ash based on their origin, composition, properties, and behaviour. *Fuel 86*, 1490-1512.

Watt, J., & Thorne, D. (1965-66). Composition and Pozzolanic Properties of Pulverized Fuel Ashes. *Journal of Applied Chemistry*.

Webb, P. A. (2000). *A Primer on Particle Sizing by Static Laser Light Scattering.* Micromeritics: Technical Workshop Series.

Wei, Y., Yao, W., & Wang, W. (2012). Effects of Internal Standards and Peak Profile Functions on Quantitative XRD Phase Analysis of Cement and its Hydrates. *Key Engineering Materials Vol. 492*, 424-428.

Winburn, R., Lerach, S., Jarabek, B., Widsom, M., Grier, D., & McCarthy, G. (2000). Quantitative XRD Analysis of Coal Combustion By-Products by the Rietveld Method. Testing with Standard Mixtures. *JCPDS- International Centre for Diffraction Data, Advances in X-ray Analysis*, 387-396.